



This is to certify that the
thesis entitled
Selective Size Reduction of poly(vinyl chloride)
and poly(ethylene terephthalate) by Impact Grinding
presented by
Janet Lynn Green
has been accepted towards fulfillment
of the requirements for
Ph.D. degree in ChE

Major professor

Date July 11, 1996

PLACE IN RETURN BOX to remove this checkout from your record.
TO AVOID FINES return on or before date due.

DATE DUE	DATE DUE	DATE DUE
SEP 23 7PM	_____	_____
_____	_____	_____
_____	_____	_____
_____	_____	_____
_____	_____	_____
_____	_____	_____
_____	_____	_____

MSU is An Affirmative Action/Equal Opportunity Institution

c:\civ\date.due.pm3-p.1

SELECTIVE SIZE REDUCTION OF POLY(VINYL CHLORIDE) AND
POLY(ETHYLENE TEREPHTHALATE) BY IMPACT GRINDING

By

Jane Lynn Green

A DISSERTATION

Submitted to
Michigan State University
in partial fulfillment of the requirements
for the degree of

DOCTOR OF PHILOSOPHY

Department of Chemical Engineering

1996

ABSTRACT

**SELECTIVE SIZE REDUCTION OF POLY(VINYL CHLORIDE) AND
POLY(ETHYLENE TEREPHTHALATE) BY IMPACT GRINDING**

By

**SELECTIVE SIZE REDUCTION OF POLY(VINYL CHLORIDE) AND
POLY(ETHYLENE TEREPHTHALATE) BY IMPACT GRINDING**

By

The separation of post-consumer thermoplastics for recycling is often difficult in cases where significant physical property differences between the materials do not exist.

Janet Lynn Green

One instance of this is the separation of Poly(ethylene terephthalate) from Poly(vinyl chloride). This research has investigated a method to selectively grind Poly(ethylene terephthalate) and Poly(vinyl chloride) in a hammer mill to different particle sizes and shapes for classification. Process variables, namely impact rate and temperature, have been related to the failure mechanisms for each thermoplastic. Single and multiple particle breakage patterns have been examined. **A DISSERTATION**

Submitted to
Michigan State University
in partial fulfillment of the requirements
for the degree of

DOCTOR OF PHILOSOPHY

Department of Chemical Engineering

1996

ABSTRACT

SELECTIVE SIZE REDUCTION OF POLY(VINYL CHLORIDE) AND POLY(ETHYLENE TEREPHTHALATE) BY IMPACT GRINDING

By

Janet Lynn Green

The separation of post-consumer thermoplastics for recycling is often difficult in cases where significant physical property differences between the materials do not exist. One instance of this is the separation of Poly(ethylene terephthalate) from Poly(vinyl chloride). This research has investigated a method to selectively grind Poly(ethylene terephthalate) and Poly(vinyl chloride) in a hammer mill to different particle sizes and shapes for classification. Process variables, namely impact rate and temperature, have been related to the failure mechanisms for each thermoplastic. Single and multiple particle breakage patterns have been examined. The brittle-ductile transitions have been compared with those predicted by tensile and compressive tests, and the β -transition process. Izod impact and ballistics testing were also conducted to explore differences in low and high speed impact. High speed videography was used to examine particle flow and breakage within the hammer mill. The surfaces of the particles were viewed by scanning electron microscopy for failure mechanism identification.

Failure mechanisms suggested by tensile and compressive deformation diagrams proved to be poor indicators of the failure mechanisms of PVC and PET during impact grinding. Izod impact testing and the β -relaxation temperature provided correlating

brittle-ductile transition information for PVC comminution, but not for PET. The ductile behavior of PET at cryogenic conditions is not fully understood.

An empirical two parameter equation proved useful in describing the size reduction behavior of PVC and PET. The model coefficients could be related to the grinding temperature, impact rate and screen size. The product sizes of PVC particles decreased with increasing impact rate and decreasing temperature, and the breakage changed from bimodal cascade failure to monomodal catastrophic failure. For PET the product size was independent of temperature, and only decreased slightly with increases in impact rate.

At cryogenic temperatures, PVC can be selectively ground to smaller particle sizes than PET. This is due to PVC particles fracturing in a brittle fashion, while PET fails in a ductile fashion. Separation of the two materials based on size is possible, however, optimization to increase purity and yield is still necessary.

This work is dedicated to my Lord and Savior, Jesus Christ, to my parents, and seven sisters, whose guidance, love and support has made the difference!

My appreciation and indebtedness to those who contributed to this work are limitless. My sincere thanks to my advisor, Dr. Eric A. Grocke, whose assistance, guidance, and support over the years have been invaluable. My gratitude to my advisor, Dr. Charles A. Petty, who stepped right in with enthusiasm, insuring the success of this project with his unrivaled ideas. To the Department of Chemical Engineering, who gave me the opportunity and support to complete this work.

I would like to thank Dr. Syed Ali for all of his assistance in obtaining the necessary equipment and guidance at the start of this project. I would like to give special thanks to Dr. Serhan Pinar for his help with the high speed videotaping and so many other aspects of this research. His tireless efforts and kindness will always be remembered. Thanks to Eric Cheslek, whose assistance with experimentation at the close of this project was immensely appreciated.

I would also like to acknowledge the Office of Naval Research, Research Excellence Fund, American Phosphor Council, Michigan Materials Processing Institute, and the Summer Acceleration Fellowship Fund, for their financial support.

Finally, to my parents, Rev. Hovious and Mrs. Julia Green, and my sisters, Dr. June Rivers, Ph.D., Dr. LaClair Bouknight, M.D., Dr. Constance Elico, Ph.D., Dr. Hazel Young, M.D., Dr. Valeria Jackson, Ph.D., Dr. Christine Quast, Ph.D., and Dr. Carroon Green-Lee, M.D., who provided the prayers, example, direction, and vision. To Eric Hopson, whose friendship, support, and companionship has made this journey an adventure. To Drewy, who helped me learn what faith, hope, and love really mean.

TABLE OF CONTENTS
ACKNOWLEDGMENTS

My appreciation and indebtedness to those who contributed to this work are limitless. My sincere thanks to my advisor, Dr. Eric A. Grulke, whose assistance, guidance, and support over the years have been invaluable. My gratitude to my advisor, Dr. Charles A. Petty, who stepped right in with enthusiasm, insuring the success of this project with his unrivaled ideas. To the Department of Chemical Engineering, who gave me the opportunity and support to complete this work.

I would like to thank Dr. Syed Ali for all of his assistance in obtaining the necessary equipment and guidance at the start of this project. I would like to give special thanks to Dr. Serban Petcu for his help with the high speed videotaping and so many other aspects of this research. His tireless efforts and kindness will always be remembered. Thanks to Eric Cheslek, whose assistance with experimentation at the close of this project was immensely appreciated.

I would also like to acknowledge the Office of Naval Research, Research Excellence Fund, American Plastics Council, Michigan Materials Processing Institute, and the Summer Acceleration Fellowship Fund, for their financial support

Finally, to my parents, Rev. Havius and Mrs. Julia Green, and my sisters, Dr. June Rivers, Ph.D., Dr. LaClaire Bouknight, M.D., Dr. Constance Price, Ph.D., Dr. Hazel Young, M.D., Dr. Valeria Jackson, Ph.D., Dr. Chiarina Owens, Ph.D., and Dr. Carmen Green-Lee, M.D., who provided the prayers, example, direction, and vision. To Eric Hopson, whose friendship, support, and companionship has made this journey an adventure. To Drewy, who helped me learn what faith, hope, and love really mean.

	2-2.4 Predicting Particle Size and Shape	17
	2-3 Failure Mechanisms	17
	2-3.1 Types of Failure Mechanisms	17
	2-3.2 Dependence on Loading Rate, Temperature, and	19
TABLE OF CONTENTS		
	2-4 Separation by Grinding	21
	2-5 References	Page
List of Tables	FAILURE MECHANISM DIAGRAMS: PVC AND PET	x
List of Figures	3-1 Introduction	xii
List of Symbols	3-2 Strain Rate - Velocity Relationship	xvii
List of Abbreviations	Tensile and Compressive Failure	xix
Chapter	3-2.2 Tensile Failure Mechanism Diagrams	27
	3-2.3 Compressive Failure Mechanism Diagrams	34
	3-3.3 Sensitivity Analysis of Model Coefficients on	38
1.	INTRODUCTION	1
	1-1. Problem Description	1
	3-4.1 Materials	40
	1-2. Background	2
	1-2.1 Plastic Recycling	2
	1-2.2 Thermoplastic Properties and Grinding	4
	1-3. Objectives	6
	3-5.1 Materials	7
	1-4. Methodology and Scope of the Study	7
	3-5.3 Results and Discussion	17
	1-5. Engineering Significance	8
	3-6 Impact Transition Temperature Estimation from	20
	1-6. References	9
2.	SURVEY OF RELEVANT LITERATURE	10
	2-1. Introduction	10
	2-2. Size Reduction	10
	2-2.1 Fracture Mechanics	12
	2-2.2 Impact Grinding	14
	2-2.3 Thermoplastics	15

4-2	2-2.4	Predicting Particle Size and Shape	17
	4-2.1	Materials	56
2-3		Failure Mechanisms	17
	2-3.1	Types of Failure Mechanisms	17
	2-3.2	Dependence on Loading Rate, Temperature, and 4-2.5 Material Properties	19
			58
	2-4	Separation by Grinding	21
	4-3.1	Empirical Breakage Models	28
	2-5	References	22
	4-3.2	Characteristic Particle Size	31
	4-3.3	Particle Breakage Mechanism	31
3		FAILURE MECHANISM DIAGRAMS: PVC AND PET	24
	4-4	Conclusions	24
	3-1	Introduction	24
	4-5	References	25
	3-2	Strain Rate - Velocity Relationship	25
5		IMPACT GRINDING OF THERMOPLASTICS: EFFECT OF 3-3 COMMINUTION	26
	3-3	Tensile and Compressive Failure	26
	3-3.2	Tensile Failure Mechanism Diagrams	27
	5-1	3-3.2 Compressive Failure Mechanism Diagrams	34
	3-3.3	Sensitivity Analysis of Model Coefficients on 5-2 Experimental Brittle-Ductile Transition	38
	5-2.1	Materials	38
	3-4	Izod Impact Failure	40
	3-4.1	Materials	40
	3-4.2	Izod Impact Testing	40
	3-4.3	Limitations	42
	3-4.4	Results and Discussion	42
	5-2.7	Limitations	42
	3-5	High Speed Ballistics	47
	5-3	3-5.1 Materials	47
	3-5.2	Ballistics Testing	47
	3-5.3	Results and Discussion	47
	5-3.3	Effect of Feed Particle Size	47
	3-6	Impact Transition Temperature Estimations from β -Relaxation Process	50
	3-3.6	Predicting Particle Size	50
	3-7	Conclusions	53
	5-3.6	Particle Size Reduction of PVC	53
	3-8	References	54
4		IMPACT GRINDING OF THERMOPLASTICS: SIZE DISTRIBUTION FUNCTION MODEL	55
6		CONCLUSIONS	55
	4-1	Introduction	55

4-2.	Experimental	55
4-2.1	Materials	56
4-2.2	Hammer Mill	56
4-2.3	Particle Size Determination	56
4-2.4	Optical Microscopy	58
4-2.5	Limitations	58
4-3.	Results and Discussion	58
4-3.1	Empirical Breakage Models	58
4-3.2	Characteristic Particle Size	62
4-3.3	Particle Breakage Mechanism	63
4-4.	Conclusions	74
4-5.	References	75
5.	IMPACT GRINDING OF THERMOPLASTICS: EFFECT OF PROCESS VARIABLES ON PARTICLE COMMUNUTION	76
5-1.	Introduction	76
5-2.	Experimental	77
5-2.1	Materials	77
5-2.2	Hammer Mill	79
5-2.3	Particle Size Determination	82
5-2.4	Size Distribution Representation	82
5-2.5	High Speed Videography	83
5-2.6	Scanning Electron Microscopy	85
5-2.7	Limitations	85
5-3.	Results and Discussion	85
5-3.1	Effect of Temperature	86
5-3.2	Effect of Impact Rate	88
5-3.3	Effect of Feed Particle Size	91
5-3.4	Effect of Screen Size	95
5-3.5	Breakage Mechanism Identification	99
5-3.6	Predicting Particle Size	105
5-3.7	Selective Size Reduction of PVC and PET	121
5-4.	Conclusions	123
5-5.	References	125
6.	CONCLUSIONS	126

7.	RECOMMENDATIONS	129
	APPENDICES	131
	Appendix A: Izod Impact Data	131
	Appendix B: Impact Grinding Data	132

Table		Page
1.1	Thermoplastic Separation Techniques	3
1.2	Properties of Typical Consumer Waste Thermoplastics	5
2.1	Factors Promoting Brittle Fracture	20
2.2	Mechanical Properties of Select Thermoplastics	20
3.1	Values of Strain Rate and Velocity for Various Stress Types	26
3.2	Constants for Tensile Brittle Behavior Model	30
3.3	Constants for Tensile Yield Behavior Model	30
3.4	Constants for Tensile Viscous Behavior Model	30
3.5	Brittle-Ductile Transition Temperatures for Tensile Failure	33
3.6	Thermal Properties	35
3.7	Requirements for Adiabatic Heating	33
3.8	Constants for Compressive Brittle Behavior Model	35
3.9	Constants for Compressive Yield Behavior Model	35
3.10	Sensitivity of Tensile Failure Strength to Model Coefficients	39
3.11	Sensitivity of Compressive Failure Strength to Model Parameters	39
3.12	β -Relaxation Temperature and Activation Energy	51

4.1	Coefficients for Cumulative Size Distribution Models for PVC	61
4.2	Coefficients for Cumulative Size Distribution Models for PET	61
4.3	Effects of Temperature and Impact Rate on PVC Comminution	73
4.4	Effects of Temperature and Impact Rate on PET Comminution	74
5.1	Apparatus for Grinding and Analytical Systems	78
Table	Physical Data for PVC and PET	Page
1.1	Thermoplastic Separation Techniques	30
1.2	Properties of Typical Consumer Waste Thermoplastics	524
2.1	Factors Promoting Brittle Fracture	20
2.2	Mechanical Properties of Select Thermoplastics	20
3.1	Values of Strain Rate and Velocity for Various Stress Types	26
3.2	Constants for Tensile Brittle Behavior Model	30
3.3	Constants for Tensile Yield Behavior Model	30
3.4	Constants for Tensile Viscous Behavior Model	30
3.5	Brittle-Ductile Transition Temperatures for Tensile Failure	33
3.6	Thermal Properties	33
3.7	Requirements for Adiabatic Heating	33
3.8	Constants for Compressive Brittle Behavior Model	35
3.9	Constants for Compressive Yield Behavior Model	35
3.10	Sensitivity of Tensile Failure Strength to Model Coefficients	39
3.11	Sensitivity of Compressive Failure Strength to Model Parameters	39
3.12	β -Relaxation Temperature and Activation Energy	51

4.1	Coefficients for Cumulative Size Distribution Models for PVC	61
4.2	Coefficients for Cumulative Size Distribution Models for PET	61
4.3	Effects of Temperature and Impact Rate on PVC Comminution	73
4.4	Effects of Temperature and Impact Rate on PET Comminution	74
5.1	Apparatus for Grinding and Analytical Systems	78
5.2	Physical Data for PVC and PET	78
5.3	Process Variable for Impact Grinding	80
5.4	Brittle-Ductile Transition Temperatures (C) for PVC	124
3.1	Tensile Failure Mechanisms	
3.2	Tensile Failure Mechanisms (Cont'd)	
3.3	Brittle-Ductile Transition for Impact Testing	
3.4	Compressive Failure Mechanisms	
3.5	Compressive Failure Mechanisms (Cont'd)	
3.6	Brittle-Ductile Transition for Impact Testing	
3.7	Schematic of Izod Apparatus	
3.8	Izod Impact Strength of PVC and PET	
3.9a	SEM (x 50) of PVC Izod Test Specimen Impact Fracture	
3.9b	SEM (x 1,000) of PVC Izod Test Specimen Impact Fracture	
3.10a	SEM (x 50) of PVC Izod Test Specimen Impact Fracture	
3.10b	SEM (x 1,000) of PVC Izod Test Specimen Impact Fracture	
3.11a	SEM (x 50) of PET Izod Test Specimen Impact Fracture	
3.11b	SEM (x 1,000) of PET Izod Test Specimen Impact Fracture	
3.12	SEM of PVC Ballistics Sample Impacted at 200 ft/s	

3.13	SEM of PET Ballistics Sample Impacted at 369 m/s	40
3.14	Brittle-Ductile Transition Predicted by β -Relaxation Temperature	52
3.15	Brittle-Ductile Transition Based on the β -Temperature in Terms of Strain-Rate	52
LIST OF FIGURES		
4.1	Schematic of Hammer M31	37
4.2	Comparison of Cumulative Size Distribution Functions Modeling Ground PVC Particles	60

Figure		Page
2.1	Schematic Diagram of Incipient Flaw	12
3.1	Tensile Failure Mechanism Diagram for PVC	31
3.2	Tensile Failure Mechanism Diagram for PET	31
3.3	Brittle-Ductile Transition for Tensile Failure	32
3.4	Compressive Failure Mechanism Diagram for PVC	36
3.5	Compressive Failure Mechanism Diagram for PET	36
3.6	Brittle-Ductile Transition for Compressive Failure	37
3.7	Schematic of Izod Apparatus	41
3.8	Izod Impact Strength of PVC and PET at Various Temperatures	42
3.9a	SEM (x 50) of PVC Izod Test Specimen Impacted at -40°C	44
3.9b	SEM (x 1,000) of PVC Izod Test Specimen Impacted at -40°C	44
3.10a	SEM (x 50) of PVC Izod Test Specimen Impacted at 20°C	45
3.10b	SEM (x 1,000) of PVC Izod Test Specimen Impacted at 20°C	45
3.11a	SEM (x 50) of PET Izod Test Specimen Impacted at 20°C	46
3.11b	SEM (x 1,000) of PET Izod Test Specimen Impacted at 20°C	46
3.12	SEM of PVC Ballistics Sample Impacted at 398 m/s	49

3.13	SEM of PET Ballistics Sample Impacted at 369 m/s of PET at 53.3 m/s and 22°C	49
3.14	Brittle-Ductile Transition Predicted by β -Relaxation Temperature	52
4.17	Density Distribution for Multiple Particle Breakage of PET at 93.2 m/s	72
3.15	Brittle-Ductile Transition Based on the β -Temperature in Terms of Strain-Rate	52
4.18	Density Distribution for Multiple Particle Breakage of PET at 93.2 m/s	72
4.1	Schematic of Hammer Mill	57
4.2	Comparison of Cumulative Size Distribution Functions Modeling Ground PVC Particles	60
5.2	Bosman Mikro-Pulverizer Hammer Mill	81
4.3	Comparison of Cumulative Size Distribution Functions Modeling Ground PET Particles	60
5.3	Setup for High Speed Videography of the Grinding Process	84
4.4	Cumulative Size Distribution of PVC Ground in a Hammer mill	63
4.5	Progeny PVC Particles from Single Particle Impact at 53.3 m/s and 22°C	65
4.6	Progeny PVC Particles from Single Particle Impact at 93.2 m/s and 22°C	65
4.7	Progeny PVC Particles from Single Particle Impact at 93.2 m/s and 0°C At Room Temperature	66
4.8	Progeny PET Particles from Single Particle Impact at 53.3 m/s and 22°C	66
5.8	Cumulative Particle Size Distribution for PET at Various Impact Rates	89
4.9	Progeny PET Particles from Single Particle Impact at 93.2 m/s and 22°C	67
4.10	Progeny PET Particles from Single Particle Impact at 93.2 m/s and 0°C At 0°C M.O.T.	67
4.11	Optical Microscopy Photograph of PVC Particle Ground at 92.3 m/s and 0°C	68
5.10	Cumulative Particle Size Distribution for PET at Various Impact Rates At 0°C M.O.T.	90
4.12	Optical Microscopy Photograph of PET Particle Ground at 92.3 m/s and 0°C	68
5.11	Cumulative Particle Size Distribution PVC for Various Feed Particle Sizes at Room Temperature	93
4.13	Density Distribution for Multiple Particle Breakage of PVC at 53.3 m/s and 22°C	70
5.12	Cumulative Particle Size Distribution PET for Various Feed Particle Sizes at Room Temperature	93
4.14	Density Distribution for Multiple Particle Breakage of PVC at 93.2 m/s and 22°C	70
5.13	Cumulative Particle Size Distributions PVC for Various Feed Particle Sizes at 0°C M.O.T.	94
4.15	Density Distribution for Multiple Particle Breakage of PVC at 93.2 m/s and 0°C M.O.T.	71
5.14	Cumulative Particle Size Distributions PVC for Various Feed Particle Sizes at 0°C M.O.T.	94

4.16	Density Distribution for Multiple Particle Breakage of PET at 53.3 m/s and 22°C	71
4.17	Density Distribution for Multiple Particle Breakage of PET at 93.2 m/s and 22°C	72
4.18	Density Distribution for Multiple Particle Breakage of PET at 93.2 m/s and 0°C M.O.T.	72
5.1	Cumulative Particle Size Distribution of Feed Thermoplastic Flakes	79
5.2	Bantam Mikro-Pulverizer Hammer Mill	81
5.3	Experimental Setup for High Speed Videography of the Grinding Process	84
5.4	Cumulative Particle Size Distribution for PET at Various Temperatures	87
5.5	Cumulative Particle Size Distribution for PVC at Various Temperatures	87
5.6	Effect of Mill Outlet Temperature on PVC Comminution	88
5.7	Cumulative Particle Size Distribution for PVC at Various Impact Rates At Room Temperature	89
5.8	Cumulative Particle Size Distribution for PET at Various Impact Rates At Room Temperature	89
5.9	Cumulative Particle Size Distribution for PVC at Various Impact Rates At 0°C M.O.T.	90
5.10	Cumulative Particle Size Distribution for PET at Various Impact Rates At 0°C M.O.T.	90
5.11	Cumulative Particle Size Distribution PVC for Various Feed Particle Sizes at Room Temperature	93
5.12	Cumulative Particle Size Distribution PET for Various Feed Particle Sizes at Room Temperature	93
5.13	Cumulative Particle Size Distribution PVC for Various Feed Particle Sizes at 0°C M.O.T.	94
5.14	Cumulative Particle Size Distribution PET for Various Feed Particle Sizes at 0°C M.O.T.	94

5.15	Self-similar size distribution of PVC for Various Feed Particle Sizes at 0°C M.O.T	95
5.16	Cumulative Particle Size Distribution PET for Various Retaining Screen Sizes at Room Temperature	97
5.17	Cumulative Particle Size Distribution PVC for Various Retaining Screen Sizes at Room Temperature	97
5.18	Cumulative Particle Size Distribution PET for Various Retaining Screen Sizes at 0°C M.O.T.	98
5.19	Cumulative Particle Size Distribution PVC for Various Retaining Screen Sizes at 0°C M.O.T.	98
5.20	SEM (x1,000) of PVC Particle Ground at Room Temperature	100
5.21	SEM (x1,000) of PET Particle Ground at Room Temperature	100
5.22	SEM (x1,000) of PVC Particle Ground at 0°C M.O.T.	101
5.23	SEM (x1,000) of PET Particle Ground at 0°C M.O.T.	101
5.24	SEM of PET Particle Shape	103
5.25	SEM of PVC Particle Shape	103
5.26	High Speed Videography of Particle Prior to Impact	104
5.27	High Speed Videography of Particle at the Point of Impact	104
5.28	Dependence of Characteristic Product Size on Feed Temperature for PET	106
5.29	Dependence of Characteristic Product Size on Feed Temperature for PVC	106
5.30	Dependence of Uniformity Index on Feed Temperature for PET	107
5.31	Dependence of Uniformity Index on Feed Temperature for PVC	107
5.32	Dependence of Characteristic Product Size on Impact Rate for PET	109
5.33	Dependence of Characteristic Product Size on Impact Rate for PVC	109
5.34	Dependence of Uniformity Index on Impact Rate for PET	110

5.35	Dependence of Uniformity Index on Impact Rate for PVC	110
5.36	Dependence of Characteristic Product Size on Feed Particle Size for PET	112
5.37	Dependence of Characteristic Product Size on Feed Particle Size for PVC	112
5.38	Dependence of Uniformity Index on Feed Particle Size for PET	113
5.39	Dependence of Uniformity Index on Feed Particle Size for PVC	113
5.40	Dependence of Characteristic Product Size on Screen Size for PET	115
5.41	Dependence of Characteristic Product Size on Screen Size for PVC	115
5.42	Dependence of Uniformity Index on Screen Size for PET	116
5.43	Dependence of Uniformity Index on Screen Size for PVC	116
5.44	Self-similar Size Distribution for PVC	118
5.45	Self-similar Size Distribution for PET	118
5.46	Cumulative Size Distributions for Separated PVC/PET Ground Mixture	122
5.47	Mass Percentage of Particles of Each Thermoplastic Retained on Sieve Size	122
5.48	Size Separation of PVC/PET Mixture Ground at -20°C M.O.T.	123

t_f	Time to failure (sec)
t_e	Exponential time constant (sec)
T	Temperature (K)
T_g	Glass transition temperature (K)
T_β	β -relaxation temperature (K)
ΔU	Activation energy (kJ/mol)
v	Velocity (m/s)

Greek

α	Fractional difference between compressive and tensile strengths
α_m	Temperature coefficient of the modulus
γ	Surface free energy per unit area (N/m ²)
$\dot{\epsilon}$	Strain rate (sec ⁻¹)
ϵ_0	Pre-exponential for strain rate (sec ⁻¹)
k	Boltzmann constant (J/K)
σ	Stress (N/m ²)

σ_b	Brittle tensile stress (N/m^2)
σ_d	Draw stress (N/m^2)
$\sigma_{f,0}$	Fracture stress at 0 K (N/m^2)
$\sigma_{y,0}$	Yield stress at 0 K (N/m^2)
η_{T_g}	Viscosity at T_g ($N\text{-sec}/m^2$)
v	Stress activation velocity

LIST OF SYMBOLS

a	Thermal diffusivity (cm^2/sec)
c	Incipient crack length (m)
C_p	Heat capacity (kJ/kg-K)
C_1, C_2	WLF constants (K)
D	Particle thickness (mm)
E	Young's Modulus (N/m^2)
E_0	Modulus at 0 K (N/m^2)
f	Frequency (Hz)
H	Activation energy (J/mol)
K_{ic}	Critical stress intensity factor ($N/m^{3/2}$)
l	Distance from center (cm)
L	Particle length (mm)
L_1	Characteristic particle size (mm)
n	Uniformity index
P	Tensile load (N)
R	Universal gas constant (J/mol-K)
t_f	Time to failure (sec)
t_0	Exponential time constant (sec)
T	Temperature (K)
T_g	Glass transition temperature (K)
T_β	β -relaxation temperature (K)
ΔU	Activation energy (kJ/mol)
v	Velocity (m/s)
Greek	
α	Fractional difference between compressive and tensile strengths
α_m	Temperature coefficient of the modulus
γ	Surface free energy per unit area (N/m^2)
$\dot{\epsilon}$	Strain rate (sec^{-1})
ϵ_0	Pre-exponential for strain rate (sec^{-1})
κ	Boltzmann constant (J/K)
σ	Stress (N/m^2)

σ_B	Brittle tensile stress (N/m^2)
σ_d	Draw stress (N/m^2)
$\sigma_{f,0}$	Fracture stress at 0 K (N/m^2)
$\sigma_{y,0}$	Yield stress at 0 K (N/m^2)
η_{T_g}	Viscosity at T_g ($N\text{-sec}/m^2$)
v	Stress activation volume (m^3)

LIST OF ABBREVIATIONS

B-D	Brittle-Ductile Transition
fps	Frames per second
HDPE	High density polyethylene
LIN	Liquid nitrogen
M.O.T.	Mill outlet temperature
PET	Poly(ethylene terephthalate)
PP	Polypropylene
PMMA	Poly(methyl methacrylate)
PS	Polystyrene
PSD	Particle size distribution
PVC	Poly(vinyl chloride)
RRB	Rosin-Rammler-Bennett equation
THF	Tetrahydrofuran

CHAPTER 1

INTRODUCTION

LIST OF ABBREVIATIONS

B-D	Brittle-Ductile Transition
fps	Frames per second
HDPE	High density polyethylene
LIN	Liquid nitrogen
M.O.T.	Mill outlet temperature
PET	Poly(ethylene terephthalate)
PP	Polypropylene
PMMA	Poly(methyl methacrylate)
PS	Polystyrene
PSD	Particle size distribution
PVC	Poly(vinyl chloride)
RRB	Rosin-Rammler-Bennett equation
THF	Tetrahydrofuran

INTRODUCTION

1-1. Problem Description

Plastic recycling has been gaining momentum due to decreasing landfill space, concerns about environmental contamination, and increasing costs of raw materials. A major research focus has been to develop technology to separate mixed plastic streams. The simplest approach to plastics separation is to use differences in physical properties, such as density. One technological challenge has been in cases where these differences between plastics do not exist, thus making separation difficult. The separation of poly(vinyl chloride) (PVC) from poly(ethylene terephthalate) (PET) is an example.

PVC and PET have overlapping density ranges, and due to their similar appearances and common applications, they are difficult to identify and separate. However, these materials can be separated if differences in size and shape can be induced during grinding (Famechon, 1990; Dreissen and Fontein, 1963). Exploratory experiments at Michigan State University have noted significant differences in the response of PVC and PET to impact stresses and have produced particle size differences for classification. The objective of this research is to explore more broadly the size reduction behavior of PVC and PET over a wide range of temperatures. The approach adopted has provided new understanding of the failure mechanisms associated with PVC and PET comminution. This study has provided a general knowledge of the mechanics of breakage for thermoplastics during impact grinding.

1-2. Background

1-2.1 Plastic Recycling

In the past two decades, the market for plastic resins has more than quadrupled in the United States. With this large increase, plastics still only make up about 7% of municipal waste. However, with the high cost of waste disposal, the large volume plastic waste takes up, the increasing cost of petroleum and natural gas (primary constituents of plastic material), the fear of environmental contamination, and the anticipation of a significant increase in the use of plastics, there has been incentive enough for the development and improvement of plastic recycling technologies. With governmental regulations encouraging and even requiring recycling, the plastic recycling industry is expanding rapidly. One limitation to this growth industry, however, is an economical separation technology.

Plastic separation techniques basically fall into three categories: namely macrosorting, microsorting, and molecular separation. Macrosorting can be defined as separating plastic waste in its existing form. This is usually done manually, but automated methods that detect color, shape, and chemical structure also have been developed. Microsorting is the separation of material that has been reduced by shredders, or granulators. The separation is usually based on some physical property differences between the plastics, such as density. Molecular separation entails separating macromolecules from each other. A brief summary of some of the techniques can be seen in Table 1.1. Most of these separation methods are still in the developmental stages.

Table 1.1 Thermoplastic Separation Techniques

TYPE OF SORTING	DEVELOPER	DESCRIPTION OF TECHNIQUE	ADVANTAGES / DISADVANTAGES	STAGE OF DEVELOPMENT
Macro (Dinger, 1992)	B. F. Goodrich	X-ray fluorescence is used to identify vinyl	Limited Applicability	Developmental
Macro (Dinger, 1992)	Rutgers	Light transmission is used to sort plastics by pigment	Contamination affects success, Limited Applicability	Developmental
Macro (Dinger, 1992)	Automation Industries, and others	Plastics sorted by resin type and color using detectors	Applicable to all common packaging resins	Developmental
Macro (Dinger, 1992)	Eastman Chemical and others	Plastics sorted by markers placed by manufacturer	Need cooperation of entire industry	Developmental
Macro (Leaversuch, 1991)	Eaglebrook Plastics	Video cameras used to sort plastic containers by shape	Difficulty sorting damaged containers	Developmental
Macro	-	Plastics sorted manually	Costly - time consuming	commercialized
Micro (Dinger, 1992)	Dev Tech Laboratories	Separation of PET and PVC based on electrostatic properties	Limited Applicability	Developmental
Micro (Dinger, 1992)	Sepco and others	Froth flotation - surfactants alter plastics floating and sinking tendencies	Limited Applicability	Pre-commercialization
Micro (Kolb, 1991)	Many	Sink/ float method using separating liquids with densities in between plastics	Significant density differences needed	Commercialized
Micro (Brewer, 1990)	AKW and others	Hydrocyclones separate plastics based on densities	Significant density differences needed	Commercialized
Micro (Dinger, 1992)	University of Pittsburgh	Supercritical CO ₂ 's density can be altered by changing pressure to be between plastics	Works with density differences as little as 0.001 g/cu cm.	Developmental
Micro (Famechon, 1990)	Micronyl	Separation of PET & PVC based on size differences after successive shock crushing	Does not rely on density differences	Developmental
Micro (Modern Plastics, 1990)	Herbold	PVC(MP-380) and PET(MP-470) can be separated by melting them selectively	Limited Applicability	Developmental
Molecular or Micro (Dinger, 1992)	Rensselaer	Selective dissolution of plastics in a solvent at various temperatures	Solvent use may be expensive	Pre-commercialization

While all of the techniques have their advantages and disadvantages, the following criteria are often looked for:

1. Economic Feasibility
2. Ease of Operation
3. Broad Applicability
4. Efficiency
5. Purity of Separated Streams

1-2.2 Thermoplastic Properties and Grinding

The vast amount of literature covering comminution deals primarily with the size reduction of brittle materials. The grinding of polymers is rarely discussed in detail. However, because of the properties that make them unique, some differences in their comminution behavior is expected. Polymers can act as a glassy solid, elastic rubber, or a viscous liquid, depending on the temperature or time scale of deformation. Thus, the study of the size reduction of PVC and PET is important, not only for the development of an approach to recycling, but also to fill a void in the knowledge base of thermoplastics comminution.

Famechon (1990) has reported a process for crushing a mixture of PVC and PET particles to give selective grinding of the PVC. The PET particles are said to be larger at each stage of the operation. An Australian firm (Mapleston, 1991) has reported an impact grinding process which also accomplishes a size difference. However, the relationship between the grinding conditions and thermoplastic properties has not been defined.

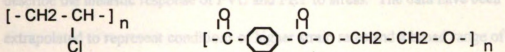
Whether a material undergoes ductile or brittle failure determines the size and shape of the comminuted particle. The brittle temperature defines the change between a brittle and a ductile failure mechanism for a thermoplastic. Ductile failure leads to long fibrils at the failure surface, higher energy-to-break, and larger particles. Brittle failure leads to lower energy-to-break and smaller particles. Table 1.2 shows the brittle temperatures for some commodity thermoplastics, as well as their ease of fracture at cryogenic conditions. PVC is listed as being easy to fracture, while PET is difficult to fracture at low temperatures. The factors that promote brittle fracture are: low temperature, high loading (impact) rate, low molecular weight, high cross-linking, low crystallinity, high glass transition temperature and low polarity (Braton, 1980; Williams, 1984). The factors which are easiest to manipulate during grinding are the polymer temperature and the impact rate. Thus, these are the process parameters that will be examined in this study to selectively grind PVC and PET to different particle sizes.

Table 1.2 Properties of Typical Consumer Waste Thermoplastics

Resin	Density (g/cm ³)	Glass Transition Temp. (C)	Fracture at Cryogenic Temp.	Brittle Temp. (C)	Crystallinity	Polarity
PP	~0.90 - 0.91	-20	Fractures	< 20	High	Low
HDPE	~0.94 - 0.97	-122	Difficult to Fracture	~ -150	High	Low
PVC	~1.32 - 1.40	75	Easy to Fracture	~ -20	Low	Polar
PET	~1.33 - 1.42	79	Difficult to Fracture	--	Inter-mediate	Polar
PS	~1.04 - 1.07	100	Fractures	~ 90	Low	Non Polar

Braton, 1980; Modern Plastics, 1994

The chemical formulas of PVC and PET are, respectively,



PVC is mainly an amorphous thermoplastic, while PET can have varying degrees of crystallinity. It is noteworthy that PVC and PET have similar glass transition temperatures, yet very different fracture behavior. Therefore, though often used, the glass transition temperature (T_g) is not a valid indicator of the brittle-ductile transition. T_g is determined by the measurement of molecular motion in a nondestructive test, while the actual brittle temperature is defined by the method of fracture. This still does not explain the behavior of PET at low temperatures. However, suggestions have been made that PET's ductile behavior in cryogenic environments may be the result of structural changes, such as strain-induced crystallization or molecular reorientation (see Yano and Yamaoka, 1995; Ward, 1983).

1-3. Objectives

The major objective of this dissertation is to identify conditions under which a mixture of PVC and PET can be selectively ground to different particle sizes. The grinding conditions will be related to the failure mechanism at the temperature and impact rate used for each thermoplastic. The subobjectives were to determine tensile, compressive and impact failure mechanism diagrams for the two homopolymers, and determine whether either of the first two diagrams could be related to the third.

Experimental data and theoretical models have been assembled in Chapter 3 to describe the inelastic response of PVC and PET to stress. The data have been extrapolated to represent conditions of higher strain rates and a broad range of temperatures in order to determine what deformation mechanism or material property could be used to estimate the behavior of PVC and PET when subjected to high speed impact processes.

In Chapter 4, classical mathematical size distribution representations were appraised for their applicability to describe thermoplastic comminution products. One function was used, along with single particle grinding tests, to examine the breakage behavior of PVC and PET. In Chapter 5, the parameters from the size distribution function were related to changes in process variables for the purpose of evaluating the size and shape differences of PVC and PET for a broad range of impact grinding conditions.

1-4. Methodology and Scope of the Study

The investigation was approached by attempting to relate the comminution process to various deformation mechanisms. Impact grinding of PVC and PET post-consumer bottle flakes was carried out in a hammer mill at various temperatures, impact rates, feed particle sizes, and grinder retaining screen sizes. The failure mechanisms were determined by noting the brittle-ductile transitions for the grinding conditions and observing the failure surfaces by scanning electron microscopy (SEM). The results were compared to those predicted by compressive and tensile deformation models. Also, high speed videotaping of the grinding chamber was done in order to gain additional breakage mechanism information.

1-5. Engineering Significance

This research project will have a direct effect on the recycling industry by providing another means for separating PET and PVC. In addition, this research may have implications in the recycling of composite materials. The controlled grinding of composite materials into distinct shape and sizes will also assist in their separation.

Valuable information needed to understand the comminution of plastics will be provided by this investigation of particle breakage patterns. By relating these patterns to particle shape, size, and comminution conditions, improvements can be made in areas ranging from scrap recovery to producing better polymer powder coatings.

Leaversuch, R., "Automated Sorting: Key to Success in Recycling," *Modern Plastics*, Nov. 1991.

Mapleston, P., "Cryogenics Improve PVC Separation," *Modern Plastics*, Nov. 1991, 32.

Modern Plastics, "PVC Melt Point Keys Scrap Separation," June 1990, 45.

Modern Plastics, "Resins and Compounds," Mid-November, 1994.

Ward, I., *Mechanical Properties of Solid Polymers*, John Wiley & Sons Ltd., New York, 1983.

Williams, J.G., *Fracture Mechanics of Polymers*, Ellis Horwood, Chichester, 1994.

Yano, O. and H. Yamacka, "Cryogenic Properties of Polymers," *Progress in Polymer Science*, 20 (1995), 585.

1-6. References

- Braton, N., *Cryogenic Recycling and Processing*, CRC Press, Boca Raton, 1980.
- Brewer, G., "Beyond PET and Milk Jug Recycling," *Resource Recycling*, Jan. 1990, 44.
- Dinger, P., "Automatic Sorting for Mixed Plastics," *Biocycle*, March 1992, 80.
- Dinger, P., "Automatic Microsorting for Mixed Plastics," *Biocycle*, April 1992, 79.
- Dreissen, H., and F. J. Fontein, "Applications of Hydrocyclones and Sieve Bends in Wet Treatment of Coal, Minerals, and Mineral Products," *SME Trans.*, March 1963.
- Famechon, R., "Separation of Waste PET and PVC for Recycling," *Patent FR2643011*, 1990.
- Kolb, K., "Method for Separating or Identifying Plastics," *Journal of Chemical Education*, 68 (1991) 348.
- Leaversuch, R., "Automated Sorting: Key to Success in Recycling," *Modern Plastics*, Nov. 1991.
- Mapleston, P., "Cryogenics Improve PVC Separation," *Modern Plastics*, Nov. 1991, 32.
- Modern Plastics*, "PVC Melt Point Keys Scrap Separation," June 1990, 15.
- Modern Plastics*, "Resins and Compounds," Mid-November, 1994.
- Ward, I., *Mechanical Properties of Solid Polymers*, John Wiley & Sons Ltd., New York 1983.
- Williams, J.G., *Fracture Mechanics of Polymers*, Ellis Horwood, Chichester, 1984.
- Yano, O. and H. Yamaoka, "Cryogenic Properties of Polymers," *Progress in Polymer Science*, 20 (1995), 585.

1-2. Size Reduction

Despite the fact that particle size reduction is a major unit operation in chemical engineering, there is not a lot of information available on how the physical properties of a material relate to the resulting shape and size of the comminuted material. The study of shape has been limited in the past due to the lack of adequate shape characterization

CHAPTER 2

SURVEY OF RELEVANT LITERATURE

2-1. Introduction

The study of the selective size reduction of poly(vinyl chloride) and poly(ethylene terephthalate) has required a review of a number of areas. An understanding of comminution in terms of fracture mechanics, modes of size reduction, material property influences, and mathematical representations were all important. Also, an awareness of how the failure mechanism of the material is related to the size reduction conditions, namely temperature and impact rate (hammer velocity), has significant relevance. A survey of other selective size reduction techniques for thermoplastics are also reviewed in this chapter.

Most available grinding data focuses on mineral processing, and very little information is available for the size reduction of plastics. Transferring grinding technology from minerals to plastics is a key issue, since mineral processing techniques are time-tested.

2-2. Size Reduction

Despite the fact that particle size reduction is a major unit operation in chemical engineering, there is not a lot of information available on how the physical properties of a material relate to the resulting shape and size of the comminuted material. The study of shape has been limited in the past due to the lack of adequate shape characterization

methods. For instance, it is still being debated whether the equipment, material type, or the reduction ratio has the biggest effect on the shape of comminuted particles. Image analyzers have opened the door to better particle shape determination and study. Particle size is usually related to grind time, feed size, method of comminution, and impact energy. The determination of what grinding conditions will give the desired size in the most energy efficient way seems to be trial and error. Tarasiewicz and Radziszewski (1990) made an attempt to bridge the gap between process parameters (such as rotation speed) and material parameters (such as tensile strength) by way of breakage energy modeling. An energy balance was done around the breakage event in terms of the elastic strain energy of the material and the energy added for breakage. This was related to constitutive equations describing the energy imparted by a ball mill rotating at various rates. Their model was not verified with experimental data, however, their study reinforces the need for better understanding of the size reduction behavior of materials. They reported that until a better relationship is established, it would be difficult to truly optimize a comminution process.

Recent experimentation investigated the relationship between the temperature and strain rate to the nature of breakage for some commercial polymers (Ahmad and Ashby, 1988). The strength of the materials were calculated using theoretical models representing brittle and ductile fracture, cold-drawing, and viscous flow. This was put in the form of diagrams summarizing mechanical response. They noted that polymers with similar structures have similar diagrams. This information will be helpful in relating the size and shape of a size reduced polymer to its brittle temperature and other properties that are

specific to polymer type. Thus, following their approach, failure mechanism diagrams have been developed for PVC and PET as a part of this research.

2-2.1 Fracture Mechanics

2-2.1.1 Nature of Breaking

In the most general sense, comminution of thermoplastics is the result of the breakage of secondary valence forces between macromolecules and chain breakage by tensile stress. Material flaws and crack propagation also affect breakage. Typically, the Griffith criterion, which defines the minimum tensile stress required for fracture, is used to describe brittle fracture. It was derived by doing an energy balance on an idealized elliptical two-dimensional flaw or crack (see Figure 2.1). The elastically stored energy within a stressed specimen was equated with the surface energy necessary to propagate the crack (Ward, 1983). The analysis gives a relationship between the tensile stress, σ_B , and the incipient crack length, $2c$, represented by :

$$\sigma_B = (2\gamma E / \pi c)^{1/2} \quad (2-1)$$

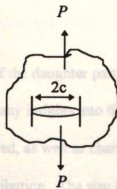


Figure 2.1 Schematic Diagram of Incipient Flaw

where E is Young's modulus, and γ is the surface free energy per unit area of surface.

Over the years, Eq. (2-1) has been transformed to

$$\sigma_B = (K_{ic}^2 / \pi c)^{1/2} \quad (2-2)$$

where K_{ic} is the critical stress intensity factor, which is a function of the load (P) and the geometry of the material. In polymers there are inherent defects that behave like the cracks described by the Griffith criteria. However, unlike other material, there is a critical flaw size below which the fracture stress is independent of the flaw size. It may be that the flaws are created by the stress. Once a critical stress around a flaw is reached, a crack can propagate at velocities of up to 40% of the speed of sound in the material (Prasher, 1987). Excess energy can lead to other cracks as well.

Prasher (1987) presents experimental work on stress patterns in poly(methyl methacrylate) (PMMA) and steel spheres to compare viscoelastic with elastic material. It was reported that, in steel, the cracks propagate around curves like onion peels, whereas in PMMA the cracks run parallel like orange slices when subject to a compressive load. The difference is mainly because of the much larger lateral tensile strain that occurs in the viscoelastic material.

2-2.1.2 Progeny Distribution

The sizes and shapes of the daughter particles (progeny distribution) from a size reduction event can provide many insights into the breakage mechanism. Catastrophic or cascade breakage can be inferred, as well as characteristic dispersion information, such as a multimodal particle size distribution. The size distribution from primary breakage is

usually bimodal or even trimodal. There are a few large pieces, and many small particles. The small particles are a result of a high concentration of stress just below the contact surface. However, continued grinding (multiple impacts) usually results in monomodal breakage, as the larger particles are more susceptible to size reduction because of the following reasons:

- larger particles have more flaws
- smaller fragments are often "hidden" by the larger particles
- smaller particles cannot store enough energy for crack propagation
- the particles are so small that plastic deformation occurs without size reduction

Therefore, for long grinding times, the size of the feed particles should not matter, as particles are reduced down to nearly the same size.

Prasher (1987) presents a case of PVC being ground in a rotary cutter at room temperature. The PVC materials had varying amounts of impact modifier (i.e. different degrees of brittleness). At low rotational speeds and high impact strengths (more ductile), the product was not only more coarse, but the resulting size distribution was bimodal. At high impact rates and low impact strengths (more brittle) the particles were smaller and more uniformly sized. This is often indicative of catastrophic breakage.

2-2.2 Impact Grinding

An understanding of the breakage mechanism of particles within the grinder is vital in order to relate low speed mechanical tests to impact grinding results. On a macroscopic

level, the main vehicle of breakage occurs when kinetic energy is transferred between the hammers and the particles. Stress waves concentrate at areas of weakness due to the particle being impacted while suspended. Lowrison (1974) reports that particles typically break immediately as opposed to just leaving residual strains for future crack propagation. The higher stress concentration is one of the reasons impact mills are commonly used to comminute soft products, because there is less deformation.

In terms of the mechano-chemistry of fracture, there is considerable debate as to the deformation mechanism polymers undergo during impact loading. In Lowrison (1974), it is reported that tensile strength is the determining parameter in particle breakage. Prasher (1987) states that impact and compression are actually the same mode of force application - just at different rates. Then, Kausch (1987) reports that deformation mechanism of impact loading is elastic compression and/or tensile deformation. All of these mechanisms will be investigated in terms of their relation to impact grinding of PVC and PET.

2-2.3 Thermoplastics

Though there are some distinct differences between the comminution behavior of brittle material and viscoelastic material, very little information is published on the latter. A thermoplastic can behave in a brittle fashion, and break without material flow, or in an elastic manner and withstand large extensions, but return to its original form after being stressed. It can also behave like a viscous liquid and deform permanently (Ward, 1983).

The fact that thermoplastic failures are deformation-controlled will affect crack propagation, stress patterns, and the responses to the deformation rate and temperature.

One important characteristic of viscoelastic material in terms of comminution is the change in deformation behavior caused by changes in deformation rate. With higher velocities, the stress is greater while the deformation is less. This is why this material is better size reduced by impact rather than by other modes of comminution. Also, plastic material requires a high amount of energy for crack propagation, and often multiple impacts are necessary before breakage occurs.

Temperature is also an important component when discussing the comminution of plastics, both on macroscopic and microscopic levels. The temperature at which size reduction takes place relates to whether deformation or fracture will occur. In addition, with the expenditure of energy for crack propagation, local heating results.

This research will investigate how these characteristics of thermoplastics will affect the usage of size distribution representations that have been established chiefly for brittle material.

One present research initiative on the size reduction of thermoplastics by Khait (1994) relates to post-consumer plastic recycling as well. This technique uses an extrusion-pulverizing process to grind commingled plastic waste by applying pressure and a shear force while rapidly cooling the plastics to temperatures between 15 and 60°C. The resulting product is used as powder feedstock for a variety of applications. The research focuses on the microstructural changes in the polymers (e.g. the recombination of macroradicals formed during comminution that leads to an *in situ* compatibilizations of

polymer blends), rather than the relationship between process parameters and product properties that is of interest to this research. However, Khait stated that the latter would be helpful in the future development of their process.

2-2.4 Predicting Particle Size and Shape

It has been a long time goal in the comminution industry to be able to predict the product of a size reduction operation from material property and process parameters. There has been very limited success. Typically, particle size distributions are represented by empirical functions. These functions range from equations based on some characteristic particle size to others based on physical properties, such as fracture initiating flaws. Prasher (1987) presents an extensive review of each type of mathematical representation.

This research will investigate the use of some of these equations to describe PVC and PET comminution. The information will be related to the failure mechanism the materials undergo at various size reduction conditions. Because thermoplastics behave different from the brittle material these models are generally used for, the validity of their use was of interest.

2-3. Failure Mechanisms

2-3.1 Types of Failure Mechanisms

2-3.1.1 Brittle and Ductile Behavior

In describing the failure mechanisms of materials in this research, the terms brittle or ductile failure will be used. Brittle failure can be defined as catastrophic fracture

without any indication of plastic deformation. Conditions of low temperature and high loading rates usually promote brittle failure. Ductile failure is characterized by yielding of the material, sometimes resulting in the appearance of a neck. Yielding is associated with temperatures above the glass transition temperature of the material. Beyond ductile failure, cold-drawing is the term used when a stabilized neck results in very large extensions of the material. Though the glass transition temperature (T_g) is often used as a reference point for brittle-ductile transitions, this is not always accurate. PET is known to exhibit ductile behavior at cryogenic temperatures, despite its T_g being around 80°C (Yano and Yamaoka, 1995). Allison (1967) noted cold-drawing of PET at temperatures as low as -50°C.

While the Griffith theory of rupture (see Eq. (2-2)) is used to describe brittle fracture, the Eyring equation is often applied to failure by yield and cold-drawing (Ward, 1971). The equation is based on the premise that yielding occurs when the internal viscosity decreases to where the applied strain rate is equal to the plastic strain rate, leading to Eq. (2-3):

$$\sigma / T = R / v \{ \Delta H / RT + \ln(2 \dot{\epsilon} / \dot{\epsilon}_0) \} \quad (2-3)$$

σ is the applied tensile stress, ΔH is the activation energy, and v is the activation volume.

2-3.1.2 Adiabatic heating

The occurrence of adiabatic heating is another aspect of interest to this research. At high loading rates, the energy is dissipated as heat at rates too high to be conducted away from the polymer. Thus, the material undergoes a localized temperature rise which

can lead to necking and cold drawing. This phenomena has been associated with PET and is used to explain its cold-drawing behavior at low temperatures (Marshall, 1954).

2-3.2 Dependence on Loading Rate, Temperature and Material Properties

A study of the relationship between the mode of failure (brittle, ductile, viscous flow) and the temperature and strain rate for various polymers was reported by Ahmad and Ashby (1988). At temperatures below about 0.8 times the glass transition temperature, brittle fracture occurs. Depending on the strain rate, ductile fracture presumably occurs above $0.8T_g$. However, there are many instances when this is not true, such as in the case of both PET and PVC. Their T_g 's are around 80°C , while the brittle temperature of PVC is around -20°C and PET does not have a clear brittle-ductile transition. Newton (1971) reported that at high impact rates polymers in the ductile region are able to absorb energy by motion, while in the brittle region there is low mobility, and therefore less energy absorption. Increasing the impact rate has a similar effect as lowering the temperature inasmuch as it encourages brittle fracture.

Shape differences between two materials might be induced by grinding if one fractured in a ductile mode and the other fractured in a brittle fashion. Also, because of the way material handles the impact energy, the breakage size should vary as the mode of fracture varies. Some other factors promoting brittle factor can be seen in Table 2.1.

Temperature and impact rate are the parameters easiest to manipulate to affect the brittle-ductile properties, and thus, the size and shape distributions of PVC and PET during impact grinding.

3-4. Table 2.2 provides some typical mechanical property values for some thermoplastics at room temperature. It is not obvious from looking at these values, how PET and PVC will respond to impact grinding. This point will become increasingly clear as this research is presented.

Table 2.1 Factors Promoting Brittle Fracture

Parameters Promoting Brittle Fracture	Effects of Additives
Low Temperature High Rate of Loading Low Molecular Weight High Cross-Linking Low Crystallinity Orientation Rings or Side Groups Short Linear-Side Chains High Glass Transition Temperature Low/No Polarity	Plasticizers Decrease Brittleness Rubbers Decrease Brittleness Inert Particles Increase Brittleness Fibers Decrease Brittleness (Glass Fibers - Dependent on Resin Type)

Braton, N. (1980); Williams, J. (1984)

Table 2.2 Mechanical Properties of Select Thermoplastics

Resin	Tensile Strength (MPa)	Tensile Modulus (GPa)	Elongation, % at break	Izod Impact Strength (J/m)
PP	33.2 - 37.9	1.1 - 1.5	100 - 600	21.6 - 324
HDPE	20.0 - 37.2	.4 - 1.2	20 - 130	43.2 - 756
PVC	37.9 - 55.2	2.4 - 2.7	2 - 80	27 - 540
PET	71.7	2.7 - 4.1	30 - 300	13.5 - 37.8
PS	41.4	2.6 - 3.2	3 - 60	10.8 - 21.6

Materials Engineering, 1992

2-4. Poly (vinyl Chloride) and Poly (ethylene Terephthalate) Separation by Grinding

The utilization of the difference in impact resistance to separate thermoplastics has gained interest in the past few years. Cryogrind Corporation (Australia) separates PVC bottle material from other plastics and paper contaminants using granulation under cryogenic conditions (Mapleston, 1991). Streams of mostly PVC particles are ground with liquid nitrogen at a temperature below -100°C . PVC particles, less than 500 microns in diameter are removed by screening from PET and other contaminants. The product is reported to be more than 99% PVC.

A French patent details the use of the differences in shock resistance of PET and PVC to obtain size differences between the two plastics. Famechon (1990) shows that successive crushing of the plastics at room temperature can be followed by sieve separation based on particle size differences. PET is said to have the larger size at each stage.

Ultron Pac Inc. (Rogers, Minnesota) uses cryogenic conditions to remove PVC from PET and HDPE (Schult, 1993). At -130°C , PET beverage-bottle and HDPE basecup flakes are hurled at a steel impact plate. Reportedly 90% of the PVC contaminate can be removed by screening.

2-5. References

Ahmad, Z. and M. Ashby, "Failure-Mechanism Maps for Engineering Polymers," *Journal of Materials Science*, 23 (1988) 2037.

Allison, S., "The Cold Drawing of Polyethylene Terephthalate," *Brit. Journal of Applied Physics*, 18 (1967) 1151.

Braton, N., *Cryogenic Recycling and Processing*, CRC Press, Boca Raton, 1980.

Famechon, R., "Separation of Waste PET and PVC for Recycling," *Patent FR2643011*, (1990).

Kausch, H., *Polymer Fracture*, Springer-Verlag, New York, 2nd ed., 1987.

Khait, K., "Novel Elastic-Deformation Grinding Process for Commingled Plastic Waste Recovery," ANTEC 94, Vol. 3 (1994) 3006.

Lowrison, G., *Crushing and Grinding*, Butterworths, Boston, 1974.

Materials Engineering, "Polymer Properties," December 1992.

Mapleston, P., "Cryogenics Improve PVC Separation," *Modern Plastics*, Nov. 1991.

Marshall, I., "The Cold Drawing of High Polymers," *Proc. Roy. Soc. London*, A221 (1954) 541.

Newton, J., "The High-Speed Impact Strength of Polymers," *Applied Polymer Symposium No. 17*, (1971) 95.

Prasher, C., *Crushing and Grinding Process Handbook*, John Wiley & Sons, Chichester 1987.

Schult, J., "Cryogenics Remove PVC From PET and HDPE Recycle," *Plastics Technology*, April. 1993.

Tarasiewicz, S. and P. Radziszewski, "Comminution Energetics," *Materials Chemistry and Physics*, 25 (1990) 1.

Ward, I., *Mechanical Properties of Solid Polymers*, John Wiley & Sons Ltd., New York 1983.

Williams, J., *Fracture Mechanics of Polymers*, Ellis Horwood, Chichester, 1984.

Yano, O. and H. Yamaoka, "Cryogenic Properties of Polymers," Progress in Polymer Science, 20 (1995), 585.

CHAPTER 3

FAILURE MECHANISM DIAGRAMS: PVC AND PET

3-1. Introduction

Ahmad and Ashby (1988) developed tensile and compressive failure mechanism diagrams for several homopolymers. Failure regions such as brittle fracture, plasticity and yielding (ductile fracture), adiabatic heating, rubbery flow, viscous flow and elastic behavior were identified. The brittle-ductile transition temperature occurred at temperatures below 0.8 times the glass transition temperature. However, the brittle temperature can be changed either by lowering the temperature of the sample, or by increasing the impact rate (Newton, 1971). Similar diagrams have been developed for PVC and PET as a part of this research to gain insight into the failure mechanisms that might occur during impact grinding. The size and shape of comminuted material is dependent on the type of failure that occurs at the grinding conditions.

It is unclear what differences a diagram for impact failure might have from one for tensile or compressive failure. Kausch (1987) has stated that the deformation mechanism for solid polymers upon grinding is compressive yielding, while that during impact loading specifically is elastic compressive and/or tensile deformation. Prasher (1987) argued that since the chief difference between impact and compression stress is the strain rate, impact failure should be similar to compressive failure. The strain rates for tensile and compression tests are typically less than 1 s^{-1} , while those of the Izod impact test are 100 s^{-1} (Kukureka and Hutchings, 1984). The strain rate for impact grinding has been

calculated to be between 10,000-20,000 s⁻¹. Thus, the failure behaviors of materials for these loading mechanisms are not expected to be the same at the same temperatures.

In this chapter the failure mechanisms of PVC and PET will be examined in terms of tensile, compressive, and impact loading. Tensile and compressive behavior have been predicted for various temperatures and strain rates utilizing theoretical equations of failure. Experimental data has been extrapolated to include conditions of very high strain rates and low temperatures for later comparison to the failure behavior seen in high speed impact grinding. It should be noted that tensile and compressive strengths are deformation properties, while impact strength is a fracture property. Thus, while they may be related, their trends are typically different (i.e. reductions in impact strengths are often associated with increases in yield strengths). Therefore, similarities in their brittle-ductile transition conditions are of primary interest. Izod and ballistics testing have also been done to study impact behavior. At the conclusion of this chapter, the β -transition temperature has been utilized to estimate brittle-ductile transitions, since the strain-rate behavior of polymers has been related to mechanical relaxations (Foot et al., 1987).

3-2. Strain Rate-Velocity Relationship

It is often helpful to define impact loading in terms of strain rates and vice versa when comparing mechanical testing and intentional mechanical degradation. Kukureka and Hutchings (1984) use the following relationship to equate the two in cases of simply-supported beams:

$$\dot{\varepsilon} = 6Dv / L^2 \quad (3-1)$$

where D is the depth of the beam, L is the span of the support points, and v is the velocity of impact. In a case of a particle being impacted by a hammer, D is the particle thickness and L is the particle length. Eq. (3-1) was used to calculate the velocities in Table 3.1.

Table 3.1 Values of Strain Rate and Velocity for Various Stress Types

Stress Type	Particle/ Specimen Thickness (mm)	Particle/ Specimen Length (mm)	Order of Magnitude of Strain Rate (s⁻¹)	Velocity (m/s)
Tensile Test	3.17	12.7	0.1	.001
Izod Impact Test	3.17	12.7	100	3.5
Impact Grinding	0.7	5.0	10,000	100
Gun Test	76.2	7.62	1,000,000	300

3-3. Tensile and Compressive Failure

Failure mechanism diagrams, based on literature data and theoretical equations for deformation and fracture, were constructed for PET and PVC. Though the diagrams are based on their possible response to tensile and compressive stresses, the data were extrapolated to conditions representative of high speed impact testing as well. Thus, the strain rates are representative of those seen in typical tensile and compressive tests, Izod

impact tests, and high speed impact grinding. The mechanism of failure is determined by which correlating equation has the lowest calculated stress.

3-3.1 Tensile Failure Mechanism Diagrams

The failure mechanisms were modeled using the following equations:

- Brittle Fracture - derived from Griffith criterion (see Ahmad, 1988)

Brittle fracture is defined by a near linear stress-strain response up to the breaking point.

$$\sigma_f = \sigma_{f,o} \left[\frac{\sigma_y}{\sigma_{y,o}} \left(1 - \alpha_m \frac{T}{T_g} \right) \right]^{1/2} \quad (3-2)$$

$\sigma_{f,o}$ and $\sigma_{y,o}$ are the fracture and yield stresses at 0°K, respectively. A negligible dependence on strain rate was assumed for $\sigma_{f,o}$ and $\sigma_{y,o}$. α_m is the temperature coefficient of the modulus estimated from literature values, using the relationship:

$$E = E_o \left(1 - \alpha_m \frac{T}{T_g} \right) \quad (3-3)$$

where E_o is the modulus, E , at 0°K.

- Plasticity - based on Eyring Theory (see Foot, 1987)

Plasticity is characterized by a drop in the stress prior to fracture, with some necking of the material.

$$\sigma_y = \frac{\kappa T}{\nu_1} \left[\frac{H_1}{RT} + \ln \left(2 \frac{\dot{\epsilon}}{\epsilon_{o1}} \right) \right] + \frac{\kappa T}{\nu_2} \sinh^{-1} \left[\left(\frac{\dot{\epsilon}}{\epsilon_{o2}} \right) \exp \left(\frac{H_2}{RT} \right) \right] \quad (3-4)$$

v is the stress activation volume, H is the activation energy, and $\dot{\epsilon}_0$ is the pre-exponential for strain rate. Subscripts 1 and 2 represent two different activated processes. Process one represents yielding at high temperatures and low strain rates, while process two is dominate for low temperatures and high strain rates. These values were obtained from literature data. $\dot{\epsilon}$ is the variable strain rate.

- Viscous Flow - (see Ahmad, 1988)

Viscous flow is distinguished by homogeneous deformation with large extensions.

$$\sigma_v = 3 \dot{\epsilon} \eta_{T_g} \exp\left[\frac{-2.303C_1(T - T_g)}{C_2 + T - T_g}\right] \quad (3-5)$$

η_{T_g} is the viscosity at the glass transition temperature, C_1 and C_2 are the WLF constants.

- Adiabatic Heating - (see Ahmad, 1988)

The local temperature rise at high loading rates when heat cannot be conducted away rapidly enough is termed adiabatic heating. This can lead to cold-drawing of polymers, where a stabilized neck results in very large extensions.

The two requirements for adiabatic heating are:

$$\sigma_d > 10C_p \rho l \dot{\epsilon} \quad (3-6)$$

$$\dot{\epsilon} > 2\alpha / l^2 \quad (3-7)$$

where C_p is the heat capacity, ρ is the density, ϵ is the strain, α is the thermal diffusivity and l is the distance from center of sample. σ_d is the drawing stress, which can be

represented by Eq. (3-4) for plastic yielding. The strain in Ineq. (3-6) can be assumed to be unity.

Figures 3.1 and 3.2 illustrate the possible failure mechanisms for PVC and PET materials in tension at various temperatures and strain rates. They were constructed using Eqs. (3-2) through (3-5), using the values in Tables 3.2 - 3.4. σ_f , σ_y , and σ_v were calculated, and the one resulting in the lowest failure strength is considered the dominant mechanism. As the temperature and strain rate changes, the dominant mechanism changes. The change from brittle failure to ductile failure is denoted in the diagrams. A summary of the brittle-ductile transition temperatures is presented in Table 3.5, with comparisons to experimental data.

The brittle-ductile transition of PET is much lower than that of PVC, which means PET will begin to exhibit ductile behavior at lower temperatures than PVC. As the strain rate is increased, the transition from brittle to ductile behavior occurs at higher temperatures.

The regions where adiabatic heating may occur were not placed in the diagrams due to the fact that from the rudimentary calculations, an adiabatic temperature rise may take place at any of the conditions where ductile failure occurs for both PVC and PET. However, adiabatic heating seems more likely to occur in PET because more plastic work must be done for failure to occur due to its higher tensile strength. The thermal properties and requirements for adiabatic heating can be seen in Tables 3.6 and 3.7, respectively.

Table 3.2 Constants for Tensile Brittle Behavior Model

Polymer	T _g (K)	α_m	$\sigma_{f,0}$ (N/m ²)	$\sigma_{y,0}$ (N/m ²)	E ₀ (N/m ²)
PVC	352	0.295 ^a	1.27x10 ⁸ ^b	1.90x10 ⁸ ^c	9.94x10 ⁹ ^a
PET	337	0.295 ^a	2.82x10 ⁸ ^b	3.69x10 ⁸ ^c	1.00x10 ¹⁰ ^e

^a Assumed.^b Estimated.^c Calculated from eq. 3-4.^d Extrapolated, using data from Polymer Handbook.^e Obtained from EDD Database.

Table 3.3 Constants for Tensile Yield Behavior Model

Polymer	v ₁ (m ³)	v ₂ (m ³)	H ₁ (J/mol)	H ₂ (J/mol)	ϵ_{01} (sec ⁻¹)	ϵ_{02} (sec ⁻¹)
PVC	3.1x10 ⁻²⁷	2.15x10 ⁻²⁷	2.95x10 ⁵	5.86x10 ⁴	1.0x10 ³⁸	2.35x10 ⁹
PET	1.21x10 ⁻²⁷	0.86x10 ⁻²⁷	1.88x10 ⁵	7.15x10 ⁴	1.28x10 ²²	1.94x10 ¹⁴

PVC data from Bauwens-Crowet et. al, 1969.

PET data from Foot et. al, 1987.

Table 3.4 Constants for Tensile Viscous Behavior Model

Polymer	η_{Tg} (N-sec/m ²)	C ₁ (K)	C ₂ (K)
PVC	1x10 ¹⁴ ^a	17.4 ^a	51.6 ^a
PET	1x10 ¹⁵ ^a	15.1 ^b	75.7 ^b

^a Assumed.^b From Duckett et. al, 1970.

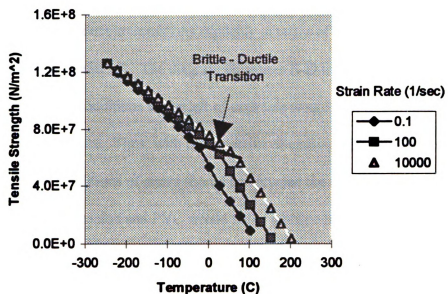


Figure 3.1 Tensile Failure Mechanism Diagram for PVC

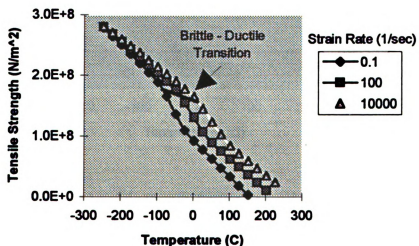


Figure 3.2 Tensile Failure Mechanism Diagram for PET

Another way of presenting the failure mechanisms of PVC and PET is by determining the brittle-ductile transitions explicitly in terms of temperature and strain rate. This has been done in Figure 3.3. The diagram illustrates B-D transition lines for which tensile deformation at conditions to the left of each line would lead to brittle fracture, and to the right, ductile failure. Thus, with the objective of causing PET and PVC to fail in different ways, the conditions of stress should lie between the two lines. In this case, PET would fail in a ductile fashion and PVC would fail in a brittle manner.

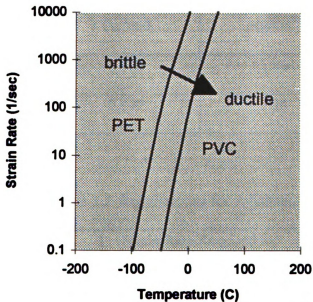


Figure 3.3 Brittle-Ductile Transition for Tensile Failure

Table 3.5 Brittle-Ductile Transition Temperatures for Tensile Failure

Strain Rates (sec^{-1})	PVC		PET	
	Predicted	Literature (Vincent, 1960)	Predicted	Literature (Foot, 1987)
0.1	-48/-23 °C	-25°C	-98/-73 °C	-80 °C
100	2/27 °C	0 °C	-48/-23 °C	-20 °C
10,000	52/77 °C	---	2/27 °C	---

Table 3.6 Thermal Properties

Material	k (W/m-K)	ρ (g/cm ³)	C_p (kJ/kg-K)
PVC	0.160	1.40	0.957
PET	0.147	1.38	1.13

Table 3.7 Requirements for Adiabatic Heating

Material	Strain Rate Required for Adiabatic Heating (sec^{-1})	Drawing Stress Required for Adiabatic Heating (N/m^2)
PVC	0.006	1.34×10^7
PET	0.005	1.56×10^7

3-3.2 Compressive Failure Mechanism

The compressive failure-mechanism behavior was modeled using Eqs. (3-8) and (3-9). Eq.(3-8) is derived from the Griffith criterion for brittle fracture (see Ahmad, 1988). Eq. (3-9) is a simplification of the Eyring theory. The mechanisms are represented as following:

- Brittle Fracture

$$\sigma_f = \sigma_{f,o} \left[\frac{\sigma_y}{\sigma_{y,o}} \left(1 - \alpha_m \frac{T}{T_g} \right) \right]^{1/2} \quad (3-8)$$

- Plasticity

$$\sigma_y = \sigma_{y,o} \left(\frac{2 + \alpha}{2} \right) \left[1 + \left(\frac{RT_g}{H} \right) \left(\frac{T}{T_g} \right) \ln \left(\frac{\dot{\epsilon}}{\dot{\epsilon}_o} \right) \right] \quad (3-9)$$

where α is the fractional difference between compressive and tensile strengths given by:

$$\alpha = 2(\sigma_c - \sigma_t) / (\sigma_c + \sigma_t) \quad (3.10)$$

σ_c and σ_t are the compressive and tensile strengths. The values of the parameters used in these equations can be seen in Tables 3.8 and 3.9. Figures 3.4 and 3.5, which illustrates the compressive failure behavior these equations predict for PVC and PET, were constructed in the same manner as the tensile failure diagrams.

For compressive failure, the brittle-ductile transitions for PET are slightly higher than for PVC, implying that PET will still exhibit brittle behavior at temperatures where

PVC will begin to act in a ductile fashion. This is the opposite of what the tensile diagrams illustrated. Also, the brittle-ductile transitions occur at much higher temperature for compressive failure.

Table 3.8 Constants for Compressive Brittle Behavior Model

Polymer	T _g (K)	α_m	$\sigma_{f,o}$ (N/m ²)	$\sigma_{y,o}$ (N/m ²)	E _o (N/m ²)
PVC	352	0.295 ^a	1.27x10 ^{8^b}	1.90x10 ^{8^c}	9.94x10 ^{9^d}
PET	337	0.295 ^a	2.82x10 ^{8^b}	3.69x10 ^{8^c}	1.00x10 ^{10^e}

^a Assumed.

^b Estimated.

^c Calculated from eqn. 3.

^d Extrapolated, using data from Polymer Handbook.

^e Obtained from EDD Database.

Table 3.9 Constants for Compressive Yield Behavior Model

Polymer	σ_c (N/m ²) ^a	σ_t (N/m ²) ^a	H (J/mol)	ϵ_o (sec ⁻¹)
PVC	5.52x10 ⁷	4.07x10 ⁷	2.95x10 ⁵	1.0x10 ⁻³⁸
PET	7.58x10 ⁷	4.83x10 ⁷	1.88x10 ⁵	1.28x10 ⁻²²

^a Modern Plastics, Encyclopedia 1993.

PVC data from Bauwens-Crowet et. al, 1969.

PET data from Foot et. al, 1987.

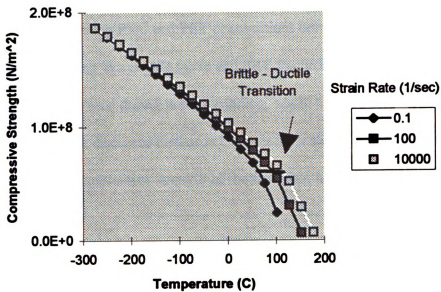


Figure 3.4 Compressive Failure Mechanism Diagram for PVC

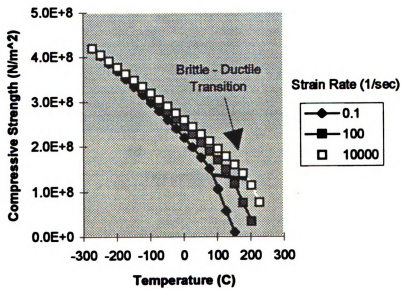


Figure 3.5 Compressive Failure Mechanism Diagram for PET

Figure 3.6 represents the brittle-ductile transition in terms of strain rate and temperature only. Deforming PVC and PET at conditions between the B-D line of each would result in PVC failing in a ductile mode and PET fracturing in a brittle fashion. This is the opposite of what is seen during impact grinding, which has a strain rate of about $10,000 \text{ sec}^{-1}$. This will be discussed further in Chapter 5. It should be noted that Figure 3.6 is a function of the compressive strength of the materials, though that cannot be seen explicitly.

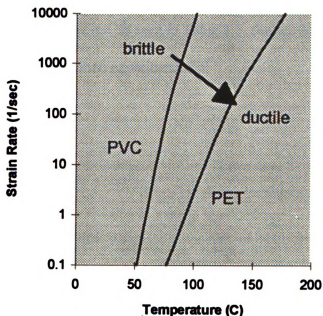


Figure 3.6 Brittle-Ductile Transition for Compressive Failure

3-3.3 Sensitivity Analysis of Model Coefficients on Brittle-Ductile Transition

Data are not readily available over the range of temperatures that were needed for the failure mechanism models. Thus, many estimations were made. In order to assess possible errors introduced by these estimations, the effect of a 20 % change in the material property values on the tensile strength and brittle-ductile transition were evaluated. This sensitivity analysis reveals that the values of σ_{f0} and σ_{y0} have the greatest effect on the failure strengths and brittle-ductile transitions calculated. Tables 3.10 and 3.11 summarize the influence of these coefficients on the material response.

The failure strength of PVC is more sensitive to error than PET, but both are significantly affected. However, as seen in Table 3.5, the brittle-ductile transitions were fairly close to those determined experimentally.

Table 3.10 Sensitivity of Tensile Failure Strength to Model Coefficients

Parameter	Effect on σ	Effect on Brittle-Ductile Transition	Example: 20% increase in Parameter
σ_{fo}	$\Delta\sigma \propto \Delta\sigma_{fo}$	An increase decreases transition temperature	Decreases transition by as much as 75° for PET and 200° for PVC
σ_{yo}	$\Delta\sigma \propto 1 / \sqrt{\Delta\sigma_{yo}}$	An increase increases transition temperature	Increases transition by as much as 25° for PET and 50° for PVC

Table 3.11 Sensitivity of Compressive Failure Strength to Model Parameters

Parameter	Effect on σ	Effect on Brittle-Ductile Transition	Example: 20% increase in Parameter
σ_{fo}	$\Delta\sigma \propto \Delta\sigma_{fo}$	An increase decreases transition temperature	Decreases transition by as much as 25° for PET and 75° for PVC
σ_{yo}	$\Delta\sigma \neq f(\Delta\sigma_{yo})$ in brittle region; $\Delta\sigma \propto \Delta\sigma_{yo}$ in ductile region	An increase increases transition temperature	Increases transition by as much as 25°

3-4. Izod Impact Failure

3-4.1 Materials

Poly(ethylene terephthalate) post-consumer bottle flakes were utilized for these experiments. The flakes were dried and then injection molded at about 260°C into impact specimens for the Izod impact tests. The poly(vinyl chloride) impact specimens were injection molded at about 185°C from general purpose GEON PVC containing 25% recycled content. The specimens had a width of 12.7 mm (0.5 in.), a length of 63.5 mm (2.5 in.), and a thickness of 3.17 mm (0.125 in.).

3-4.2 Izod Impact Testing

A notch cutter (Testing Machine Inc., Model TMI 22-05) was used to produce the indented impact site on the samples. The samples were impacted on an Izod impactor (Testing Machines Inc., Model 43-02). A 10 lb. pendulum was used for the PVC samples, while a 1 lb. pendulum was used for the PET samples. The fracture surfaces were evaluated using a JEOL T-330 Scanning Electron Microscope (SEM) to obtain fracture mechanism information.

The impact testing was conducted according to ASTM-D256 standard test for impact resistance. The Izod apparatus is illustrated in Figure 3.7. The desired test temperatures were obtained by placing the samples in a Nalgene Dewar containing a heat-transfer media for 3 minutes. The temperature was adjusted by placing dry ice in a methanol bath below room temperature and an immersion heater in a water bath above room temperature. A temperature range from -40°C to 80°C was used.

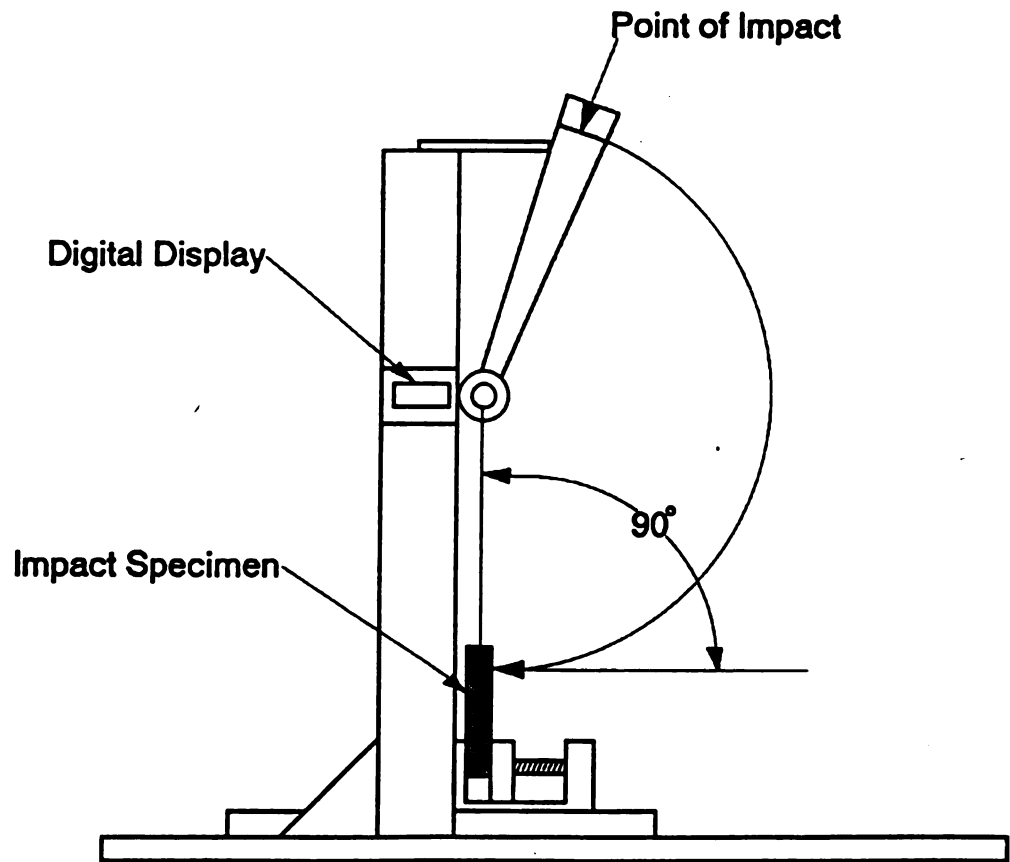


Figure 3.7 Schematic of Izod Apparatus

3-4.3 Limitations

Though the testing was done as quickly as possible, the temperature of the test specimens may not be exactly as recorded at the time of the tests.

3-4.4 Results and Discussion

Poly(vinyl Chloride). The data for the Izod impact strength versus testing temperature are shown in Figure 3.8 (see tabular data in Appendix A). The amount of energy required to break a PVC test specimen varies widely with temperature. At temperatures less than -10°C , the impact strengths were low and were all less than 27 J/m. Photomicrographs of the fracture surface showed characteristics typical of brittle fracture. Figure 3.9 a and b show the surface for samples tested at -40°C . The lower magnification (Fig. 3.9a; x 50) shows a sharp fracture edge, and no obvious necking at higher magnifications (Fig 3.9b: x 1000). Both observations are consistent with brittle fracture.

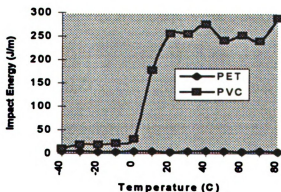


Figure 3.8 Izod Impact Strength for PVC and PET at Various Temperatures

There is a step change in PVC Izod impact strength over the temperature range, $0\text{ }^{\circ}\text{C} < T < 20\text{ }^{\circ}\text{C}$. The impact energy increases by an order of magnitude. Inspection of the samples for PVC specimens above $0\text{ }^{\circ}\text{C}$ showed that only partial breaks occurred. Fracture surfaces were whitish in color from deformation during impact, which is consistent with a ductile failure mechanism. Photomicrographs taken for samples tested at 0 , 20 and $80\text{ }^{\circ}\text{C}$ all showed ductile fracture. Figure 3.10 a and b ($20\text{ }^{\circ}\text{C}$) show obvious necking at low and high magnifications. The circular depressions in Fig. 3.10a are similar in size to PVC suspension macroparticles. At temperature above $20\text{ }^{\circ}\text{C}$, the Izod impact strength is independent of temperature and ductile failure occurs.

Poly(ethylene Terephthalate). The PET impact test specimens all break via a brittle fracture mechanism over this temperature range. Photomicrographs of fracture surfaces taken over the entire range were all quite similar (Figure 3.11 a and b), showing no obvious necking even at high magnification.

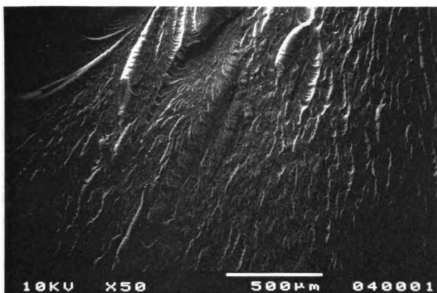


Figure 3.9a SEM (x 50) of PVC Izod Test Specimen Impacted at -40°C

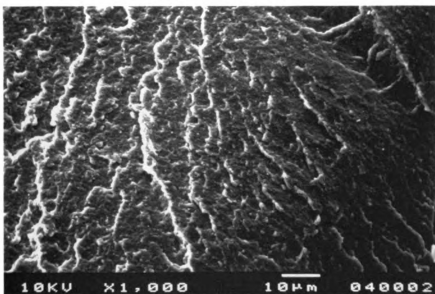


Figure 3.9b SEM (x 1,000) of PVC Izod Test Specimen Impacted at -40°C

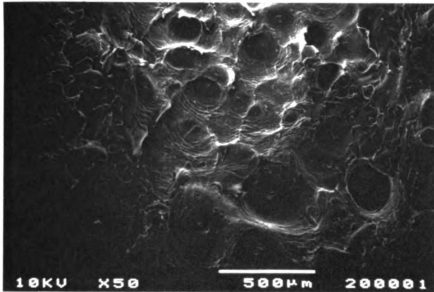


Figure 3.10a SEM (x50) of PVC Izod Test Specimen Impacted at 20°C

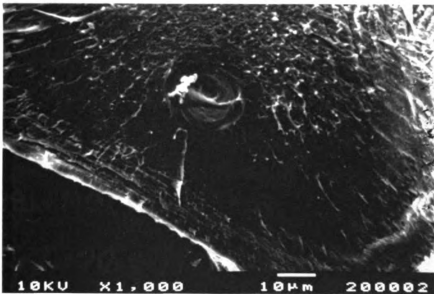


Figure 3.10a SEM (x1,000) of PVC Izod Test Specimen Impacted at 20°C

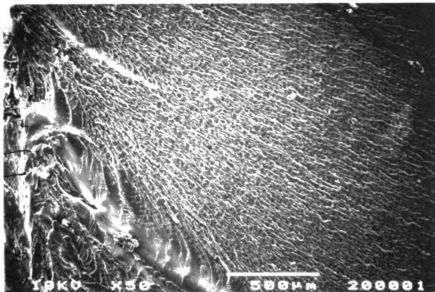


Figure 3.11a SEM (x50) of PET Izod Test Specimen Impacted at 20°C

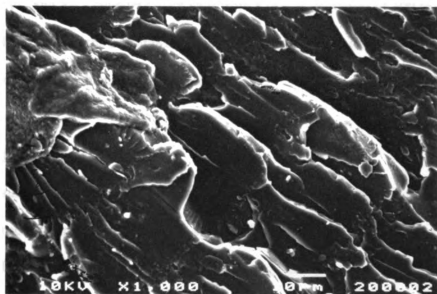


Figure 3.11a SEM (x1,000) of PET Izod Test Specimen Impacted at 20°C

3-5. High Speed Ballistics

The velocities of impact for Izod impact testing are much smaller than those seen during impact grinding. For Izod testing, the specimens are impacted at 3.4 m/s compared with nearly 100 m/s during impact grinding. Therefore, ballistics testing was done at room temperature in order to evaluate the impact failure mechanisms at higher speeds.

3-5.1 Materials

PET and PVC material molded into 9.53 mm (.375 in) diameter rods were cut to lengths of 38.1 mm (1.5 in.), 57.15 mm (2.25 in.), and 76.2 mm (3 in.) and used as projectiles.

3-5.2 Ballistics Testing

The PVC and PET cylinders were shot from a gun at velocities of 300 to 600 m/s into a wall. The final lengths and appearances of the samples were noted. SEM was used to observe the failure mechanism of the materials.

3-5.3 Results and Discussion

The failure mechanisms of PVC and PET were the same as observed for Izod impacting at room temperature. The PVC samples deformed and decreased in length, while the PET samples shattered. The SEM photographs in Figures 3.12 and 3.13 depict the yielding of the PVC material, and the brittle fractured surface of the PET material.

The PVC material flowed, as if stretched, while the PET material has blunt edges, from stable crack propagation.



Figure 3.12 SEM of PVC Ballistics Sample Impacted at 398 m/s

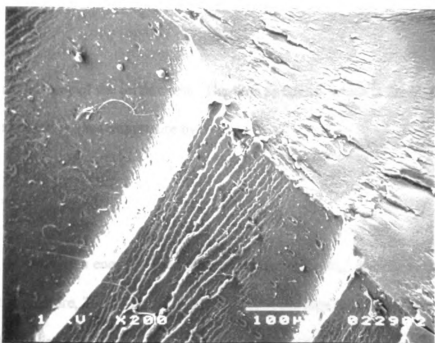


Figure 3.13 SEM of PET Ballistics Sample Impacted at 369 m/s

3-6. Impact Transition Temperature Estimations from β -Relaxation Process

As the temperature of a polymer is lowered, various molecular motions (or relaxations) occur. The secondary relaxation, known as the β -relaxation process, and its corresponding temperature, T_β , have been related to transitions that are observed in impact behavior with changes in loading rate and temperature (Foot et al., 1987; Yano and Yamaoka, 1995). The β -relaxation temperature occurs at the secondary peak, below that of the glass transition temperature, and is associated with the motion of polymer side-groups. This process is evaluated by determining the dynamic mechanical responses at various temperatures using a free oscillating torsion pendulum. A method for estimating the brittle-ductile transition using the β -relaxation temperature as a function of the time to failure and temperature has been presented by Menges and Boden (1986). The time to failure is give as

$$t_f = 1/(2\pi f) \quad (3-11)$$

where f is the frequency of the torsion test. The time to failure, which is the inverse of the strain rate, is related to the temperature by

$$t_{ref} = t_o e^{\frac{\Delta U}{RT_{ref}}} \quad (3-12)$$

where ΔU is the activation energy. The reference temperature, T_{ref} , was chosen to be the β -transition temperature, T_β , at 1 Hz. The variable t_{ref} is the time to failure at T_β . Values for T_β and ΔU are listed in Table 3.12. To determine the B-D transitions, the time

constant, t_0 , was calculated for T_β and a strain rate of 0.160 sec^{-1} (1 Hz). Eq.(2-12) was rearranged to calculate the β -temperatures for a range of times to failure.

Table 3.12 β -relaxation Temperature and Activation Energy

Material	T_β at 1 Hz (K)	ΔU (kJ/mol)	t_0 (sec)
PVC	218 ^a	54.4 ^a	1.46×10^{-14}
PET	200 ^b	71.5 ^c	3.39×10^{-20}

^aMenges

^bArmeniades

^cFoot

Figure 3.14 illustrates the brittle-ductile transition for PVC and PET as predicted by the β -relaxation temperature in terms of the time to failure. The region of brittle fracture is to the right of the transition line. The estimates for the B-D transitions for PVC are -80 and -35°C for times to failure equivalent to those for tensile and Izod testing, respectively, while those for PET were -85 and -60°C . According to these values, PET will begin to exhibit ductile behavior at lower temperature than PVC. At a time to failure of 1×10^{-4} sec., which is comparable to the time scale for impact grinding, the B-D transition for PVC is estimated to be about 12°C for PVC and -35°C for PET. Figure 3.15 is a replot of Figure 3.14 in terms of the strain rate. It can be easily compared to the tensile and compressive B-D transition diagrams presented earlier in this chapter. This information will be referred to in Chapter 5.

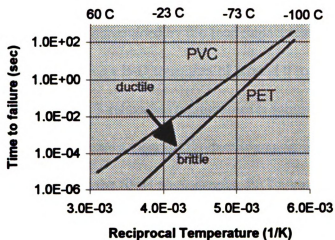


Figure 3.14 Brittle-Ductile Transition Predicted by β -relaxation Temperature

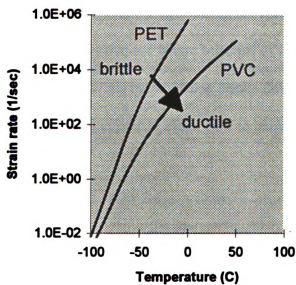


Figure 3.15 Brittle-Ductile Transition Based on the β -Temperature in Terms of Strain-Rate

3-7. Conclusions

The values for the brittle-ductile transition temperatures as estimated by the tensile failure diagrams and that determined by the Izod impact test are in agreement for PVC, but not for PET. Both give a B-D transition of around 0 to 20°C for PVC. The value predicted for PVC by the β -relaxation temperature is somewhat lower than observed. PET does not appear to have a clear brittle-ductile transition for the range of temperatures tested by Izod impact. In the SEM photographs, PET appears to be consistently brittle, while the tensile theoretical failure diagrams and β -relaxation process predict PET to be ductile for these temperatures. Ballistics tests also indicate brittle behavior for PET at room temperature.

The brittle behavior of PET specimens in Izod and ballistics tests at room temperature may be due to property changes during the specimen molding process. Another possible explanation is that the failure behavior of PET is too complex to be modeled by one mechanism. While extrapolating tensile failure models seemingly works for PVC, very high strain rates appear to cause PET to behave in an unexpected manner.

3-8. References

Ahmad, Z. and M. Ashby, *Journal of Materials Science*, **23** (1988) 2037.

Armeniades, C. and I. Kuriyama, "Mechanical Behavior of Poly(ethylene terephthalate) at Cryogenic Temperatures," in Serafini, T. and J. Koenig, ed. *Cryogenic Properties of Polymers*, Marcel Dekker, Inc., New York, 1968.

Bauwens-Crowet, C., Bauwens, J.C. and G. Homes, *Journal of Polymer Science: Part A-2*, **7** (1969) 735.

Duckett, R.A., Rabinowitz, S., and I.M. Ward, *Journal of Materials Science*, **5** (1970) 909.

Foot, J.S., Truss, R.W., Ward, I.M., and R.A. Duckett, *Journal of Materials Science*, **22** (1987) 1437.

GE Plastics, Engineering Design Database, 1992.

Kausch, H., *Polymer Fracture*, Springer-Verlag, Berlin, 1987.

Kukureka, S.N., and I.M. Hutchings, *International Journal of Mechanical Science*, **26** (11/12), (1984), 617.

Menges, G. and H. Boden, "Deformation and Failure of Thermoplastics on Impact," in Brostow, W. and R. Corneliussen, ed. *Failure of Plastics*, New York, 1986.

Modern Plastics Encyclopedia '93, Mid-December. 1992.

Newton, J., "The High-Speed Impact Strength of Polymers," *Applied Polymer Symposium No. 17*, (1971) 95.

Prasher, C.L., *Crushing and Grinding Process Handbook*, Wiley, New York, 1987.

Yano, O. and H. Yamaoka, "Cryogenic Properties of Polymers," *Progress in Polymer Science*, **20** (1995), 585.

CHAPTER 4

IMPACT GRINDING OF THERMOPLASTICS: SIZE DISTRIBUTION FUNCTION MODEL

4-1 Introduction

It has long been a goal of the comminution industry to be able to predict product particle size distributions. Various mathematical functions have been modified to model comminution results with some success. However, it is unclear how well these functions would describe the breakage of thermoplastics, due to their dependence on breakage mechanism.

It is the objective of this chapter to develop and demonstrate empirical breakage mechanisms and models for impact grinding of plastics. Results from multiple and single particle breakage in a hammer mill will be utilized. This information will assist in bridging the gap between material properties and process parameters and their relationship to comminution results.

4-2. Experimental

PET and PVC chipped bottles (typically 80 grams) were ground in a laboratory hammer mill at temperatures ranging from -196°C to room temperature. The bottle flakes were soaked in liquid nitrogen prior to grinding and liquid nitrogen was also added continuously into the grinding chamber, for the low temperatures. The temperature of the grinding chamber was measured using a thermocouple probe. Temperatures are reported

in terms of the mill outlet temperature (M.O.T), and not necessarily the exact temperature of the flakes. The impact rate of grinding was varied from 53 m/s (8,000 RPM) to 93 m/s (14,000 RPM) by changing pulleys controlling the hammers. The particle size distributions of the ground particles were determined by sieving. Most of the grinding results are the average of eight replicated experiments. The tabular data are in Appendix B.

4-2.1 Materials

Post-consumer PET and PVC bottle flakes were used. The characteristic size of the PET and PVC flakes were 4.6 and 7.4 mm, respectively.

4-2.2 Hammer Mill

A laboratory hammer mill was used for grinding the particles. The model CF Bantam Mikro-Pulverizer (Micron Powder Systems) contains six swing hammers on a rotor disc. The grinding chamber is 130 mm in diameter. The maximum speed is 14,000 RPM (93.2 m/s). A retaining screen size of 3.175 mm was used for these experiments. A schematic of the equipment can be seen in Figures 4.1.

4-2.3 Particle Size Determination

A series of Tyler sieves ranging from 212 μm to 8 mm (70 - 2 1/2 Mesh) was used to determine the particle size distributions (PSD). The set of sieves were subjected to a sieve shaker for size classification.

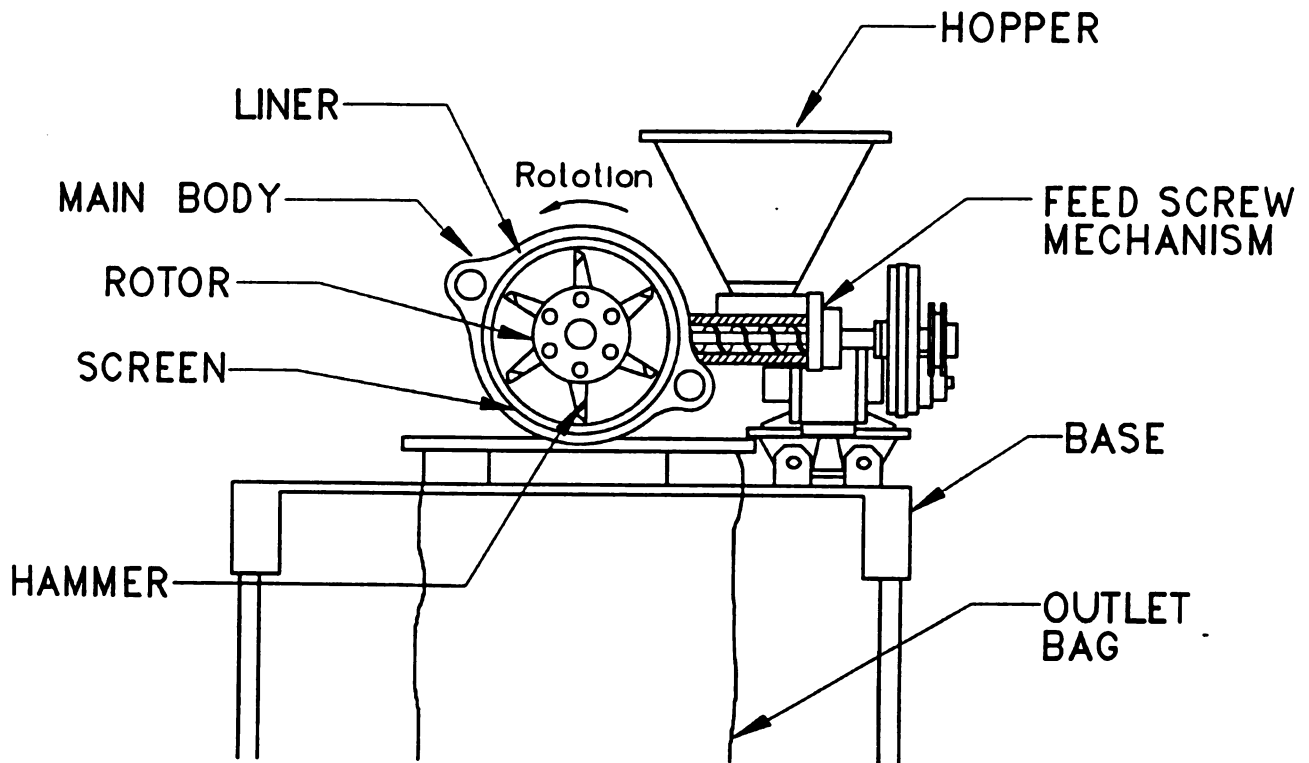


Figure 4.1 Schematic of Hammer Mill

4-2.4 Optical Microscopy

An optical microscope (Olympus BH-2) was used to examine the surface structure of ground particles. This was done to gain insight into the breakage mechanism of PVC and PET. Surface magnifications of 50 x were photographed.

4-2.5 Limitations

The collection of particle fines is often difficult. Though only a small amount of fines is typically lost, this can affect the data's representation by empirical models.

4.3. Results and Discussion

4.3.1. Empirical Breakage Models

Four mathematical functions were examined for their usefulness in describing PVC and PET breakage in an impact grinder. The models were fitted to the data by the least-squares method. The data are tabulated in Appendix B. Because sieves were used to determine the particle size distributions and the number of particles per impact were low, cumulative particle size distributions were used to interpret the results.

The following cumulative size distribution representations were used (see Prasher, 1987):

-Rosin-Rammler-Bennett

$$F(l) = 1 - e^{-(l/L_{50})^n \ln(5)} \quad (4-1)$$

-Gaudin-Schuhmann

$$F(l) = (l/L_{100})^n \quad (4-2)$$

-Broadbent-Callcott

$$F(l) = \frac{1 - e^{-l/L_{100}}}{1 - e^{-1}} \quad (4-3)$$

-Gaudin-Meloy

$$F(l) = 1 - (1 - l/L_{100})^n \quad (4-4)$$

where l is the particle size, and n is a power exponent sometimes referred to as the uniformity index. Small values of n mean the distribution is broad, while large values of n signify uniform-sized particles. L_{80} and L_{100} represent, respectively, the characteristic size for which 80% and 100% of the particles are smaller. The equations are bound by the lower limit $F(l) = 0$ at $l=0$, and $F(l)=1$ at $l=L_{100}$.

It should be noted that Eq. (4-1) is a modification of the Rosin-Rammler-Bennett function. The equation presented here has been altered for use with a characteristic size based on 80% passing rather than the original 63.2% passing. The reason for this choice will be discussed in the next section.

In Figures 4.2 and 4.3, it can be seen that each function fits the data with varying success. Coefficient values were determined by minimizing the error between the data and the models. This was done using the Solver program by Microsoft Excel. The values of the coefficients for PVC and PET can be seen in Tables 3.1 and 3.2. The Rosin-Rammler-Bennett gives the best overall fit. However, the Gaudin-Meloy and the Gaudin-Schumann functions give a better fit for the fines.

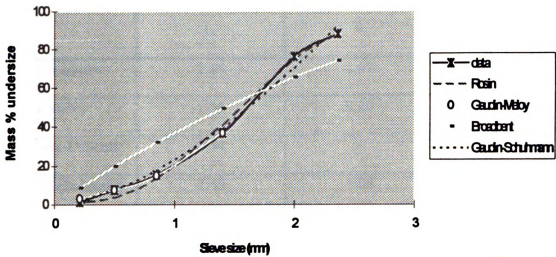


Figure 4.2 Comparison of Cumulative Size Distribution Functions Modeling Multiple Particle Breakage of PVC Particles

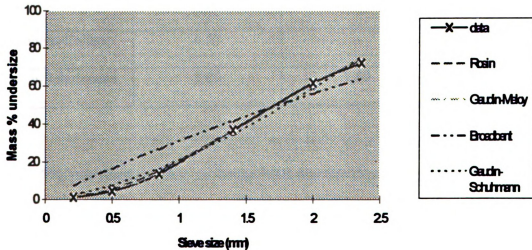


Figure 4.3 Comparison of Cumulative Size Distribution Functions Modeling Multiple Particle Breakage of PET Particles

Table 4.1 Coefficients for Cumulative Size Distribution Models for PVC

Model	Characteristic Size, L_i	Uniformity Index, n	Error Sum of Squares
Rosin-Rammler-Bennett	2.14	2.67	42.8
Gaudin-Meloy	1.56	0.20	2.92
Broadbent-Callcott	3.74	-	955.78
Gaudin-Schuhmann	2.48	1.64	59.93

Table 4.2 Coefficients for Cumulative Size Distribution Models for PET

Model	Characteristic Size, L_i	Uniformity Index, n	Error Sum of Squares
Rosin-Rammler-Bennett	2.60	2.07	4.18
Gaudin-Meloy	1.47	0.15	6.04
Broadbent-Callcott	4.63	-	472
Gaudin-Schuhmann	2.86	1.50	39.57

The two fitted coefficients for the RRB function describe the data well. The standard deviations of replicated data for L_{90} are 0.07 and 0.12 for PVC and PET, respectively. The standard deviations for n are 0.35 for PVC, and 0.21 for PET.

4.3.2 Characteristic Particle Size

The various mathematical models utilize different characteristic particle lengths. The most common are L_{50} , $L_{63.2}$, L_{80} , and L_{100} , with the subscripts representing the percentage of particles under the sieve size denoted by L_i . Although L_{80} is generally thought to better characterize a particle size distribution (Lowrison, 1974), most values are chosen out of convenience or by default from the mathematical function employed. In using the appropriate variations of the Rosin-Rammler-Bennett equation, the same fit is obtained for either L_{50} , $L_{63.2}$, or L_{80} . This is not surprising inasmuch as the particle size distributions are self-similar (Prasher, 1987). Thus, there exists a transformation between each of the RRB modifications because the characteristic lengths are proportional to one another. Eqs. (4-5) and (4-6) represent RRB when $L_{63.2}$ and L_{50} are used.

$$F(l) = 1 - e^{-(l/L_{63.2})^n} \quad (4-5)$$

$$F(l) = 1 - e^{-(l/L_{50})^n \ln(2)} \quad (4-6)$$

When the cumulative distribution is plotted logarithmically (see Figure 4.4) a nearly straight line is obtained up to 80%. This observation partially motivates the arbitrary selection of L_{80} as a characteristic size parameter.

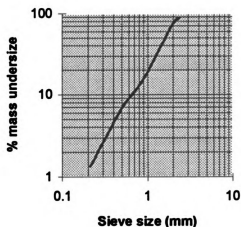


Figure 4.4 Cumulative Size Distribution of PVC Ground in a Hammer mill

4-3.3 Particle Breakage Mechanism

Progeny particles from single particle grinding experiments and density distributions determined from multiple particle testing were analyzed to obtain information about the breakage mechanisms for PVC and PET. The results are sometimes discussed in terms of coarse or fine particles, meaning particle sizes of 1-10 mm or 0.1-1 mm, respectively. Monomodal and multimodal behavior has been identified. Also, evidence suggesting catastrophic (i.e. an impact producing many fine particles) vs. cascade (i.e. repeated impacts needed to reduce particle to screen size) breakage is examined.

4-3.3.1 Single Particle Grinding

Single post-consumer bottle flakes, roughly 6 mm in length, were subjected to impact grinding in order to gain information about the progeny particles. The impact rate

of grinding was controlled by varying the rotation rate of the mill. Single particles were dropped directly into the grinding chamber. At the lowest impact rate of 53.3 m/s, the progeny PVC particles were made up of a few (~6) nearly equally sized coarse particles and some fines (Figure 4.5). At 93.2 m/s the fragments were made up of a few coarse pieces and quite a few fines (Figure 4.6). Grinding done at a M.O.T. of 0°C (feed conditions typically below -196°C) and a rotational speed of 93.2 m/s resulted in mostly midsize to fine particles (Figure 4.7). Single particle tests for PET produced a few (~6) coarse particles at room temperature and 53.3 m/s (Figure 4.8). At 93.2 m/s the PSD is broad, but is made up of mostly a number of larger particle (Figure 4.9). A liquid nitrogen soaked PET particle broke into quite a few coarse and fine particles (Figure 4.10).

As the impact rate is increased and the temperature decreased, the PVC particles ground to smaller and more uniform sizes. This seems to infer that the breakage mechanism changes from being cascade to catastrophic. The results for PET are different in that at low temperatures and high impact rates, the size of the ground particles are still comparatively large, though there are more fines. Cascade breakage may be occurring at these conditions.

Examination by optical microscopy of PVC and PET particles ground at 93 m/s and a M.O.T. of 0°C, gives further clues about the breakage mechanism. In Figure 4.11, PVC appears to break perpendicular to the bottle surface. The edges are blunt. However, PET seems to craze throughout the sample (see Figure 4.12). This seems to give credence to catastrophic break for PVC and cascade breakage for PET at low temperatures.



Figure 4.5 Progeny PVC Particles from Single Particle Impact at 53.3 m/s and 22°C:
3.175 mm Retaining Screen, Magnification x 5.8



Figure 4.6 Progeny PVC Particles from Single Particle Impact at 92.3 m/s and 22°C:
3.175 mm Retaining Screen, Magnification x 5.8



**Figure 4.7 Progeny PVC Particles from Single Particle Impact at 92.3 m/s and 0°C
M.O.T.: -196°C Feed Temperature, 3.175 mm Retaining Screen, Magnification x 5.8**



**Figure 4.8 Progeny PET Particles from Single Particle Impact at 53.3 m/s and 22°C:
3.175 mm Retaining Screen, Magnification x 5.8**



**Figure 4.9 Progeny PET Particles from Single Particle Impact at 92.3 m/s and 22°C:
3.175 mm Retaining Screen, Magnification x 5.8**

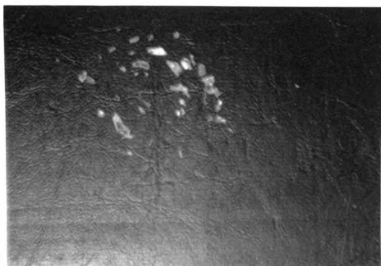


**Figure 4.10 Progeny PET Particles from Single Particle Impact at 92.3 m/s and 0°C
M.O.T. : -196°C Feed Temperature, 3.175 mm Retaining Screen, Magnification x 5.8**



Figure 4.11 Optical Microscopy Photograph of PVC Particle Ground at 92.3 m/s and 0°C
M.O.T.: -196°C Feed Temperature, 3.175 mm Retaining Screen, Magnification x 50

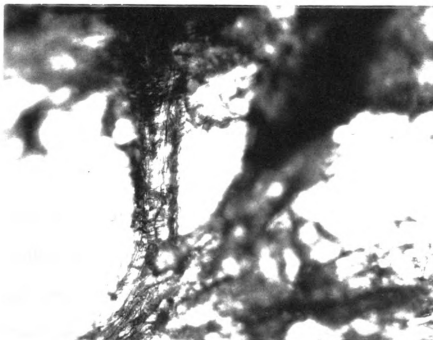


Figure 4.12 Optical Microscopy Photograph of PET Particle Ground at 92.3 m/s and 0°C
M.O.T.: -196°C Feed Temperature, 3.175 mm Retaining Screen, Magnification x 50

4-3.3.2 Density Distributions

One method for determining changes in breakage mechanism is to observe density (or differential) distributions. Density distributions are the derivatives of cumulative distributions. They offer the advantage of revealing multimodal behavior. Thus, information about the number and size of progeny particles from multiple particle impact grinding can be obtained. This information should correlate with what is seen in single particle testing.

PVC and PET flakes were ground at impact rates of 53 and 93 m/s and at room temperature and a M.O.T. of 0°C (feed temperature below -196°C, see Section 4-2). The resulting size distributions were arranged in the form of the change in % mass undersize divided by the change in the representative sieve sizes. PVC exhibits bimodal characteristics and coarser particles at room temperature for impact rates of 53.3 and 93.2 m/s, though at the higher impact rate there is a decrease in the bimodal component (see Figures 4.13 and 4.14). At a M.O.T. of 0°C, the PVC density distribution is monomodal (Figure 4.15). The narrowness of the peak suggests a more uniform distribution, and possibly catastrophic failure. In Figures 4.16 - 4.18, PET appears to exhibit monomodal breakage at room temperature, but is slightly bimodal, with finer particles at 0°C. This bimodal distribution may be the result of cascade breakage or PET may be exhibiting both ductile and brittle behaviors, leading to both fine and coarse size particles.

Though these density plots are based on actual data, it is interesting to note that of the PSD functions presented at the beginning of this chapter, only the RRB equation gives a differential distribution which represents the data.

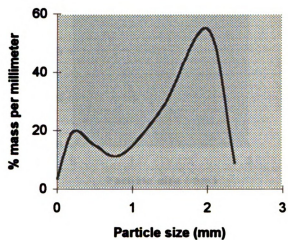


Figure 4.13 Density Distribution for Multiple Particle Breakage of PVC at 53.3 m/s and 22°C: 3.175 mm Retaining Screen

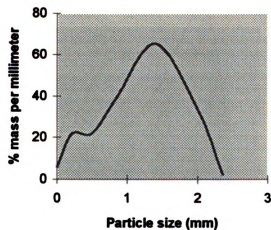


Figure 4.14 Density Distribution for Multiple Particle Breakage of PVC at 93.2 m/s and 22°C: 3.175 mm Retaining Screen

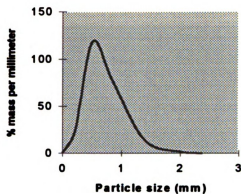


Figure 4.15 Density Distribution for Multiple Particle Breakage of PVC at 93.2 m/s and 0°C M.O.T.: -196°C Feed Temperature, 3.175 mm Retaining Screen

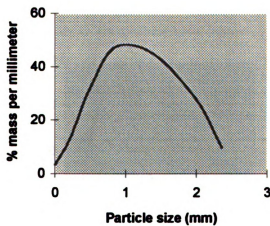


Figure 4.16 Density Distribution for Multiple Particle Breakage of PET at 53.3 m/s and 22°C: 3.175 mm Retaining Screen

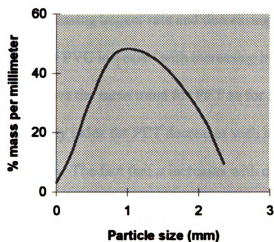


Figure 4.17 Density Distribution for Multiple Particle Breakage of PET at 93.2 m/s and 22°C: 3.175 mm Retaining Screen

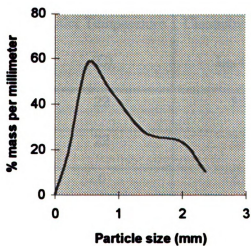


Figure 4.18 Density Distribution for Multiple Particle Breakage of PET at 93.2 m/s and 0°C M.O.T.: -196°C Feed Temperature, 3.175 mm Retaining Screen

The coefficients for the RRB equation representing each condition given in the density distributions are presented in Tables 4.3 and 4.4 for PVC and PET, respectively. L_{80} decreases with increasing impact rate and decreasing temperature for PVC. The uniformity index, n , for PVC increases with increasing impact rate and decreasing temperature. L_{80} follows the same trend for PET as for PVC except to a smaller extent. However, the uniformity index for PET decreases with increasing impact rate and decreasing temperature. The fact that n increases with decreasing temperature and increasing impact rate for PVC, by definition, means the distribution is more uniform, again suggesting a change toward catastrophic failure. By the same logic, since n decreases for PET for these conditions, the distribution is becoming increasingly scattered, implying multiple breakage mechanisms. Thus, the behavior for PET at low temperatures is quite different from that of PVC.

Table 4.3 Effects of Temperature and Impact Rate on PVC Comminution

Impact Rate (m/s)	Outlet Temperature (C)	Characteristic Size, L_{80} (mm)	Uniformity Index, n
53.3	22	3.12	2.52
93.2	22	2.14	2.67
93.2	0	1.17	3.25

Table 4.4 Effects of Temperature and Impact Rate on PET Comminution

Impact Rate (m/s)	Outlet Temperature (C)	Characteristic Size, L_{90} (mm)	Uniformity Index, n
53.3	22	2.67	2.89
93.2	22	2.57	2.09
93.2	0	2.41	1.68

4-4. Conclusions

The Rosin-Rammler-Bennett equation adequately models PVC and PET behavior over the entire range of the cumulative size distribution. The two fitted coefficients, L_{90} and n , describe the data well. The breakage mechanism for multiple particle size reduction agree with what is seen in single particle breakage. PVC breaks in a bimodal fashion at room temperature, and in a monomodal fashion at low temperatures. The breakage behavior of PET is the reverse. Grinding at low temperatures and/or high impact rates appears to cause PVC flakes to break catastrophically, while the breakage pattern for PET seems to be both catastrophic and cascade at those conditions.

4-5. References

Lowrison, G., *Crushing and Grinding*, Butterworths, Boston, 1974.

Prasher, C., *Crushing and Grinding Process Handbook*, John Wiley & Sons Ltd., New York, 1987.

CHAPTER 5

IMPACT GRINDING OF THERMOPLASTICS: EFFECT OF PROCESS VARIABLES ON PARTICLE COMMINUTION

5-1. Introduction

The impact failure behavior of thermoplastics is generally described in terms of their responses to low speed tests at room temperature. However, failure behavior is dependent on the rate of impact loading, and on the temperature. Very little work has been done at high impact rates and low temperatures. For various applications, whether exposed to intentional or inadvertent impact stresses, information at these condition is very important.

In this chapter the failure behavior of PVC and PET will be examined during high speed impact grinding. The effect that process variables, namely impact rate, temperature, retaining screen size, and feed particle size, have on the comminuted product will be discussed. The particle size distribution (PSD) data are represented by the Rosin-Rammler-Bennett (RRB) distribution.

Due to the self-preserving nature of particle size distributions, a similarity solution exists that is only disrupted with changes in the mode and/or mechanism of size reduction. In addition, beyond initial grinding periods the observed similarity behavior is independent of grinding time. Since each of the process variables has an effect on the residence time of the particles, this is an important fact.

The breakage and failure mechanisms have been observed using scanning electron microscopy and high speed videography.

5-2. Experimental

The grinding experiments were carried out on a Bantam Mikro-Pulverizer impact grinder with cryogenic apparatus made by Micron Powder Systems. The temperatures of the bottle flakes (ranging from -196 to 80°C) were lowered using liquid nitrogen or refrigeration, and raised by heating in an oven. The flakes were placed on a vibratory feeder and fed into the hopper of the impact grinder. The hammer speed was varied between experiments from 53 to 93 m/s. The retaining screens, with slots ranging from 0.254 to 3.175 mm, were also varied. The ground material was collected, and the particle size distribution was determined. The data and the curves representing the empirical size distribution model are presented as cumulative mass percent of particles under a given sieve size. The data, in tabular form, are presented in Appendix B. Scanning electron microscopy was employed to determine shape and failure mechanism information. Table 5.1 lists the apparatus employed.

5-2.1 Materials

Post-consumer PET and PVC bottle flakes were used. Relevant physical property data are summarized by Table 5.2. The initial cumulative size distributions of the flakes are plotted in Figure 5.1.

Table 5.1 Apparatus for Grinding and Analytical Systems

EQUIPMENT	MAKE	MODEL
Testing Sieve Shaker	Tyler	RO-TAP Model B
High Speed Motion Analyzer	Eastman Kodak	EKTAPRO EM
Scanning Electron Microscope	Joel	T-330
Micro-Pulverizer Hammer Mill	Micron Powder Systems	BANTAM
Electromagnetic Vibratory Feeder	Syntron	FTO-C
Thermocouple Thermometer	McMaster Carr	Model C, Type K

Table 5.2 Physical Data for PVC and PET

Material	Density (g/cm ³)	Glass Transition Temperature (C)	Melting Temperature (C)	Characteristic Feed Particle Length (mm)	Particle Thickness (mm)
PET	~1.30-1.40	80	250-255	4.6	0.68
PVC	~1.30-1.35	85	150-200	7.4	0.72

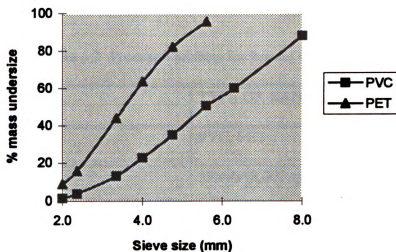


Figure 5.1 Cumulative Particle Size Distribution of Feed Thermoplastic Flakes

5-2.2 Hammer Mill

A laboratory hammer mill containing six “T” head swing-hammers was used for grinding the particles. The hammers are attached to a rotor in the 12.7 cm diameter grinding chamber. The hammer speed, which is the circumference of the grinding chamber multiplied by the number of revolution of the rotor per min. (RPM), can be varied by changing pulleys and belts. The grinding chamber has a liquid nitrogen purge for lowering the temperature. There are retaining screens of different slot sizes that fit in the bottom of the chamber. Herringbone perforated screens were used for this experimentation. A herringbone screen has a series of slotted holes at 45 degrees to the length of the screen. The opening without a screen is 5 cm x 12 cm. There are multiple deflector liners which

supplement the impacts of the hammers. A list of the process variable can be seen in Table 5.3. A photograph of the equipment can be seen in Figures 5.2.

Table 5.3 Process Variables for Impact Grinding

VARIABLE	TYPE OR RANGE
Material	PVC, PET
Impact Rate	53 m/s (8,000 rpm), 67 m/s (10,000 rpm), 93 m/s (14,000 rpm)
Screen Slot Size	0.254 mm, 1.57 mm, 2.36 mm, 3.175 mm, no screen (50mm)
Temperature	-196°C to 80°C
Screen Type	Herringbone
Feed Size	up to 8 mm
Feed Rate	up to 100 g/min.

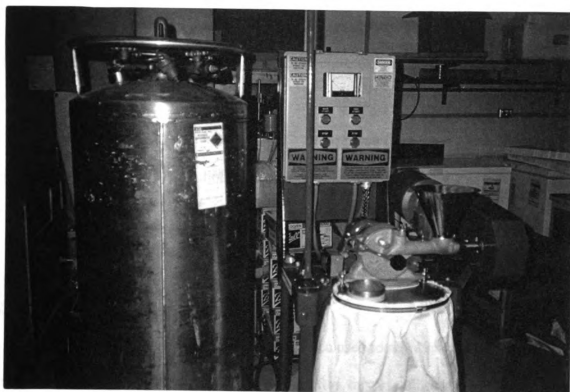


Figure 5.2 Bantam Mikro-Pulverizer Hammer Mill

5-2.3 Particle Size Determination

The particle size distributions of the feed and product were determined by standard sieving methods. The representative size of the particles in a sample was taken to be that of the sieve screen size through which 80% of the particles passed. This size is thought to more accurately characterize the material, without placing too much emphasis on the larger or smaller size fractions (Lowrison, 1974). The large size fractions may contain particles that have not been reduced or just odd particles that are not representative of the batch. Smaller size fractions (i.e. below 50% undersize) neglect some characteristic particles.

A series of Tyler sieves ranging from 212 μm to 8 mm (70 - 2 1/2 Mesh) were used to determine the size distributions. The set of sieves were subjected to a sieve shaker for size classification.

5-2.4 Size Distribution Representations

A number of mathematical equations have been used to represent particle size distributions. Though empirical in nature, they are often very useful for mapping changes in size distributions with changes in design parameters and operating conditions. They are also helpful in exposing changes in the mode and the mechanism of comminution.

In the previous chapter, the Rosin-Rammler-Bennett equation (Eq. 5-1) was determined to adequately model PVC and PET comminution. Thus, the RRB equation will be used to represent the size distribution data presented in this chapter:

$$F(l) = 1 - e^{-(l/L_{80})^n \ln(5)} \quad (5-1)$$

$F(l)$ is the cumulative size distribution function. L_{80} is the fineness index representing the characteristic 80 % passing size, and the exponent n is the uniformity index. Large values of n imply nearly uniform particle sizes, while smaller values denote a scattered distribution (Prasher, 1987). Note that when $l = L_{80}$, Eq. (5-1) implies that $F(L_{80})=0.80$.

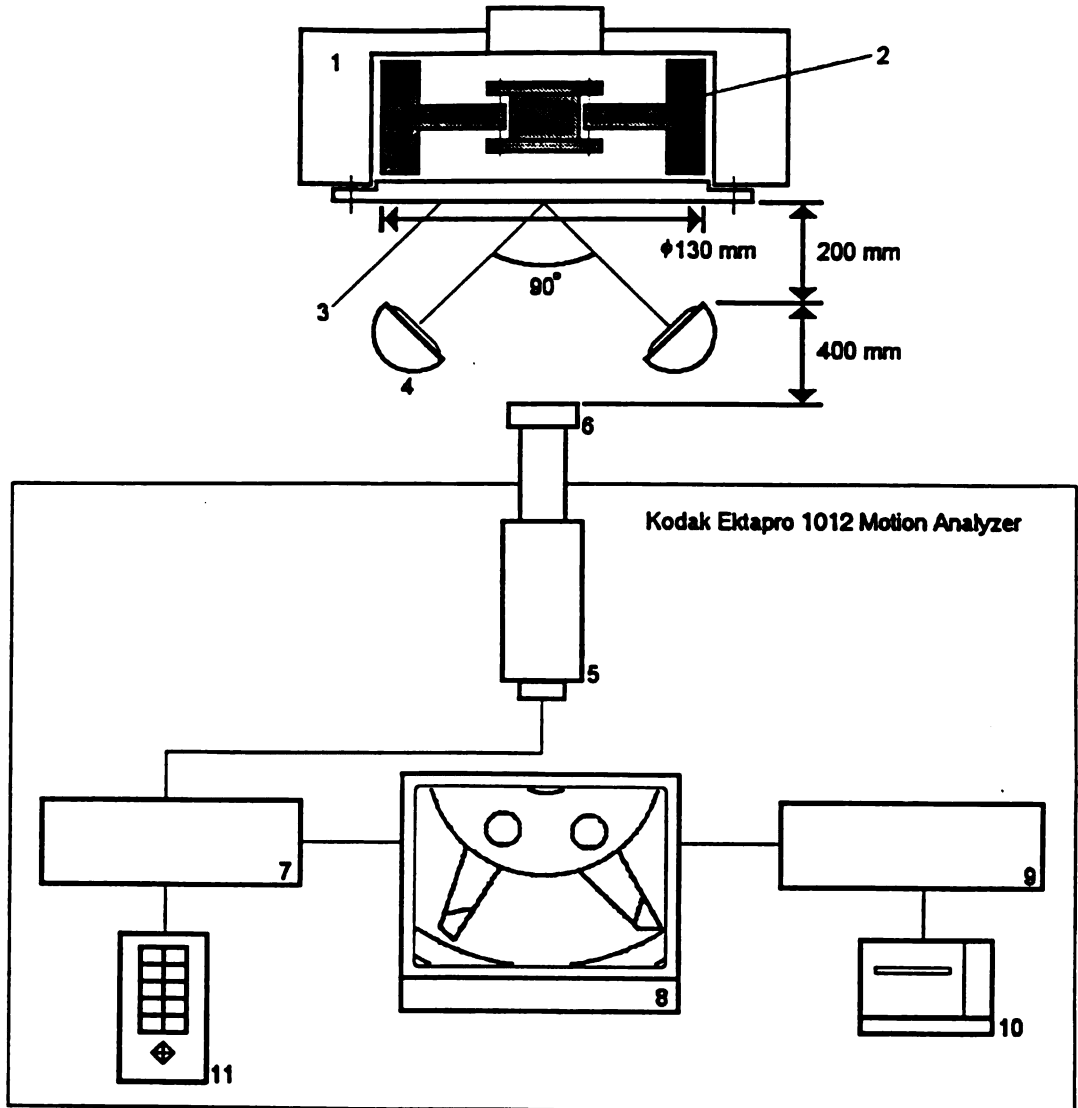
The measured PSD are given as cumulative plots of mass percentage of particles below a given sieve size.

5-2.5 High Speed Videography

A high speed motion analyzer was used to observe the particles within the grinding chamber, which was retrofitted with a 12 mm thick transparent acrylic window. The comminution was recorded at 1,000-6,000 frames per second (fps) using a 67 mm diameter lens with a macro focusing zoom. The objective for using high speed videography was to capture the following:

- number of impacts to break a particle;
- number of impacts to break a particle to screen size;
- number of fragments per impact (i.e. catastrophic or cascade breakage) and,
- the breakage mechanism (i.e. particle-particle, particle-hammer, particle-wall).

The setup for the high speed videography is illustrated in Figure 5.3



Key:

- | | |
|--|---|
| 1. Top view of grinder (Model CF, Micron Powder Systems, Summit, NJ) | 6. ϕ 67 mm lens with macro focusing zoom |
| 2. Oscillatory hammer | 7. Processor |
| 3. Transparent window | 8. Video monitor |
| 4. Quartz lamp with dichroic reflector | 9. Super-VHS VCR |
| 5. High-speed video imager, 192x239 NMOS pixel array | 10. Video copy printer |
| | 11. Keypad |

Figure 5.3 Experimental Setup for High Speed Videography of the Grinding Process

5-2.6 Scanning Electron Microscopy

The intensity of the secondary electrons is monitored to form the image from the specimen topography. The sample is gold-covered to obscure emission variations due to surface composition and surface charging. Magnifications up to 1,000 times were used. Particle shape and the fracture mechanism were observed.

5-2.7 Limitations

When liquid nitrogen was used as the cooling method, it was added to the feed prior to processing and was also fed directly into the grinding chamber during testing. The actual temperature of the plastic flakes was not known. Thus, the temperature was measured just outside the grinding chamber using a thermocouple probe, and is reported as the mill outlet temperature (M.O.T.).

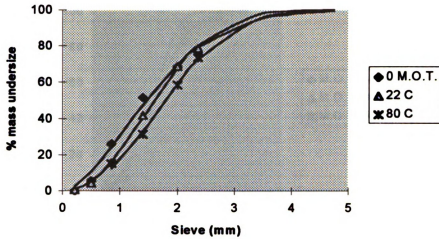
5-3 Results and Discussion

The influence of temperature, impact rate, feed particle size, and retaining screen size on PVC and PET grinding have been evaluated. This has been done in terms of cumulative size distribution plots, surface morphology photographs, and the assessment of breakage model parameters. High speed videotaping of the grinding event was also done to examine particle breakage.

5-3.1 Effect of Temperature

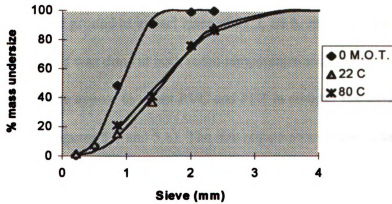
Using a 3.175 mm retaining screen and an impact rate of 93.2 m/s, PVC and PET flakes were ground in the hammer mill. The temperature of the feed was varied from -196 to 80°C. Temperature plays only a small role in the particle size distribution for PET. As seen in Figure 5.4, the PSD at room temperature nearly coincides with that at a M.O.T. of 0°C for the coarser particles. For PVC, the size distribution remains relatively unchanged for room temperature and above, but changes quite a bit at 0°C (Figure 5.5). Nearly 100 % of PVC is under 1.4 mm, while only about 50 % of PET is under that size at 0°C.

When liquid nitrogen was used, the actual temperature of the flakes during grinding was not known. Thus, the mill outlet temperature was varied by adjusting the amount of liquid nitrogen injected into the mill to determine whether the flakes were near or at liquid nitrogen (LIN) temperature (-196°C). From Figure 5.6, the amount of LIN injected does not appear to change the PSD significantly for sizes below L_{50} .



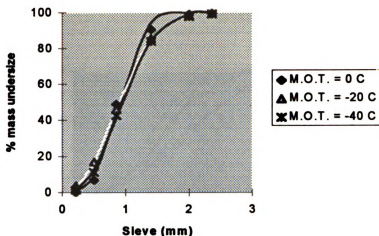
Temperature	L_{90}	n
0°C M.O.T.	2.41	1.68
22°C	2.57	2.09
80°C	2.61	2.22

Figure 5.4 Cumulative Particle Size Distribution for PET at Various Temperatures: 3.175 mm retaining screen, 93.2 m/s



Temperature	L_{90}	n
0°C M.O.T.	1.17	3.25
22°C	2.14	2.67
80°C	2.19	2.21

Figure 5.5 Cumulative Particle Size Distribution for PVC at Various Temperatures: 3.175 mm retaining screen, 93.2 m/s

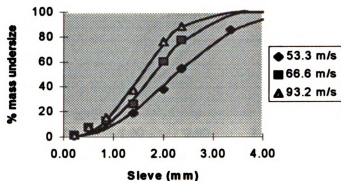


Temperature	L_{90}	n
0°C M.O.T.	1.17	3.25
-20°C M.O.T.	1.69	2.58
-40°C M.O.T.	1.32	2.51

Figure 5.6 Effect of Mill Outlet Temperature on PVC Comminution: 3.175 mm retaining screen, 93.2 m/s

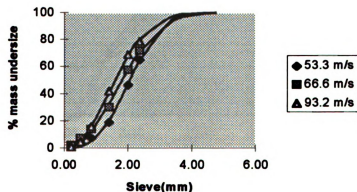
5-3.2 Effect of Impact Rate

Bottle flakes were ground at impact rates of 53.2, 66.6, and 93.2 m/s using a 3.175 mm retaining screen. This was done at both room temperature and a M.O.T. of 0°C. Changes in the impact rate appear to affect PVC and PET in roughly the same way at room temperature (see Figures 5.7 and 5.8). The size reduction increases with increasing impact rate, as expected. At lower temperatures, the impact rate seems to have a greater effect on PVC (Figure 5.9), and a lesser effect on PET (Figure 5.10). PVC particles are ground to a much smaller size, with 100% of the particles being under 2 mm at 93.2 m/s, and 70% of the PET particles being smaller than that size.



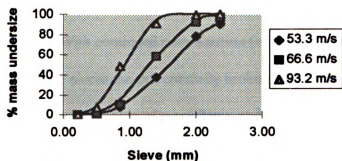
Impact Rate (m/s)	L_{80}	n
53.3	3.12	2.52
66.6	2.48	2.64
93.2	2.14	2.67

Figure 5.7 Cumulative Particle Size Distribution for PVC at Various Impact Rates at Room Temperature: 3.175 mm retaining screen



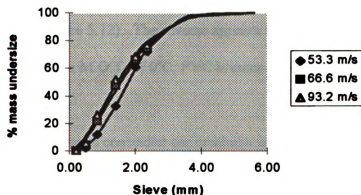
Impact Rate (m/s)	L_{80}	n
53.3	2.76	2.89
66.6	2.68	2.15
93.2	2.42	2.09

Figure 5.8 Cumulative Particle Size Distribution for PET at Various Impact Rates at Room Temperature: 3.175 mm retaining screen



Impact Rate (m/s)	L_{50}	n
53.3	2.05	3.24
66.6	1.69	3.25
93.2	1.17	3.25

Figure 5.9 Cumulative Particle Size Distribution for PVC at Various Impact Rates at 0°C
M.O.T. : 3.175 mm retaining screen, -196°C Feed Temperature



Impact Rate (m/s)	L_{50}	n
53.3	2.57	2.31
66.6	2.50	1.78
93.2	2.41	1.68

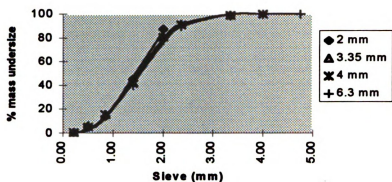
Figure 5.10 Cumulative Particle Size Distribution for PET at Various Impact Rates at 0°C
M.O.T. : 3.175 mm retaining screen, -196°C Feed Temperature

5-3.3 Effect of Feed Particle Size

As grinding proceeds, breakage changes from multimodal to monomodal (Prasher, 1987). In primary breakage, the particles break in many small fragments and fewer large pieces (bimodal breakage). With continued comminution (or longer residence time in the grinding chamber), the larger pieces are preferentially broken, both because larger particles are weaker due to the existence of more flaws, and because the smaller particles are often shielded. This leads to more uniform-sized particles (monomodal breakage). Thus, the product size distribution should be independent of the feed size distribution for extended grinding times. To examine whether this is true, the feed streams were sieved to narrow size fractions. Particle fractions close to sizes of 2 mm, 2.36 mm, 3.35 mm, 4.0 mm, and 6.3 mm were ground separately using a 3.175 mm retaining screen. This was done at room temperature and a mill outlet temperature of 0°C. PVC appears to be independent of the size of the feed particles at room temperature (Figure 5.11), while this is not the case for PET (Figure 5.12). The reverse appears to be true at low temperatures (Figures 5.13 and 5.14). At a M.O.T. of 0°C, PVC is more dependent on feed particle size than PET.

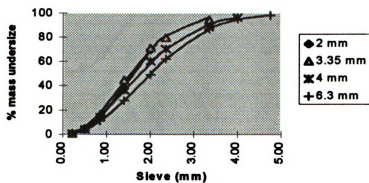
This information seems to contradict the breakage pattern results presented in the last chapter (see Section 4-3.3). At conditions for which bimodal breakage was predicted, the feed particle size does not affect the product size distribution. When monomodal breakage occurs, feed particle size does appear to affect the resulting product distribution. However, Figure 5.15 illustrates that the curves for the different feed particle sizes collapse on one curve when plotted against a dimensionless size l/L_{80} , which represents

the sieve size over the characteristic particle size. This means that the feed size effect is a residence time issue perhaps linked to a breakage mechanism change. If it were simply a breakage mode or mechanism change, this self-preserving nature would not be seen. The reason for monomodal breakage for short residence times may be a result of catastrophic breakage, as oppose to cascade breakage at other conditions.



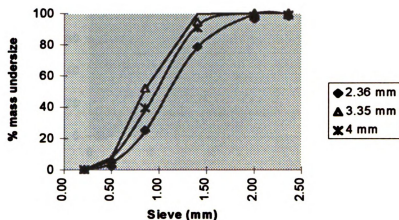
Feed Particle Size (mm)	L_{90}	n
2.00	1.88	3.13
3.35	2.02	2.72
4.00	2.03	2.74
6.3	2.09	2.70

Figure 5.11 Cumulative Particle Size Distribution PVC for Various Feed Particle Sizes at Room Temperature: 3.175 mm retaining screen, 93.2 m/s



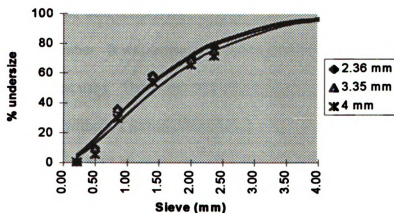
Feed Particle Size (mm)	L_{90}	n
2.00	2.29	2.37
3.35	2.33	2.07
4.00	2.74	1.93
6.3	3.01	2.10

Figure 5.12 Cumulative Particle Size Distribution PET for Various Feed Particle Sizes at Room Temperature: 3.175 mm retaining screen, 93.2 m/s



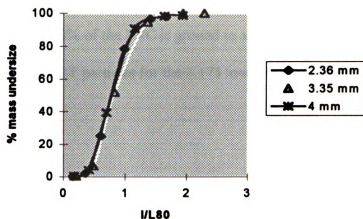
Feed Particle Size (mm)	L_{90}	n
2.36	1.42	3.39
3.35	1.03	4.07
4.00	1.22	3.35

Figure 5.13 Cumulative Particle Size Distribution PVC for Various Feed Particle Sizes at 0°C M.O.T: 3.175 mm retaining screen, 93.2 m/s, -196°C Feed Temperature



Feed Particle Size (mm)	L_{90}	n
2.36	2.34	1.44
3.35	2.43	1.39
4.00	2.60	1.48

Figure 5.14 Cumulative Particle Size Distribution PET for Various Feed Particle Sizes at 0°C M.O.T: 3.175 mm retaining screen, 93.2 m/s, -196°C Feed Temperature



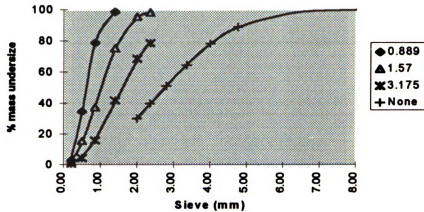
Feed Particle Size (mm)	L_{80}	n
2.36	1.42	3.39
3.35	1.03	4.07
4.00	1.22	3.35

Figure 5.15 Self-similar size distribution of PVC for Various Feed Particle Sizes at 0°C
M.O.T.: 3.175 mm retaining screen, 93.2 m/s, -196°C Feed Temperature

5-3.4 Effect of Screen Size

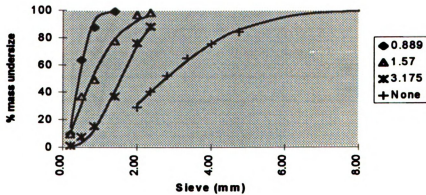
Grinding was done with herringbone screens, with varying slot sizes, placed at the base of the grinding chamber. It was expected that the product particles would have sizes close to that of the screen used. The screen slot sizes ranged from 0.889 to 3.175 mm. Grinding was also done without a screen, thus leaving a 50 mm exit space for the particles. Figures 5.16 and 5.17 illustrate the effect grinder screen size has on the particle size distributions of PET and PVC when ground at room temperature. The size distributions are nearly identical for the two materials at that condition, with the particles basically grinding closer to the size of the screen as the screen size decreases. At 0°C M.O.T., it can be seen that with the larger screen, PET (see Figure 5.18) is much less inclined to grind than PVC (Figure 5.19). This shows that in order to produce the largest

difference between the average particle sizes of the two plastics, a larger screen size will likely work best. Nearly 90% of the PVC is ground to a size smaller than 1.40 mm, compared to 40% of the PET particles for the 3.175 mm retaining screen. Therefore no screen is needed.



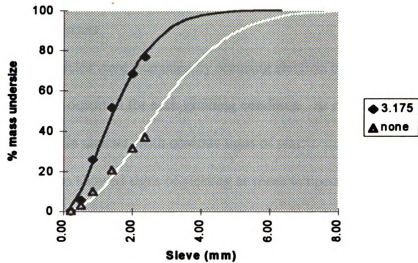
Screen Size (mm)	L_{80}	n
0.889	0.86	2.51
1.57	1.50	2.14
3.175	2.57	2.09
none	4.11	2.09

Figure 5.16 Cumulative Particle Size Distribution PET for Various Retaining Screen Sizes at Room Temperature: 93.2 m/s



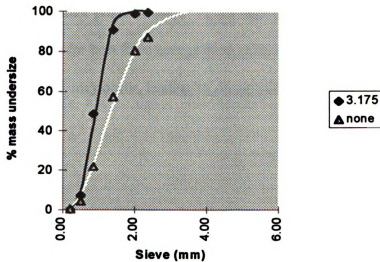
Screen Size (mm)	L_{80}	n
0.889	0.67	2.04
1.57	1.42	1.4
3.175	2.14	2.67
none	4.28	1.92

Figure 5.17 Cumulative Particle Size Distribution PVC for Various Retaining Screen Sizes at Room Temperature: 93.2 m/s



Screen Size (mm)	L_{90}	n
3.175	2.41	1.68
none	4.22	1.94

Figure 5.18 Cumulative Particle Size Distribution PET for Various Retaining Screen Sizes at 0°C M.O.T. : 93.2 m/s, -196°C Feed Temperature



Screen Size (mm)	L_{90}	n
3.175	1.17	3.25
none	1.98	2.15

Figure 5.19 Cumulative Particle Size Distribution PVC for Various Retaining Screen Sizes at 0°C M.O.T. : 93.2 m/s, -196°C Feed Temperature

5-3.5 Breakage Mechanism Identification

5-3.5.1 Failure Mechanisms

The ground particles were examined by scanning electron microscopy to determine the type of fracture that occurred for each grinding condition. At room temperature PVC particles failed in a ductile manner, with obvious signs of plastic yielding, as documented in Figure 5.20. PET also showed signs of yielding at room temperature (Figure 5.21). At a mill outlet temperature of 0°C, the PVC particles had more distinct crack patterns identifiable with brittle fracture (Figure 5.22). PET particles appear to have some characteristics of brittle failure and some of ductile (Figure 5.23). It is not well understood why PET would exhibit ductile behavior at cryogenic conditions. Yano et al. (1995) reported that studies have indicated that a nodular structure and small isometric crystallites might increase the ductility of PET by providing an energy absorbing structure. Adiabatic heating is another possible cause. At the high strain rates of impact grinding, there is insufficient time for heat from energy dissipation to be conducted away. Therefore, local heating may occur, leading to plastic yielding.

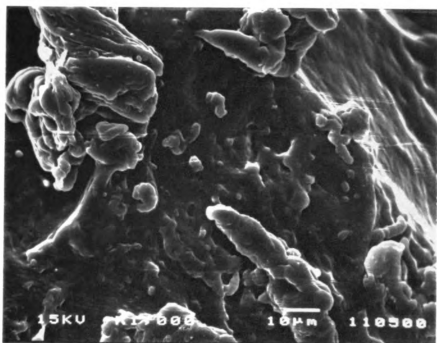


Figure 5.20 SEM (x1,000) of PVC Particle Ground at Room Temperature

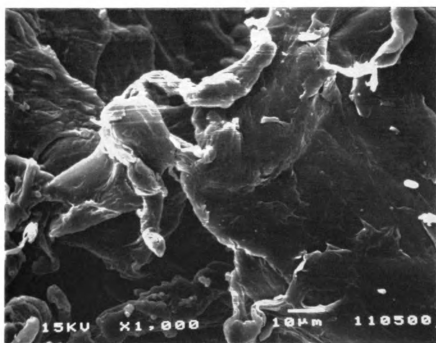


Figure 5.21 SEM (x1,000) of PET Particle Ground at Room Temperature

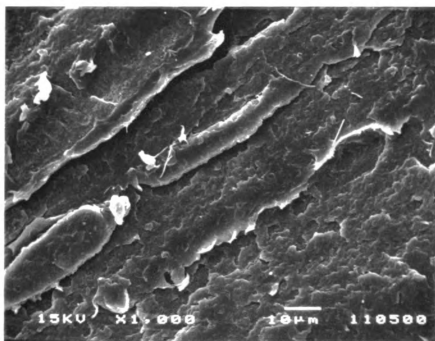


Figure 5.22 SEM (x1,000) of PVC Particle Ground at 0°C M.O.T.

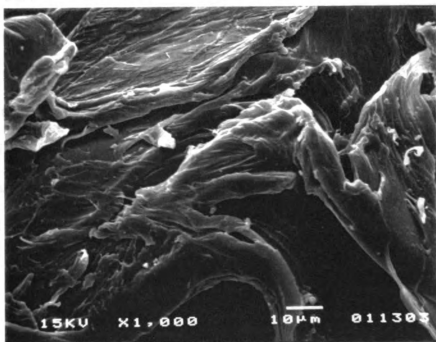


Figure 5.23 SEM (x1,000) of PET Particle Ground at 0°C M.O.T.

5-3.5.2 Differences in Particle Shapes

The fracture mechanisms of PET and PVC not only have an effect on their particle size distributions, but on their particle shapes as well. Because of the ductile mode in which PET fails during grinding, its particles have a high aspect ratio due to elongation (see Figure 5.24). PVC particles have a low aspect ratio because of their brittle fracture, as seen in Figure 5.25. The particles were comminuted after being soaked in liquid nitrogen, and at an impact rate of 93 m/s. A 3.175 mm screen was used.

5-3.5. 3 Particle Flow and Breakage

High speed videotaping of impact grinding of PVC and PET revealed two key points. The first being that particle are caught up in the air flow and often avoid being hit by the hammers. The second revelation is that the particles appear to be impacted many times before actual breakage takes place, though PVC particles seem to require fewer hits than PET particles. It was difficult to determine how many impacts that were required and the number of progeny particles that resulted because of the speed of the comminution action and the limited viewing area. Each viewing frame represented between 0.5-1 ms. After initial breakage the progeny particles appeared to be hit many more times before falling through the retaining screen. Figures 5.26 and 5.27 illustrate a particle prior to and at the point of impact, respectively.

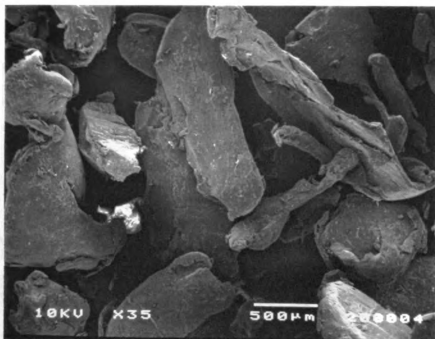


Figure 5.24 SEM of PET Particle Shape: 93.2 m/s, 0°C M.O.T.

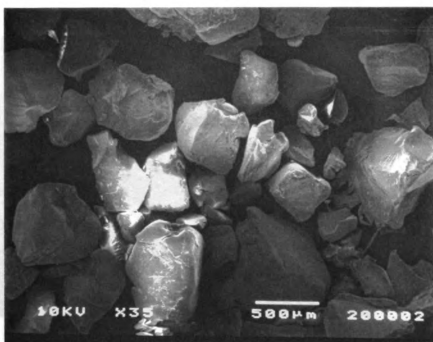


Figure 5.25 SEM of PVC Particle Shape: 93.2 m/s, 0°C M.O.T.

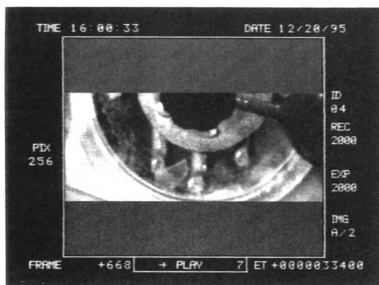


Figure 5.26 High Speed Videography of PVC Particle Prior to Impact: 93.2 m/s, 22°C, 2000 fps

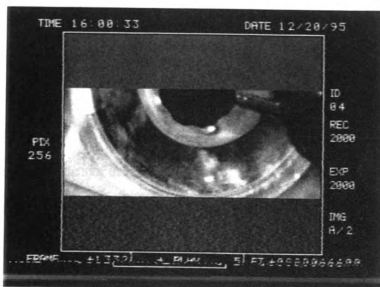


Figure 5.27 High Speed Videography of PVC Particle at the Point of Impact: 93.2 m/s, 22°C, 2000 fps

5-3.6 Predicting Particle Size

The two coefficients, L_{80} and n , of the Rosin-Rammler-Bennett equation have been evaluated in terms of the process variables (see Chapter 4 for further discussion). Since temperature seems to be a key variable, all of the other process parameters have been evaluated in relation to temperature as well. It should be noted that the standard deviations for L_{80} and n for PET is 0.12 and 0.21, respectively, while those for PVC are 0.07 and 0.35. These values were obtained by doing a statistical analysis on eight replicated experiments.

5-3.6.1 Temperature

Below the glass transition temperature of 80°C, the product size of PET appears to be nearly independent of temperature (Figure 5.28). L_{80} is generally around 2.5 mm. However, the characteristic particle size of PVC decreases significantly as the temperature decreases from 22°C to about -196°C (Figure 5.29). Above room temperature, L_{80} remains relatively constant. PVC appears to undergo a brittle-ductile transition between 0°C and -20°C.

The uniformity index for PET decreases with decreasing temperature (Figure 5.30), while the uniformity index for PVC increases with decreasing temperature (Figure 5.31). This indicates that the PVC particles are becoming more uniformly sized as they become more brittle with decreasing temperature. The slight decrease in n for PET may be related to the partial ductile nature observed at cryogenic temperatures, leading to a broader size distribution.

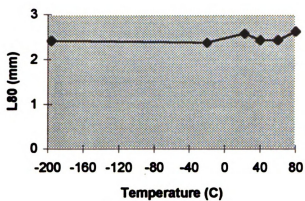


Figure 5.28 Dependence of Characteristic Product Size on Feed Temperature for PET:
3.175 mm Retaining Screen, 93.2 m/s

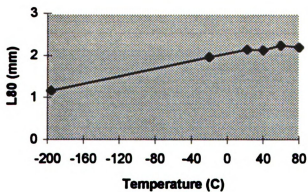


Figure 5.29 Dependence of Characteristic Product Size on Feed Temperature for PVC:
3.175 mm Retaining Screen, 93.2 m/s

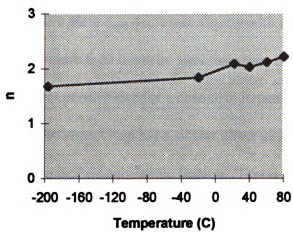


Figure 5.30 Dependence of Uniformity Index on Feed Temperature for PET: 3.175 mm Retaining Screen, 93.2 m/s

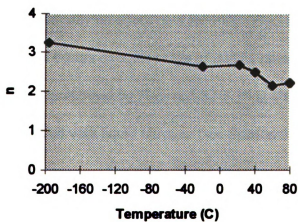


Figure 5.31 Dependence of Uniformity Index on Feed Temperature for PVC: 3.175 mm Retaining Screen, 93.2 m/s

5-3.6.2 Impact Rate

PVC is affected more by impact rate than PET. This fact was not obvious when looking at cumulative plots. L_{90} decreases slightly with increasing impact rate for PET (Figure 5.32). In Figure 5.33 it can be seen that there can be as much as a millimeter difference in product particle size for a change in impact rate from 53 m/s to 93 m/s for PVC. Increasing the impact rate has a similar affect as lowering the temperature - the particles break in an increasingly brittle fashion. This is a result of the higher concentration of stress, and the less time for molecular mobility.

For PET, the uniformity index decreases significantly with a change in the impact rate from 53 m/s to 66 m/s, then remains relatively unchanged with a further increase in the impact rate to 93 m/s (Figure 5.34). This seems to indicate a mechanism change. However, as with the anomalous response of n to decreasing the grinding temperature, the decrease in n with increasing impact rate signifies a broader distribution, possibly the result of the both brittle and ductile properties of PET observed by SEM. Increases in impact rate have virtually no effect on n for PVC (Figure 5.35). No apparent failure mechanism change occurs over the range of impact rates tested.

The data summarized by Figures 5.32-5.34 at 0°C were obtained for feed material which was pretreated with liquid nitrogen (see Section 5.2-7).

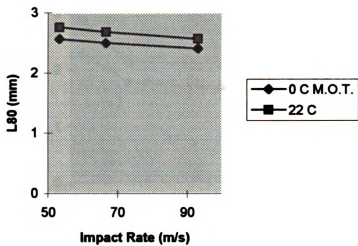


Figure 5.32 Dependence of Characteristic Product Size on Impact Rate for PET: 3.175 mm Retaining Screen

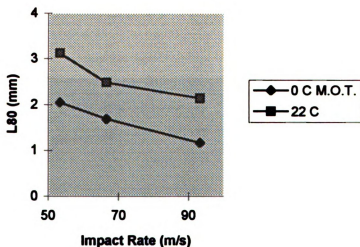


Figure 5.33 Dependence of Characteristic Product Size on Impact Rate for PVC: 3.175 mm Retaining Screen

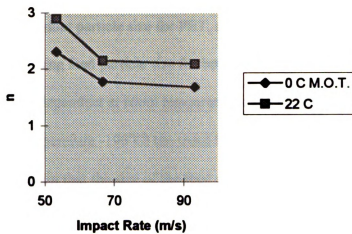


Figure 5.34 Dependence of Uniformity Index on Impact Rate for PET: 3.175 mm Retaining Screen

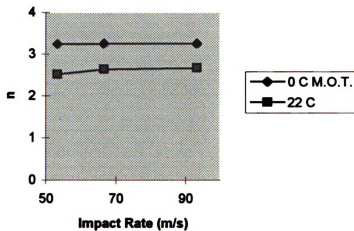


Figure 5.35 Dependence of Uniformity Index on Impact Rate for PVC: 3.175 mm Retaining Screen

5-3.6.3 Feed Particle Size

The characteristic product particle size for PET, as illustrated in Figure 5.36, increases slightly with increasing feed particle size for both room temperature and low temperature. L_{80} is nearly independent at room temperature for PVC (Figure 5.37). At a M.O.T. of 0°C (i.e., feed temperature -196°C) the trend for L_{80} is unclear.

It should be noted again that the size of the feed particles is actually an estimate from a narrow particle size distribution. As a result, the value of L_{80} for PET for a 2 mm feed is slightly above 2 mm. This may indicate that no size reduction occurred and the particles simply fell through the retaining screen.

The uniformity indexes for both PET and PVC (see Figures 5.38 and 5.39) are nearly independent of feed particle size except for the smallest size of 2 mm. Once again, an explanation is unclear.

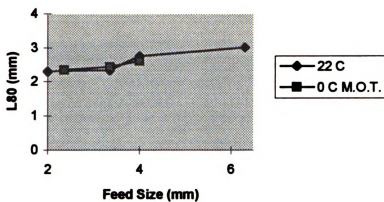


Figure 5.36 Dependence of Characteristic Product Size on Feed Particle Size for PET: 3.175 mm Retaining Screen, 93.2 m/s

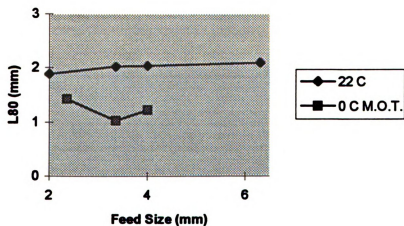


Figure 5.37 Dependence of Characteristic Product Size on Feed Particle Size for PVC: 3.175 mm Retaining Screen, 93.2 m/s

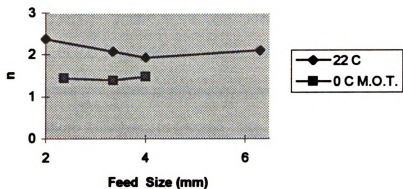


Figure 5.38 Dependence of Uniformity Index on Feed Particle Size for PET: 3.175 mm Retaining Screen, 93.2 m/s

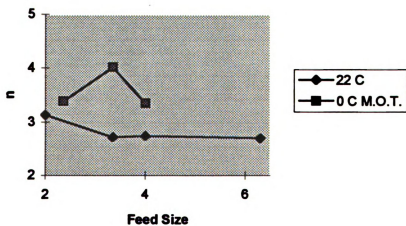


Figure 5.39 Dependence of Uniformity Index on Feed Particle Size for PVC: 3.175 mm Retaining Screen, 93.2 m/s

5-6.6.4 Retaining Screen Size

When no screen was used the opening is 5 cm x 12 cm, however, the screen size was taken to be the size of the characteristic feed particle size. Both PET and PVC particles grind to just under the screen size at room temperature (Figures 5.40 and 5.41). However, at a M.O.T. of 0°C (i.e., feed temperature -196°C), PVC particles grind to well below the retaining screen size, again signifying the brittleness of the particles at these conditions and, thus, more willingness to fracture. The uniformity index for PET increases with decreasing screen size, while that for PVC fluctuates quite a bit (Figures 5.42 and 5.43). For both PVC and PET there seems to be a transition point at screen size 1.57 mm, where L_{90} is no longer a function of temperature, and the particles become more uniformly-sized.

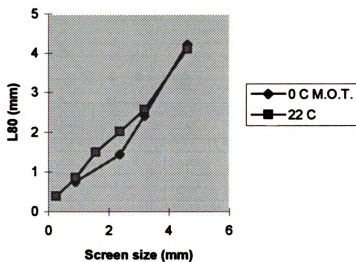


Figure 5.40 Dependence of Characteristic Product Size on Screen Size for PET: 93.2 m/s

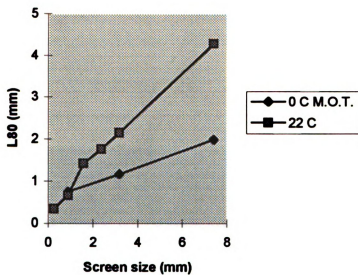


Figure 5.41 Dependence of Characteristic Product Size on Screen Size for PVC: 93.2 m/s

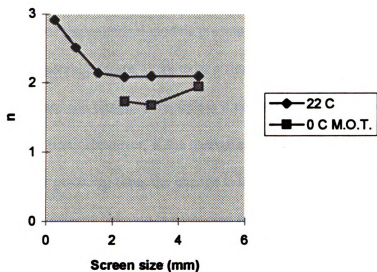


Figure 5.42 Dependence of Uniformity Index on Screen Size for PET: 93.2 m/s

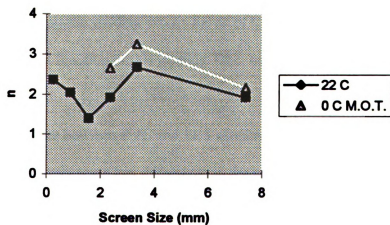
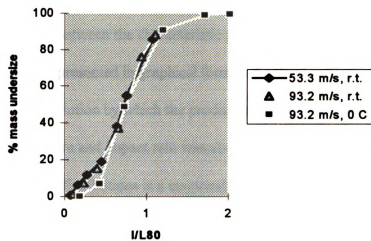


Figure 5.43 Dependence of Uniformity Index on Screen Size for PVC: 93.2 m/s

5-3.6.5 Similarity Solution

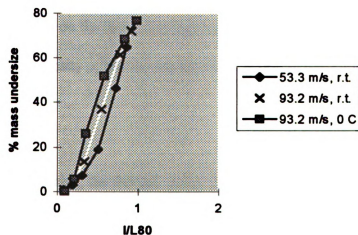
One implication of the empirical models presented in the last section is that, because of their self-preserving nature, there exist a single dimensionless curve that is independent of impact rate and temperature, unless there is a change in mode and/or the mechanism of size reduction. However, if the change in mode and/or the mechanism is a function of residence (or grinding) time, the change is incorporated in the normalizing parameter L_{90} , and the similarity solution is preserved (Prasher, 1987). The empirical model is then presented as the mass % undersize verses the sieve size made dimensionless by the characteristic particle size. In Figures 5.44 and 5.45 the similarity solutions for PVC and PET can be seen. Regardless of temperature or impact rate, the dimensionless curve for PVC is basically the same. However, there is some variance for PET. This indicates that there is a factor in the breakage mechanism of PET that cannot be related to grinding time. For PVC, the breakage mechanism changes caused by changes in temperature and impact rate are expressed in a time scale factor incorporated in L_{90} . In the case of PET, since plastic yielding occurs for all of the grinding conditions tested, L_{90} may be a more complex function of this yielding, thus, making it insufficient as a grinding time scale factor.

These differences between PVC and PET observed in this examination of the similarity solution suggests some key differences in the comminution behavior of brittle and ductile materials. That is, the relationship between plastic yielding and the size of the resulting particle is needed for ductile material if the similarity solution is to be used to map the particle size distribution for various grinding conditions.



Impact Rate (m/s)	Temperature (C)	L_{80}	n
53.3	22	3.12	2.52
93.2	22	2.14	2.67
93.2	0 M.O.T.	1.17	3.25

Figure 5.44 Self-similar Size Distribution for PVC



Impact Rate (m/s)	Temperature (C)	L_{80}	n
53.3	22	2.76	2.89
93.2	22	2.57	2.09
93.2	0 M.O.T.	2.41	1.68

Figure 5.45 Self-similar Size Distribution for PET

5-3.6.6 Scaling Laws

The relationships between the characteristic product size, L_{80} , and the impact grinding conditions were presented in graphical form in the previous sections. The existence of a similarity solution by which the product size distribution could be mapped with changes in temperature and impact rate was also presented. The missing component to predicting particle size distributions is an empirical relationship between L_{80} (and, the uniformity index n) and the process variables. Thus, a scaling analysis was done to try to bridge this gap for L_{80} .

The cumulative particle size distribution modeled with the RRB equation can be presented in the following form by normalizing the particle size with L_{80} :

$$F = F(l/L_{80}, n) \quad (5-2)$$

If L_{80} is assumed to depend on the thermal energy required for breakage (i.e., $\sim \kappa T$, where κ is Boltzmann's constant), the density ρ , and the impact rate u , then

$$f(L_{80}, \kappa T, \rho, u) = 0 \quad (5-3)$$

Thus, by dimensional reasoning, the thermal energy of the particle should be proportional to the kinetic energy of the particle. Hence,

$$\frac{\kappa T}{\frac{1}{2} V_p \rho u^2} = C \quad (5-4)$$

where V_p is the volume of the particle, and is proportional to L_{80}^3 , and C is some constant.

Rearranging Eq. (5-4) gives the following scaling relationship between L_{80} and the grinding temperature and impact rate:

$$L_{80} = CT^{1/3}/u^{2/3} \quad (5-5).$$

Over the range of temperatures and impact rates studied, this relationship works for the size reduction of PVC, but not for PET. This may be due to the ductile nature of PET.

The following examples illustrate how the characteristic product size can be determined for PVC at various grinding temperatures and impact rates from a knowledge of L_{80} at one set of conditions.

Examples of Scaling Law Utilization for PVC

Temperature: $L_{80} \sim T^{1/3}$

$$\begin{aligned} L_{80 \text{ at } 22\text{C}} &= L_{80 \text{ at } -200\text{C}} (T_{22\text{C}}/T_{-200\text{C}})^{1/3} \\ &= 2.05(295^\circ\text{K}/73^\circ\text{K})^{1/3} \\ &= 3.26 \text{ mm} \end{aligned}$$

Experimentally, $L_{80 \text{ at } 22\text{C}} = 3.12 \text{ mm}$ (see Figures 5.7 and 5.9)

Impact Rate: $L_{80} \sim u^{-2/3}$

$$\begin{aligned} L_{80 \text{ at } 93.2 \text{ m/s}} &= L_{80 \text{ at } 53.3 \text{ m/s}} [(u_{53.3 \text{ m/s}})/(u_{93.2 \text{ m/s}})]^{2/3} \\ &= 3.12 (53.3/93.2)^{2/3} \\ &= 2.15 \text{ mm} \end{aligned}$$

Experimentally, $L_{80 \text{ at } 93.2 \text{ m/s}} = 2.14 \text{ mm}$ (see Figure 5.7)

Empirical relationships can be developed from this scaling analysis for PVC. However, the relationships between L_{80} and the grinding conditions for PET need to be investigated further.

5-3.7 Selective Size Reduction of PVC and PET

A 50/50 mixture of PVC and PET flakes were pre-soaked in liquid nitrogen and ground at a M.O.T. of -20°C using a 3.175 mm retaining screen and an impact rate of 93.2 m/s. The PVC and PET particles were separated by dissolving PVC in tetrahydrofuran (THF). Since PET is insoluble in THF, the quality of the size separation could be evaluated by determining the weight of the remaining particles. In Figure 5.46, the cumulative size distributions for the ground mixture can be seen. The values for L_{80} determined from these distributions were 2.55 and 0.92 for PET and PVC, respectively. The values for n were 1.57 and 3.07. These values are close to what was obtained when PET and PVC were ground separately.

Most of the fines from the ground mixture were PVC particles, while the coarser particles were mainly PET, as illustrated in Figure 5.47. This was an expected and necessary result for size separation. The purity and yield of PET can be seen in Figure 5.48. However, with the understanding of how the process variables affect the product size, future optimization is possible.

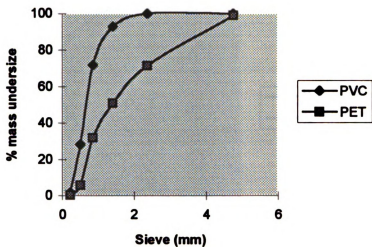


Figure 5.46 Cumulative Size Distributions for Separated PVC/PET Ground Mixture: 93.2 m/s, 3.175 mm Retaining Screen, -20°C M.O.T.

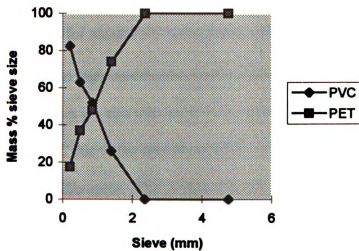


Figure 5.47 Mass Percentage of Particles of Each Thermoplastic Retained on Sieve Size: 93.2 m/s, 3.175 mm Retaining Screen, -20°C M.O.T.

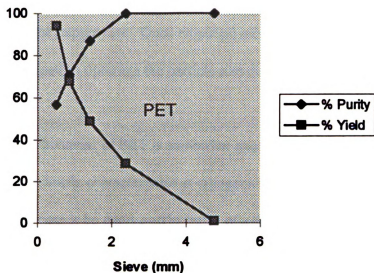


Figure 5.48 Size Separation of PVC/PET Mixture Ground at -20°C M.O.T.

5-4. Conclusions

There are conditions for which PVC bottle flakes will grind finer than PET flakes. Temperatures below 0°C and high impact rates produce the most substantial size differences. Shape differences are also created at these conditions. PET has a much higher aspect ratio than PVC due to the ductility of PET. Using larger size screens also seems to improve the size differences. PET is insensitive to temperature or impact rate, while the opposite is true for PVC.

It is possible to estimate the characteristic particle product size from the relationships between L_{50} and the grinding temperature, impact rate, and retaining screen size. The scaling laws validate this for PVC. The characteristic product size has been

found to be proportional to the 1/3 power of the temperature, and inversely proportional to the 2/3 power of the impact rate. Once empirical modeling has been completed, these relationships can be used to optimize the particle size differences between the two materials.

The breakage behavior of PET is somewhat anomalous in that PET exhibits seemingly ductile and brittle characteristics at cryogenic temperatures and high strain rates. This behavior cannot be expressed in terms of a time-dependent scale factor, as in the case of PVC.

Tensile and compressive failure mechanism behaviors do not predict the failure mechanisms seen during impact grinding, though the tensile failure mechanism diagram accurately predicts the brittle-ductile transition for PVC (see Table 5.4). The Izod impact experiments also predicts the brittle-ductile transition for PVC, as well as the failure mechanisms. They also show that the impact behavior of PET is not affected much by temperature. However, the SEM photographs show that PET Izod impact specimens fail in a brittle fashion, while PET fails in a ductile fashion during impact grinding.

Table 5.4 Brittle-Ductile Transition Temperatures (C) for PVC

Strain Rate (s ⁻¹)	Tensile ^a	Compressive ^a	Izod ^b	β-Relaxation ^a	Grinding ^b
0.1	-48/-23	52/77	-	-80	-
100	2/27	77/102	0/20	-35	-
10,000	52/77	102/127	-	12	-20

^aEstimated

^bExperimental

5-5. References

Lowrison, G., *Crushing and Grinding*, Butterworths, Boston, 1974.

Prasher, C., *Crushing and Grinding Process Handbook*, John Wiley & Sons Ltd., New York, 1987.

Yano, O. and H. Yamaoka, "Cryogenic Properties of Polymers," *Progress in Polymer Science*, 20 (1995), 585.

CHAPTER 6

CONCLUSIONS

This research has provided a framework for studying thermoplastics comminution. The applicability of using theoretical deformation processes and conventional mechanical testing to model impact grinding result was examined. The suitability of various mathematical representations to model particle size distributions from the size reduction of PVC and PET was also investigated. Lastly, the development of relationships between impact grinding process variables to the size of the resulting particles was desired. The purpose of these undertakings were for the ultimate goal of selectively grinding mixtures of PVC and PET material to different particle sizes and shapes.

Classical impact theory developed for low speed mechanical testing is not sufficient to predict the high speed impact behavior of thermoplastics. While the brittle-ductile transitions for PVC at various temperatures and impact rates were forecasted, those for PET could not be anticipated. Tensile and compressive theoretical models were not useful in describing PVC and PET behavior at high strain rates. The brittle-ductile transition temperatures determined from Izod impact testing and the β -relaxation temperature were comparable to the failure mechanism transition seen during impact grinding for PVC. However, neither of these methods, nor high speed ballistics testing, predicted the ductile behavior of PET at cryogenic conditions. This could be due to the uniqueness of thermoplastics as viscoelastic material. Factors such as notch sensitivity and

sample thickness must be taken into consideration. In the latter case, orientation affects for thinner samples may affect the failure mechanism.

Empirical breakage mechanism and model information was developed from single and multiple particle comminution in a hammer mill. A two parameter empirical model was used to describe PVC and PET comminution at various conditions. One parameter, L_{90} , provided information about how the characteristic particle product size varied with temperature, impact rate, and screen size. The other parameter, n , described the uniformity of the particles and whether the breakage was catastrophic or cascade in nature. The product sizes of PVC particles decreased with increasing impact rate and decreasing temperature, as expected. The breakage changed from bimodal cascade failure to monomodal catastrophic failure as the temperature decreased and the impact rate increased. For PET, the product size was independent of temperature, and only decreased slightly with increases in impact rate. The breakage mode changed from monomodal to bimodal as temperature was decreased and the impact rate increased.

Empirical models can be constructed to estimate a characteristic product particle size using the relationships established between L_{90} and the process variables. The characteristic product size, L_{90} , was found to be proportional to the one-third power of temperature, and inversely proportional to the two-thirds power of the impact rate. A complete particle size distribution can be determined for PVC based on a similarity solution. However, further information about the yield behavior of PET (i.e. the elongation at break) is needed to model its complete particle size distribution for various process parameters.

At cryogenic temperatures, PVC can be selectively ground to smaller particle sizes than PET. This is due to PVC particles fracturing in a brittle fashion, while PET particles fail in a ductile fashion. Separation of the two materials based on size is possible, however, optimization to increase purity and yield is still necessary. Shape differences can also be created, with PET having a larger aspect ratio than PVC.

The failure behavior of PET at low temperatures and high impact rates is somewhat anomalous to what was expected. Even though PET is known to exhibit some ductility at cryogenic conditions, PET seemed to display just as much, or perhaps even more ductile behavior at these conditions than at room temperature. This could be due to factors such as stress-induced crystallization, chain reorientation, or adiabatic heating.

CHAPTER 7

RECOMMENDATIONS

This work has provided a framework for studying the comminution of thermoplastics, in addition to presenting a method for selectively grinding mixed component streams for classification. However, a number of areas of this research invoke the need for further investigations. One of the key questions that remains is how can material be evaluated to gain insight into the probable failure mechanisms that will occur during comminution? This can be examined by studying the material properties and deformation behaviors of other thermoplastics, such as polyethylene and polypropylene. Further high speed mechanical testing at low temperatures also needs to be done to understand brittle-ductile transitions at those conditions.

Using the relationships developed between the process variables and the characteristic product size, empirical equations should be developed. The scaling analysis provided the starting point for this empirical modeling. Then the optimal conditions for affecting the desired separation can be estimated and verified through experimentation.

The ductile behavior of PET at cryogenic conditions should be examined more thoroughly to determine causes, such as strain-induced crystallization or molecular reorientation. Experimentation, such as grinding spherical shape particles rather than flakes, could provide information about morphological changes, since the inclination for

structural changes are often related to sample thickness. Thermal analysis on ground material could give insight to whether changes in crystallinity are occurring.

The final recommendation is that the actual separation of PVC and PET by size and/or shape should be carried out in a hydrocyclone, by sieving, or some other method. This research provided some answers to why this is possible. Now it needs only to be done.

APPENDICES

APPENDIX A

APPENDIX A

IZOD IMPACT DATA

Temperature (C)	PET Impact Strength (J/m)	STD. DEV.
-40	5.29	1.512
-30	4.81	1.836
-20	3.94	0.594
-10	4.27	1.026
0	4.64	0.54
10	4.59	0.378
20	3.02	0.756
30	4.86	0.702
40	5.83	1.566
50	4.75	1.188
60	3.58	0.648
70	4.97	0.756
80	2.97	0.54

Temperature (C)	PVC Impact Strength (J/m)	STD. DEV.
-40	10	2.538
-30	19	18.63
-20	19	4.536
-10	22	8.316
0	31	13.122
10	178	37.314
20	256	22.14
30	255	33.372
40	275	28.782
50	241	23.328
60	251	27.756
70	240	28.404
80	287	19.872

APPENDIX B

APPENDIX B

IMPACT GRINDING DATA

Material	Temperature (C)	Impact Rate (m/s)	Screen Size (mm)	Characteristic Feed Size (mm)
PVC	23 M.O.T.	93.2	3.175	7.4

Sieve Size (mm)	Mass % undersize	RRB Model
2.36	86.85	87.98
2	73.85	72.14
1.4	33.44	34.93
0.85	9.67	8.93
0.5	3.65	1.8
0.212	0.79	0.13

Characteristic Product Size, $L_{90} = 2.16$ Uniformity Index, $n = 3.06$

Material	Temperature (C)	Impact Rate (m/s)	Screen Size (mm)	Characteristic Feed Size (mm)
PVC	22	93.2	3.175	7.4

Sieve Size (mm)	Mass % undersize	RRB Model
2.36	91.49	92.42
2	79.78	78.53
1.4	38.68	39.68
0.85	10.59	10.11
0.5	3.37	2.01
0.212	0.48	0.14

Characteristic Product Size, $L_{90} = 2.03$ Uniformity Index, $n = 3.12$

Material	Temperature (C)	Impact Rate (m/s)	Screen Size (mm)	Characteristic Feed Size (mm)
PVC	22	93.2	3.175	7.4

Sieve Size (mm)	Mass % undersize	RRB Model
2.36	86.56	85.96
2	73.61	72.25
1.4	36.72	40.06
0.85	15.25	13.20
0.5	7.05	3.55
0.212	1.31	0.40

Characteristic Product Size, $L_{90} = 2.18$ Uniformity Index, $n = 2.57$

Material	Temperature (C)	Impact Rate (m/s)	Screen Size (mm)	Characteristic Feed Size (mm)
PVC	22	93.2	3.175	7.4

Sieve Size (mm)	Mass % undersize	RRB Model
2.36	85.23	84.55
2	72.03	70.59
1.4	35.16	38.89
0.85	15.03	12.88
0.5	7.71	3.50
0.212	1.57	0.40

Characteristic Product Size, $L_{50} = 2.23$

Uniformity Index, $n = 2.55$

Material	Temperature (C)	Impact Rate (m/s)	Screen Size (mm)	Characteristic Feed Size (mm)
PVC	22	93.2	3.175	7.4

Sieve Size (mm)	Mass % undersize	RRB Model
2.36	90.36	88.12
2	11.07	77.38
1.4	35.03	49.56
0.85	22.40	20.64
0.5	9.38	7.03
0.212	7.6	1.12

Characteristic Product Size, $L_{50} = 2.07$

Uniformity Index, $n = 2.17$

Material	Temperature (C)	Impact Rate (m/s)	Screen Size (mm)	Characteristic Feed Size (mm)
PET	22	93.2	3.175	4.6

Sieve Size (mm)	Mass % undersize	RRB Model
2.36	72.97	72.82
2	63.27	62.82
1.4	41.45	42.13
0.85	20.48	21.24
0.5	10.79	9.41
0.212	3.03	2.35

Characteristic Product Size, $L_{50} = 2.68$

Uniformity Index, $n = 1.66$

Material	Temperature (C)	Impact Rate (m/s)	Screen Size (mm)	Characteristic Feed Size (mm)
PET	22	93.2	3.175	4.6

Sieve Size (mm)	Mass % undersize	RRB Model
2.36	70.10	74.47
2	59.20	58.27
1.4	34.42	33.05
0.85	11.30	12.63
0.5	2.79	4.15
0.212	0.53	0.64

Characteristic Product Size, $L_{90} = 2.65$

Uniformity Index, $n = 2.18$

Material	Temperature (C)	Impact Rate (m/s)	Screen Size (mm)	Characteristic Feed Size (mm)
PET	22	93.2	3.175	4.6

Sieve Size (mm)	Mass % undersize	RRB Model
2.36	70.07	71.42
2	59.21	58.27
1.4	34.44	33.12
0.85	11.39	12.71
0.5	2.91	4.20
0.212	0.66	0.66

Characteristic Product Size, $L_{90} = 2.65$

Uniformity Index, $n = 2.17$

Material	Temperature (C)	Impact Rate (m/s)	Screen Size (mm)	Characteristic Feed Size (mm)
PET	22	93.2	3.175	4.6

Sieve Size (mm)	Mass % undersize	RRB Model
2.36	71.25	72.69
2	60.39	59.44
1.4	35.21	33.79
0.85	11.55	12.88
0.5	2.75	4.21
0.212	0.41	0.65

Characteristic Product Size, $L_{90} = 2.60$

Uniformity Index, $n = 2.20$

Material	Temperature (C)	Impact Rate (m/s)	Screen Size (mm)	Characteristic Feed Size (mm)
PET	22.	93.2	3.175	4.6

Sieve Size (mm)	Mass % undersize	RRB Model
2.36	75.53	77.02
2	64.89	64.02
1.4	38.70	37.32
0.85	13.30	14.45
0.5	3.32	4.75
0.212	0.53	0.74

Characteristic Product Size, $L_{90} = 2.46$

Uniformity Index, $n = 2.20$

Material	Temperature (C)	Impact Rate (m/s)	Screen Size (mm)	Characteristic Feed Size (mm)
PET	22.	93.2	2.36	4.6

Sieve Size (mm)	Mass % undersize	RRB Model
2.36	88.28	89.05
2	79.24	79.17
1.4	53.38	52.67
0.85	23.31	23.31
0.5	7.51	8.44
0.212	1.01	1.47

Characteristic Product Size, $L_{90} = 2.02$

Uniformity Index, $n = 2.08$

Material	Temperature (C)	Impact Rate (m/s)	Screen Size (mm)	Characteristic Feed Size (mm)
PVC	22	93.2	2.36	7.4

Sieve Size (mm)	Mass % undersize	RRB Model
2.36	96.61	94.14
2	91.32	87.33
1.4	59.84	64.75
0.85	31.64	33.00
0.5	19.00	13.48
0.212	3.93	2.76

Characteristic Product Size, $L_{90} = 1.76$

Uniformity Index, $n = 1.92$

Material	Temperature (C)	Impact Rate (m/s)	Screen Size (mm)	Characteristic Feed Size (mm)
PET	22	93.2	0.254	4.6

Sieve Size (mm)	Mass % undersize	RRB Model
2.36	100.00	100
2	100.00	100
1.4	100.00	100
0.85	99.39	99.99
0.5	96.34	96.34
0.212	23.78	23.78

Characteristic Product Size, $L_{80} = 0.39$

Uniformity Index, $n = 2.91$

Material	Temperature (C)	Impact Rate (m/s)	Screen Size (mm)	Characteristic Feed Size (mm)
PVC	22	93.2	.254	7.4

Sieve Size (mm)	Mass % undersize	RRB Model
2.36	100.00	100
2	99.17	100
1.4	98.33	100
0.85	99.17	99.99
0.5	97.5	97.50
0.212	38.33	38.33
		0.35

Characteristic Product Size, $L_{80} = 0.35$

Uniformity Index, $n = 2.37$

Material	Temperature (C)	Impact Rate (m/s)	Screen Size (mm)	Characteristic Feed Size (mm)
PVC	-20 M.O.T.	93.2	3.175	7.4

Sieve Size (mm)	Mass % undersize	RRB Model
2.36	98.99	99.79
2	97.36	98.35
1.4	82.16	81.93
0.85	39.82	39.58
0.5	11.93	12.79
0.212	2.64	1.65

Characteristic Product Size, $L_{80} = 1.37$

Uniformity Index, $n = 2.45$

Material	Temperature (C)	Impact Rate (m/s)	Screen Size (mm)	Characteristic Feed Size (mm)
PVC	0 M.O.T.	93.2	3.175	2.36

Sieve Size (mm)	Mass % undersize	RRB Model
2.36	97.98	99.99
2	96.42	99.40
1.4	78.38	78.23
0.85	25.19	24.49
0.5	2.18	4.54
0.212	0.16	0.25

Characteristic Product Size, $L_{90} = 1.42$

Uniformity Index, $n = 3.39$

Material	Temperature (C)	Impact Rate (m/s)	Screen Size (mm)	Characteristic Feed Size (mm)
PVC	0 M.O.T.	93.2	3.175	3.35

Sieve Size (mm)	Mass % undersize	RRB Model
2.36	100.00	100.00
2	100.00	100.00
1.4	94.54	99.58
0.85	51.97	51.33
0.5	6.55	7.98
0.212	0.44	0.25

Characteristic Product Size, $L_{90} = 1.04$

Uniformity Index, $n = 4.07$

Material	Temperature (C)	Impact Rate (m/s)	Screen Size (mm)	Characteristic Feed Size (mm)
PVC	0 M.O.T.	93.2	3.175	4.00

Sieve Size (mm)	Mass % undersize	RRB Model
2.36	98.80	100.00
2	98.29	99.98
1.4	90.75	92.06
0.85	39.55	37.79
0.5	4.28	7.69
0.212	0.34	0.45

Characteristic Product Size, $L_{90} = 1.22$

Uniformity Index, $n = 3.36$

Material	Temperature (C)	Impact Rate (m/s)	Screen Size (mm)	Characteristic Feed Size (mm)
PVC	0 M.O.T.	53.3	3.175	7.4

Sieve Size (mm)	Mass % undersize	RRB Model
2.36	90.35	91.97
2	78.09	77.12
1.4	37.49	37.14
0.85	7.74	8.80
0.5	1.01	1.64
0.212	0.10	0.10

Characteristic Product Size, $L_{90} = 2.05$

Uniformity Index, $n = 3.24$

Material	Temperature (C)	Impact Rate (m/s)	Screen Size (mm)	Characteristic Feed Size (mm)
PVC	0 M.O.T.	93.2	3.175	7.4

Sieve Size (mm)	Mass % undersize	RRB Model
2.36	99.48	100.00
2	98.83	99.99
1.4	90.64	94.29
0.85	48.63	43.19
0.5	7.15	9.59
0.212	0.13	0.62

Characteristic Product Size, $L_{90} = 1.17$

Uniformity Index, $n = 3.25$

Material	Temperature (C)	Impact Rate (m/s)	Screen Size (mm)	Characteristic Feed Size (mm)
PVC	0 M.O.T.	66.6	3.175	7.4

Sieve Size (mm)	Mass % undersize	RRB Model
2.36	96.66	99.14
2	91.99	93.80
1.4	58.21	58.20
0.85	10.15	15.83
0.5	0.27	3.03
0.212	0.00	0.19

Characteristic Product Size, $L_{90} = 1.69$

Uniformity Index, $n = 3.25$

Material	Temperature (C)	Impact Rate (m/s)	Screen Size (mm)	Characteristic Feed Size (mm)
PVC	-20 Refrig.	53.3	3.175	7.4

Sieve Size (mm)	Mass % undersize	RRB Model
2.36	60.73	57.48
2	42.52	44.97
1.4	20.75	24.08
0.85	13.21	8.91
0.5	8.05	2.91
0.212	1.01	0.45

Characteristic Product Size, $L_{90} = 3.03$

Uniformity Index, $n = 2.36$

Material	Temperature (C)	Impact Rate (m/s)	Screen Size (mm)	Characteristic Feed Size (mm)
PVC	-20 Refrig..	66.6	3.175	7.4

Sieve Size (mm)	Mass % undersize	RRB Model
2.36	82.79	81.96
2	66.24	65.73
1.4	28.98	32.25
0.85	12.29	9.02
0.5	6.60	2.08
0.212	1.03	0.18

Characteristic Product Size, $L_{90} = 2.31$

Uniformity Index, $n = 2.84$

Material	Temperature (C)	Impact Rate (m/s)	Screen Size (mm)	Characteristic Feed Size (mm)
PVC	-20 Refrig..	93.2	3.175	7.4

Sieve Size (mm)	Mass % undersize	RRB Model
2.36	92.87	92.70
2	83.83	81.59
1.4	45.30	48.40
0.85	17.24	16.29
0.5		
0.212		

Characteristic Product Size, $L_{90} = 1.96$

Uniformity Index, $n = 2.63$

Material	Temperature (C)	Impact Rate (m/s)	Screen Size (mm)	Characteristic Feed Size (mm)
PVC	22	53.3	3.175	7.4

Sieve Size (mm)	Mass % undersize	RRB Model
2.36	54.62	51.84
2	37.95	40.45
1.4	18.95	21.91
0.85	11.67	8.41
0.5	6.41	2.88
0.212	0.77	0.49

Characteristic Product Size, $L_{90} = 3.13$

Uniformity Index, $n = 2.52$

Material	Temperature (C)	Impact Rate (m/s)	Screen Size (mm)	Characteristic Feed Size (mm)
PVC	22	66.6	3.175	7.4

Sieve Size (mm)	Mass % undersize	RRB Model
2.36	77.27	75.81
2	60.22	60.01
1.4	25.98	30.04
0.85	12.72	9.12
0.5	7.71	2.33
0.212	1.35	0.24

Characteristic Product Size, $L_{90} = 2.48$

Uniformity Index, $n = 2.64$

Material	Temperature (C)	Impact Rate (m/s)	Screen Size (mm)	Characteristic Feed Size (mm)
PVC	22	93.2	3.175	7.4

Sieve Size (mm)	Mass % undersize	RRB Model
2.36	88.03	87.77
2	76.07	74.12
1.4	36.87	40.69
0.85	15.24	12.90
0.5	7.55	3.30
0.212	1.28	0.34

Characteristic Product Size, $L_{90} = 2.14$

Uniformity Index, $n = 2.67$

Material	Temperature (C)	Impact Rate (m/s)	Screen Size (mm)	Characteristic Feed Size (mm)
PVC	40.	53.3	3.175	7.4

Sieve Size (mm)	Mass % undersize	RRB Model
3.35	88.20	80.24
2.36	60.42	69.32
2.00	43.51	44.99
1.4	30.97	20.57
0.85	13.37	8.01
0.50	8.78	1.61

Characteristic Product Size, $L_{90} = 2.35$

Uniformity Index, $n = 1.91$

Material	Temperature (C)	Impact Rate (m/s)	Screen Size (mm)	Characteristic Feed Size (mm)
PVC	40	66.6	3.175	7.4

Sieve Size (mm)	Mass % undersize	RRB Model
2.36	75.42	73.01
2	58.82	58.96
1.4	27.03	32.15
0.85	15.06	11.42
0.5	9.14	3.46
0.212		

Characteristic Product Size, $L_{90} = 2.58$

Uniformity Index, $n = 2.33$

Material	Temperature (C)	Impact Rate (m/s)	Screen Size (mm)	Characteristic Feed Size (mm)
PVC	40	93.2	3.175	7.4

Sieve Size (mm)	Mass % undersize	RRB Model
2.36	88.67	87.83
2	77.21	75.24
1.4	39.45	43.76
0.85	17.45	15.35
0.5	9.11	4.36
0.212		

Characteristic Product Size, $L_{90} = 2.12$

Uniformity Index, $n = 2.48$

Material	Temperature (C)	Impact Rate (m/s)	Screen Size (mm)	Characteristic Feed Size (mm)
PVC	60	53.2	3.175	7.4

Sieve Size (mm)	Mass % undersize	RRB Model
2.36	52.56	53.51
2	37.48	41.42
1.4	21.23	21.84
0.85	15.47	8.00
0.5		
0.212		

Characteristic Product Size, $L_{50} = 3.32$

Uniformity Index, $n = 2.17$

Material	Temperature (C)	Impact Rate (m/s)	Screen Size (mm)	Characteristic Feed Size (mm)
PVC	60	66.6	3.175	7.4

Sieve Size (mm)	Mass % undersize	RRB Model
2.36	71.82	70.22
2	54.65	56.87
1.4	28.05	31.82
0.85	18.35	11.97
0.5		
0.212		

Characteristic Product Size, $L_{50} = 2.68$

Uniformity Index, $n = 2.21$

Material	Temperature (C)	Impact Rate (m/s)	Screen Size (mm)	Characteristic Feed Size (mm)
PVC	60	93.2	3.175	7.4

Sieve Size (mm)	Mass % undersize	RRB Model
2.36	85.34	83.37
2	72.79	71.63
1.4	39.63	44.46
0.85	22.59	18.34
0.5		
0.212		

Characteristic Product Size, $L_{50} = 2.24$

Uniformity Index, $n = 2.14$

Material	Temperature (C)	Impact Rate (m/s)	Screen Size (mm)	Characteristic Feed Size (mm)
PVC	80	53.2	3.175	7.4

Sieve Size (mm)	Mass % undersize	RRB Model
2.36	57.22	57.29
2	41.48	44.35
1.4	21.46	23.08
0.85	14.69	8.18
0.5		
0.212		

Characteristic Product Size, $L_{90} = 3.13$

Uniformity Index, $n = 2.25$

Material	Temperature (C)	Impact Rate (m/s)	Screen Size (mm)	Characteristic Feed Size (mm)
PVC	80	66.6	3.175	7.4

Sieve Size (mm)	Mass % undersize	RRB Model
2.36	75.1	73.23
2	58.45	59.52
1.4	29.23	33.08
0.85	17.56	12.11
0.5		
0.212		

Characteristic Product Size, $L_{90} = 2.58$

Uniformity Index, $n = 2.28$

Material	Temperature (C)	Impact Rate (m/s)	Screen Size (mm)	Characteristic Feed Size (mm)
PVC	80	93.2	3.175	7.4

Sieve Size (mm)	Mass % undersize	RRB Model
2.36	86.14	93.23
2	75.74	84.47
1.4	41.08	72.83
0.85	21.05	45.31
0.5		
0.212		

Characteristic Product Size, $L_{90} = 2.14$

Uniformity Index, $n = 2.26$

Material	Temperature (C)	Impact Rate (m/s)	Screen Size (mm)	Characteristic Feed Size (mm)
PET	0 M.O.T.	53.2	3.175	4.6

Sieve Size (mm)	Mass % undersize	RRB Model
2.36	72.14	73.46
2	60.95	59.56
1.4	32.85	32.80
0.85	11.8	11.81
0.5	2.07	3.63
0.212	0.24	0.51

Characteristic Product Size, $L_{90} = 2.57$

Uniformity Index, $n = 2.31$

Material	Temperature (C)	Impact Rate (m/s)	Screen Size (mm)	Characteristic Feed Size (mm)
PET	0 M.O.T.	66.6	3.175	4.6

Sieve Size (mm)	Mass % undersize	RRB Model
2.36	74.36	76.7
2	66.23	66.24
1.4	47.32	43.80
0.85	21.56	21.13
0.5	4.34	8.83
0.212	0.13	1.99

Characteristic Product Size, $L_{90} = 2.50$

Uniformity Index, $n = 1.78$

Material	Temperature (C)	Impact Rate (m/s)	Screen Size (mm)	Characteristic Feed Size (mm)
PET	0 M.O.T.	93.2	3.175	4.6

Sieve Size (mm)	Mass % undersize	RRB Model
2.36	76.73	78.97
2	68.37	69.29
1.4	51.63	47.71
0.85	26.01	24.45
0.5	5.375	10.86
0.212	0.13	2.68

Characteristic Product Size, $L_{90} = 2.41$

Uniformity Index, $n = 1.68$

Material	Temperature (C)	Impact Rate (m/s)	Screen Size (mm)	Characteristic Feed Size (mm)
PET	-20 Refig.	53.2	3.175	4.6

Sieve Size (mm)	Mass % undersize	RRB Model
2.36	65.43	64.14
2	48.04	48.87
1.4	21.55	23.57
0.85	9.54	7.20
0.5	5.05	1.90
0.212	1.46	0.21

Characteristic Product Size, $L_{90} = 2.81$

Uniformity Index, $n = 2.56$

Material	Temperature (C)	Impact Rate (m/s)	Screen Size (mm)	Characteristic Feed Size (mm)
PET	-20 Refig.	66.6	3.175	4.6

Sieve Size (mm)	Mass % undersize	RRB Model
2.36	71.93	72.86
2	60.37	59.07
1.4	32.17	32.66
0.85	11.68	11.89
0.5	3.85	3.69
0.212	0.87	0.53

Characteristic Product Size, $L_{90} = 2.59$

Uniformity Index, $n = 2.28$

Material	Temperature (C)	Impact Rate (m/s)	Screen Size (mm)	Characteristic Feed Size (mm)
PET	-20 Refig.	93.2	3.175	4.6

Sieve Size (mm)	Mass % undersize	RRB Model
2.36	78.82	79.81
2	69.29	69.25
1.4	47.24	45.71
0.85	21.18	21.61
0.5	7.29	8.74
0.212	2.12	1.86

Characteristic Product Size, $L_{90} = 2.37$

Uniformity Index, $n = 1.84$

Material	Temperature (C)	Impact Rate (m/s)	Screen Size (mm)	Characteristic Feed Size (mm)
PET	22	53.2	3.175	4.6

Sieve Size (mm)	Mass % undersize	RRB Model
2.36	64.76	63.98
2	46.08	46.89
1.4	19.02	20.20
0.85	7.31	5.19
0.5	3.06	1.14
0.212	0.93	0.10

Characteristic Product Size, $L_{90} = 2.76$

Uniformity Index, $n = 2.89$

Material	Temperature (C)	Impact Rate (m/s)	Screen Size (mm)	Characteristic Feed Size (mm)
PET	22	66.6	3.175	4.6

Sieve Size (mm)	Mass % undersize	RRB Model
2.36	71.74	70.51
2	57.42	57.47
1.4	30.05	32.73
0.85	13.94	12.65
0.5	7.29	4.22
0.212	2.17	0.68

Characteristic Product Size, $L_{90} = 2.68$

Uniformity Index, $n = 2.15$

Material	Temperature (C)	Impact Rate (m/s)	Screen Size (mm)	Characteristic Feed Size (mm)
PET	23 M.O.T.	93.2	3.175	4.6

Sieve Size (mm)	Mass % undersize	RRB Model
2.36	78.51	80.00
2	68.6	67.62
1.4	41.74	40.79
0.85	15.70	16.42
0.5	4.41	5.57
0.212	0.69	0.90

Characteristic Product Size, $L_{90} = 2.36$

Uniformity Index, $n = 2.15$

Material	Temperature (C)	Impact Rate (m/s)	Screen Size (mm)	Characteristic Feed Size (mm)
PET	40	53.2	3.175	4.6

Sieve Size (mm)	Mass % undersize	RRB Model
2.36	67.8	65.91
2	50.22	51.17
1.4	23.08	25.82
0.85	10.99	8.40
0.5	6.29	2.36
0.212		

Characteristic Product Size, $L_{90} = 2.78$

Uniformity Index, $n = 2.45$

Material	Temperature (C)	Impact Rate (m/s)	Screen Size (mm)	Characteristic Feed Size (mm)
PET	40	66.6	3.175	4.6

Sieve Size (mm)	Mass % undersize	RRB Model
2.36	71.93	72.86
2	60.37	59.07
1.4	32.17	32.66
0.85	11.68	11.88
0.5	3.85	3.69
0.212	0.87	0.53

Characteristic Product Size, $L_{90} = 2.48$

Uniformity Index, $n = 2.06$

Material	Temperature (C)	Impact Rate (m/s)	Screen Size (mm)	Characteristic Feed Size (mm)
PET	40	93.2	3.175	4.6

Sieve Size (mm)	Mass % undersize	RRB Model
2.36	78.82	79.81
2	69.29	69.25
1.4	47.24	45.71
0.85	21.18	21.61
0.5	7.29	8.74
0.212	2.12	1.86

Characteristic Product Size, $L_{90} = 2.42$

Uniformity Index, $n = 2.03$

Material	Temperature (C)	Impact Rate (m/s)	Screen Size (mm)	Characteristic Feed Size (mm)
PET	60	53.2	3.175	4.6

Sieve Size (mm)	Mass % undersize	RRB Model
2.36	62.47	61.04
2	43.83	45.36
1.4	19.65	20.70
0.85	8.69	5.89
0.5		
0.212		

Characteristic Product Size, $L_{90} = 2.88$

Uniformity Index, $n = 2.69$

Material	Temperature (C)	Impact Rate (m/s)	Screen Size (mm)	Characteristic Feed Size (mm)
PET	60	66.6	3.175	4.6

Size (mm)	Mass % undersize	RRB Model
2.36	70.07	68.35
2	54.8	54.52
1.4	27.34	29.42
0.85	12.07	10.53
0.5		
0.212		

Characteristic Product Size, $L_{90} = 2.73$

Uniformity Index, $n = 2.29$

Material	Temperature (C)	Impact Rate (m/s)	Screen Size (mm)	Characteristic Feed Size (mm)
PET	60	93.2	3.175	4.6

Size (mm)	Mass % undersize	RRB Model
2.36	79.00	78.34
2	67.2	65.96
1.4	38.25	39.74
0.85	16.75	16.15
0.5		
0.212		

Characteristic Product Size, $L_{90} = 2.42$

Uniformity Index, $n = 2.12$

Material	Temperature (C)	Impact Rate (m/s)	Screen Size (mm)	Characteristic Feed Size (mm)
PET	80	53.2	3.175	4.6
	Size (mm)	Mass % undersize		RRB Model
	2.36	63.35		62.65
	2	46.1		47.53
	1.4	22.17		22.81
	0.85	9.45		6.97
	0.5			
	0.212			

Characteristic Product Size, $L_{90} = 2.86$

Uniformity Index, $n = 2.56$

Material	Temperature (C)	Impact Rate (m/s)	Screen Size (mm)	Characteristic Feed Size (mm)
PET	80	66.6	3.175	4.6
	Size (mm)	Mass % undersize		RRB Model
	2.36	66.58		65.68
	2	50.26		50.58
	1.4	23.65		24.95
	0.85	9.64		7.85
	0.5			
	0.212			

Characteristic Product Size, $L_{90} = 2.78$

Uniformity Index, $n = 2.52$

Material	Temperature (C)	Impact Rate (m/s)	Screen Size (mm)	Characteristic Feed Size (mm)
PET	80	93.2	3.175	4.6
	Size (mm)	Mass % undersize		RRB Model
	2.36	73.31		72.39
	2	85.4		58.98
	1.4	31.35		33.24
	0.85	15.16		12.48
	0.5			
	0.212			

Characteristic Product Size, $L_{90} = 2.61$

Uniformity Index, $n = 2.22$

Material	Temperature (C)	Impact Rate (m/s)	Screen Size (mm)	Characteristic Feed Size (mm)
PET	0 M.O.T.	93.2	3.175	2.36

Size (mm)	Mass % undersize	RRB Model
2.36	77.42	80.43
2	70.18	72.35
1.4	58.42	53.69
0.85	35.94	31.32
0.5	9.78	16.07
0.212	0.38	4.97

Characteristic Product Size, $L_{80} = 2.34$

Uniformity Index, $n = 1.44$

Material	Temperature (C)	Impact Rate (m/s)	Screen Size (mm)	Characteristic Feed Size (mm)
PET	0 M.O.T.	93.2	3.175	3.35

Size (mm)	Mass % undersize	RRB Model
2.36	74.55	78.60
2	68.99	70.61
1.4	57.88	52.52
0.85	36.05	31.05
0.5	9.56	16.27
0.212	0.78	5.23

Characteristic Product Size, $L_{80} = 2.43$

Uniformity Index, $n = 1.39$

Material	Temperature (C)	Impact Rate (m/s)	Screen Size (mm)	Characteristic Feed Size (mm)
PET	0 M.O.T.	93.2	3.175	4.00

Size (mm)	Mass % undersize	RRB Model
2.36	71.34	75.16
2	65.33	66.40
1.4	53.47	47.46
0.85	29.74	26.49
0.5	5.53	13.10
0.212	0.46	3.87

Characteristic Product Size, $L_{80} = 2.60$

Uniformity Index, $n = 1.48$

Material	Temperature (C)	Impact Rate (m/s)	Screen Size (mm)	Characteristic Feed Size (mm)
PET	22	93.2	1.57	4.6

Size (mm)	Mass % undersize	RRB Model
2.36	98.14	98.59
2	95.35	94.91
1.4	75.3	75.09
0.85	37.18	38.04
0.5	15.41	14.29
0.212	2.12	2.44

Characteristic Product Size, $L_{90} = 1.50$

Uniformity Index, $n = 2.14$

Material	Temperature (C)	Impact Rate (m/s)	Screen Size (mm)	Characteristic Feed Size (mm)
PVC	22	93.2	1.57	7.4

Size (mm)	Mass % undersize	RRB Model
2.36	98.21	96.20
2	96.57	92.51
1.4	77.35	79.20
0.85	49.03	54.12
0.5	36.81	3091
0.212	9.24	10.49

Characteristic Product Size, $L_{90} = 1.42$

Uniformity Index, $n = 1.40$

Material	Temperature (C)	Impact Rate (m/s)	Screen Size (mm)	Characteristic Feed Size (mm)
PET	22	93.2	none	4.6

Size (mm)	Mass % undersize	RRB Model
4.75	88.69	88.59
4.00	78.27	78.02
3.35	64.42	64.83
2.80	51.08	51.22
2.36	39.77	39.46
2.00	29.86	29.87

Characteristic Product Size, $L_{90} = 4.12$

Uniformity Index, $n = 2.09$

Material	Temperature (C)	Impact Rate (m/s)	Screen Size (mm)	Characteristic Feed Size (mm)
PVC	22	93.2	none	7.4
	Size (mm)	Mass % undersize		RRB Model
	4.75	84.2		85.89
	4.00	75.33		75.73
	3.35	64.75		63.26
	2.80	52.09		50.81
	2.36	40.34		40.01
	2.00	28.85		31.05

Characteristic Product Size, $L_{90} = 2.73$

Uniformity Index, $n = 2.29$

Material	Temperature (C)	Impact Rate (m/s)	Screen Size (mm)	Characteristic Feed Size (mm)
PVC	0 M.O.T	93.2	2.36	7.4
	Size (mm)	Mass % undersize		RRB Model
	2.36	99.47		99.72
	2	97.6		97.75
	1.4	77.39		77.09
	0.85	31.91		32.47
	0.5	9.84		9.17
	0.212	1.33		0.98

Characteristic Product Size, $L_{90} = 1.47$

Uniformity Index, $n = 2.65$

Material	Temperature (C)	Impact Rate (m/s)	Screen Size (mm)	Characteristic Feed Size (mm)
PET	0 M.O.T.	93.2	2.36	4.6
	Size (mm)	Mass % undersize		RRB Model
	2.36	80.19		80.41
	2	69.66		70.62
	1.4	49.54		48.38
	0.85	25.70		24.37
	0.5	8.36		10.56
	0.212	0.93		2.50

Characteristic Product Size, $L_{90} = 2.34$

Uniformity Index, $n = 1.73$

Material	Temperature (C)	Impact Rate (m/s)	Screen Size (mm)	Characteristic Feed Size (mm)
PET/PVC	22	93.2	3.175	-
	Size (mm)	Mass % undersize		RRB Model
	2.36	85.87		86.61
	2	75.72		74.53
	1.4	44.20		44.90
	0.85	16.67		17.01
	0.5	6.52		5.28
	0.212	1.09		0.73

Characteristic Product Size, $L_{80} = 2.14$

Uniformity Index, $n = 2.33$

Material	Temperature (C)	Impact Rate (m/s)	Screen Size (mm)	Characteristic Feed Size (mm)
PET/PVC	0 M.O.T.	93.2	3.175	-
	Size (mm)	Mass % undersize		RRB Model
	2.36	83.28		86.95
	2	77.70		78.19
	1.4	60.28		55.67
	0.85	28.57		28.71
	0.5	8.71		12.47
	0.212	1.05		2.90

Characteristic Product Size, $L_{80} = 2.06$

Uniformity Index, $n = 1.76$

Material	Temperature (C)	Impact Rate (m/s)	Screen Size (mm)	Characteristic Feed Size (mm)
PET/PVC	-20 M.O.T.	93.2	3.175	-
	Size (mm)	Mass % undersize		RRB Model
	2.36	85.03		87.69
	2	78.91		79.77
	1.4	62.59		59.02
	0.85	32.99		32.61
	0.5	12.58		15.28
	0.212	2.38		4.00

Characteristic Product Size, $L_{80} = 2.01$

Uniformity Index, $n = 1.63$

Material	Temperature (C)	Impact Rate (m/s)	Screen Size (mm)	Characteristic Feed Size (mm)
PVC	0 M.O.T	93.2	0.889	7.4
	Size (mm)	Mass % undersize		RRB Model
	2.36	100		100
	2	100		99.99
	1.4	100		99.83
	0.85	86.19		87.88
	0.5	49.72		47.66
	0.212	6.08		9.14

Characteristic Product Size, $L_{90} = 0.75$

Uniformity Index, $n = 2.23$

Material	Temperature (C)	Impact Rate (m/s)	Screen Size (mm)	Characteristic Feed Size (mm)
PET	0 M.O.T.	93.2	0.889	4.6
	Size (mm)	Mass % undersize		RRB Model
	2.36	99.62		100
	2	99.62		99.99
	1.4	98.86		99.88
	0.85	87.55		87.69
	0.5	45.28		45.05
	0.212	7.17		7.60

Characteristic Product Size, $L_{90} = 0.76$

Uniformity Index, $n = 2.36$

Material	Temperature (C)	Impact Rate (m/s)	Screen Size (mm)	Characteristic Feed Size (mm)
PVC	-20 M.O.T.	93.2	3.175	7.4
	Size (mm)	Mass % undersize		RRB Model
	2.36	99.34		99.80
	2	98.34		98.59
	1.4	85.43		85.16
	0.85	46.02		46.18
	0.5	16.89		17.08
	0.212	3.64		2.67

Characteristic Product Size, $L_{90} = 1.30$

Uniformity Index, $n = 2.25$

Material	Temperature (C)	Impact Rate (m/s)	Screen Size (mm)	Characteristic Feed Size (mm)
PVC	-40 M.O.T.	93.2	3.175	7.4

Size (mm)	Mass % undersize	RRB Model
2.36	99.06	99.90
2	97.59	98.93
1.4	83.91	84.31
0.85	42.35	41.07
0.5	11.26	13.02
0.212	1.34	1.60

Characteristic Product Size, $L_{90} = 1.32$

Uniformity Index, $n = 2.51$

Material	Temperature (C)	Impact Rate (m/s)	Screen Size (mm)	Characteristic Feed Size (mm)
PET	-20 M.O.T.	93.2	3.175	4.6

Size (mm)	Mass % undersize	RRB Model
2.36	79.06	80.68
2	71.79	71.89
1.4	53.42	51.64
0.85	29.49	28.31
0.5	11.11	13.51
0.212	2.14	3.72

Characteristic Product Size, $L_{90} = 2.32$

Uniformity Index, $n = 1.56$

Material	Temperature (C)	Impact Rate (m/s)	Screen Size (mm)	Characteristic Feed Size (mm)
PET	-40 M.O.T.	93.2	3.175	4.6

Size (mm)	Mass % undersize	RRB Model
2.36	78.16	79.09
2	69.97	70.56
1.4	52.56	51.26
0.85	30.72	28.94
0.5	12.29	14.35
0.212	2.05	4.22

Characteristic Product Size, $L_{90} = 2.40$

Uniformity Index, $n = 1.49$

Material	Temperature (C)	Impact Rate (m/s)	Screen Size (mm)	Characteristic Feed Size (mm)
PET	-20 M.O.T.	53.2	3.175	4.6

Size (mm)	Mass % undersize	RRB Model
2.36	65.66	66.20
2	56.57	55.77
1.4	35.35	35.69
0.85	17.17	17.05
0.5	7.07	7.22
0.212	1.68	1.70

Characteristic Product Size, $L_{90} = 2.97$

Uniformity Index, $n = 1.72$

Material	Temperature (C)	Impact Rate (m/s)	Screen Size (mm)	Characteristic Feed Size (mm)
PET/PVC	-20 M.O.T.	93.2	3.175	-

Size (mm)	Mass % undersize	RRB Model
4.75	99.47	99.96
2.36	87.73	93.24
1.40	71.91	70.72
0.85	51.80	44
0.5	17.02	22.97
0.212	.99	6.93

Characteristic Product Size, $L_{90} = 1.67$

Uniformity Index, $n = 1.50$